


Doctoral Dissertation
Doctoral Program in Electrical, Electronics and Communications Engineering
(33.rd cycle)

Analysis and Reduction of the Scattering by Cloaked Metallic Cylinders Beyond the Quasi-static Limit

Barbara Cappello
* * * * * *

Supervisor
Prof. Ladislau Matekovits

Politecnico di Torino
2021

I hereby declare that, the contents and organisation of this dissertation constitute my own original work and does not compromise in any way the rights of third parties, including those relating to the security of personal data.

Barbara Cappello
Turin, 2021

Summary

The main topic discussed in this dissertation is the electromagnetic cloaking of conductive cylinders and the analysis of the field scattered by metasurface cloaked cylinders. Among the different cloaking techniques, here the mantle cloaking is investigated. This method is based on the scattering cancellation approach and it aims to reduce (ideally to annul) the field scattered by an object such that the total field surrounding the object resembles the incident field pattern. To do so, the object is covered by a metasurface coating layer which consists of a periodically repeated metallic pattern, printed on a dielectric layer. The latter is necessary in the cloaking of conductive structures to avoid short circuits between the cylinder and the metasurface metallic pattern.

Electromagnetic cloaking can find application in the reduction of interference between nearby antennas, or of disturbances introduced by obstacles presents in the proximity of an antenna, such to avoid interference and distortions of the antenna radiation pattern.

The dissertation presents a comprehensive and deep investigation of the mantle cloaking method. In the first part, the main focus is the theoretical analysis of the scattering by a metasurface coated cylinder. For this purpose, the metasurface is modelled as a surface impedance boundary condition at the object-background interface. The scattered field is examined in terms of harmonic composition, and a great attention is given to the computation of the scattering coefficients, which are a measure of the presence of a specific harmonic in the total scattering. In a first time, a homogeneous value of surface impedance is considered, and a closed formulation to express the scattering coefficients is derived. From this formulation, the surface impedance condition which annuls one harmonic of the scattered field is computed in a closed form, valid also beyond the quasi-static limit.

Moreover, the surface impedance condition that leads to a minimum of the scattered field is investigated, with particular focusing of non-electrically small structure. Indeed, since the initial development of cloaking devices, numerous studies

addressing different aspects of the cloaking problem have been proposed in literature, however, the cloaking beyond the quasi-static limit is still challenging, especially with the use of passive metasurface coatings.

In this framework, a possible solution to address this problem is proposed by using a single layer passive metasurface. It is found that, with an appropriate choosing of the dielectric layer properties, and with the use of an inductive surface impedance, a partial reduction of the scattering can be obtained with a homogeneous metasurface.

The analytical results are then applied to the design of a practical metasurface cloaking. An example of cloaking for electrically small structure is given, and then it is adapted to the cloaking of cylinders with radius comparable with the wavelength of the incident field. Moreover, the effect of the metasurface conformal shape on the scattering reduction is investigated.

In the second part of the thesis, the use of an inhomogeneous surface is investigated with the aim of improving the cloaking effect. Two inhomogeneous metasurfaces are presented based on the the combination of unit cells with same shape but different dimension. Both metallic square patch and strips are considered as unit cell and it is shown that with a specific arrangement of the unit cells, a further increase of the cloaking bandwidth and of the scattering reduction can be obtained.

Acknowledgements

First of all I would like to thank Prof. Ladislau Matekovits, for being my PhD tutor, and for believing in me since my Master thesis. For supporting me both professionally and personally along this journey, and for helping me overcome the obstacles that inevitably come up during the PhD. His support and his encouragement were fundamental to get to the end of the PhD program and to write this thesis.

Thanks to Prof. Oscar Quevedo-Teruel for hosting me at KTH university and for welcoming me into his research group. The time spent in Stockholm was really precious.

Thanks to Maxim Gorlach and his entire research group for hosting me at ITMO University and giving me the opportunity to participate in their research project.

Thanks to Prof. Alexey Basharin and to Anar Ospanova for the collaboration and the contribution on the anapole modes research.

Finally, I would like to thank Giuseppe Labate, who was a great inspiration during these years, even if at a distance.

Contents

List of Figures

List of Scientific Publications

Journal Papers

J1. B. Cappello, A.K. Ospanova, L. Matekovits, and A.A. Basharin, "Mantle cloaking due to ideal magnetic dipole scattering", *Sci. Rep.*, vol. 10, 2413, 2020.

J2. N.A. Olekhno, E.I.Kretov, A.A. Stepanenko, P.A. Ivanova, V.V. Yaroshenko, E.M. Puhtina, D.S. Filonov, B. Cappello, L. Matekovits and M.A. Gorlach, "Topological edge states of interacting photon pairs emulated in a topolectrical circuit", *Nat. Commun.*, vol. 11, 1436, 2020.

J3. B. Cappello and L. Matekovits, "Harmonic analysis and reduction of the scattered field from electrically large cloaked metallic cylinders", *Appl. Opt.*, vol. 59, no. 12, pp. 3742-3750, 2020.

Conference Papers

C1. B. Cappello, G. Labate and L. Matekovits, "A Surface Impedance Model for a Microstrip-line based Metasurface", 2017 International Conference on Electromagnetics in Advanced Applications (ICEAA), pp. 429-432, 2017.

C2. G. Labate, B. Cappello and L. Matekovits, "A radial transmission line model for mantle cloaking with impedance metasurfaces", 12th European Conference on Antennas and Propagation (EuCAP 2018), pp. 1-3, 2018.

C3. B. Cappello and L. Matekovits, "Effect of Geometrical Parameters of a Width Modulated Microstrip Line Based Mantle-Cloak", 2018 IEEE International Symposium on Antennas and Propagation & USNC/URSI National Radio Science Meeting, pp. 1859-1860, 2018.

C4. B. Cappello and L. Matekovits, "Spectral Composition of the Scattered Field from a Large Metallic Cloaked Cylinder", 2018 International Conference on Electromagnetics in Advanced Applications (ICEAA), pp. 240-243, 2018.

C5. B. Cappello, L. Matekovits and K. Naishadham, "Preliminary Study of a Cylindrical Microstrip Metasurface Using the State Space Method", 2019 IEEE International Symposium on Antennas and Propagation and USNC-URSI Radio Science Meeting, pp. 2035-2036, 2019.

C6. B. Cappello, A. Ospanova, A. A. Basharin and L. Matekovits, "Ideal Magnetic Dipole: Scattering and Mantle Cloaking Effects", 2019 International Conference on Electromagnetics in Advanced Applications (ICEAA), pp. 1182-1184, 2019.

C7. B. Cappello, Y. Shestopalov and L. Matekovits, "Analysis of the Surface Impedance of a Sinusoidally Modulated Metasurface", 2019 International Conference on Electromagnetics in Advanced Applications (ICEAA), pp. 0075-0077, 2019.

C8. N.A. Olekhno, E.I. Kretov, A.A. Stepanenko, P.A. Ivanova, V.V. Yaroshenko, E.M. Puhtina, D.S. Filonov, B. Cappello, L. Matekovits and M.A. Gorlach, "Topological States of Interacting Photon Pairs Emulated in a Topolectrical Circuit", 2019 Photonics & Electromagnetics Research Symposium - Fall (PIERS - Fall), pp. 1082-1086, 2019.

C9. B. Cappello and L. Matekovits, "Inhomogeneous metasurface to enlarge cloaking bandwidth", 2020 IEEE International Symposium on Antennas and Propagation and North American Radio Science Meeting, pp. 813-814, 2019.

Chapter 1

Purpose and Overview of the Dissertation

1.1 Thesis aim

The aim of this dissertation is the investigation and the study of the mantle cloaking problem and the analysis of the field scattered by cloaked cylinders. Cloaking and invisibility have always been a fascinating topic and they have found space in the scientific community especially in last decade, thanks also to the study of metamaterials.

The purpose of electromagnetic cloaking is to conceal the presence of a scatterer object illuminated by an incident electromagnetic wave. To achieve this effect, the object is covered with an opportunely designed material, such that the object presence does not influences the incident field. Therefore, the field surrounding the cloaked object should be equal to the field if the object were not present, such that the object is invisible for an observer placed in any point external to the object.

During the years different cloaking techniques were proposed, which will be briefly examined in the first part of this dissertation, however the main method which is presented and investigated here is the mantle cloaking approach. This consists in using a thin patterned metasurface coat in order to reduce the field scattered by the object to be cloaked.

A metasurface is a thin layer composed of a basic unit cell periodically repeated, and when it is used to cover the scattered object, it changes the boundary condition at the interface between the object and the background medium, giving the possibility to control the propagation of an incident electromagnetic field.

Indeed, as it will be detailed, the metasurface can be modelled as an impedance boundary conditions, and its characteristic impedance can be directly related to

the unit cell shape and dimension. Therefore, acting on the metasurface unit cells characteristics and arrangement it is possible to control the interaction between the incident field and the scatterer object, such to obtain and tune the cloaking effect.

In this work, the scatterer object is considered to be a metallic cylinder with a circular section. This choice is made for two principal reasons. The first, is that the cylindrical geometry allows to write a canonical formulation of the scattered field problem. Indeed, a closed form solution of the scattering is derived for a cloaked cylinder, and all the reasoning carried out considering this particular geometry can be than adapted to different scatterer shapes (for example elliptical cylinders). Therefore, considering a cylindrical scatterer is a fundamental step to conduct before evaluating more complex geometry. The second reason is that a metallic cylinders can characterise different real-life problem, as for example antennas struts or sensors.

Indeed, cloaking can find application for example in reducing unwanted interference from obstacles of different nature present in the proximity of an antenna, in order to avoid distortion in the radiation pattern. Moreover, cloaking can be also useful for reducing the mutual coupling between nearby antennas, which is of growing importance due to the increasing of locations with high density of antennas presence, and in general to the realisation of low noise communication networks.

Moreover, the analysis of electromagnetic cloaking can be the basis for cloaking application in other fields of study, and the concepts and principles proposed in electromagnetics can be adjusted and reformulated for other disciplines. Indeed, in last years, different types of cloaking were proposed in literature such as mechanical, thermal or seismic.

Therefore, throughout this dissertation, the mantle cloaking topic is exposed in a comprehensive way. Starting from the in-depth analytical study of the scattering phenomena, and the rigorous analytical derivation of the field scattered by coated metallic cylinders and its harmonic composition, investigating in particular the effect of the impedance boundary condition on the scattering.

Then, a real-life design of the cloaking metasurface is proposed, different metasurface shapes are presented, focusing on both electrically small and electrically large cylinders.

Two main evaluation criteria of the cloaking performance are taken into account. The first is the scattering reduction, which is evaluated as the difference between the field scattered by the bare metallic cylinder, and the one scattered by the cloaked cylinder. The second criteria is the cloaking operational bandwidth, i.e. the frequency range in which the cloaking metasurface has an appreciable effect on the scattering reduction.

1.2 Novelty of the work

The principal obstacles in the design of a cloaking device are considered in the thesis. In particular, it is shown that mantle cloaking technique is very effective for the reduction of the scattered field from electrically small structures (with dimension much smaller than the wavelength of the incident field), while presents more difficulties when electrically large objects are taken into consideration.

Indeed, in the past decade the cloaking phenomena has been of great interest and its characteristics have been examined in different literature papers, nonetheless, the cloaking of non electrically small structures remains challenging, especially if passive metasurface coatings are employed, as it is considered throughout the dissertation.

Therefore, in this framework, this dissertation aims to carefully examine analytically and numerically the cloaking beyond the quasi-static limit, proposing a solution for the cloaking of non electrically small structure.

In the first analytical section a closed form formulation is derived to compute the scattering coefficients associated to a dielectric coated metallic cylinder with a surface impedance boundary condition. From the expression of the coefficients is then derived an expression to compute the surface impedance which suppress an harmonic of the scattered field. Most important, this expression is valid also beyond the quasi-static limit, and can be therefore applied to the cloaking of electrically large cylinders.

Then, an investigation of the surface impedance condition which leads to a minimum of the scattering is performed and it is demonstrated that a single layer passive and homogeneous metasurface can partially reduce the scattered field even when the cylinder radius is comparable with the incident field wavelength, if opportunely designed and if an inductive surface impedance boundary condition is considered.

Moreover, the design of two inhomogeneous metasurfaces is also proposed, and it is shown that it gives the possibility to increase both the scattering reduction and the cloaking bandwidth.

1.3 Thesis outline

This thesis is an overall view of all the studies, the reasoning and the main findings carried out during the PhD years, which have been partially collected also in different conference and journal papers. For this reason, at the beginning of each Chapter it will be underlined if part of the presented results have been previously

published in a conference or journal article.

Moreover it should be noticed that a nomenclature section is not present because all acronyms and variables are defined at the first occurrence in the text, and that all the Equations are numbered for an easiest reading.

The thesis is organised as follows:

- In Chapter 1 an introduction of the thesis aim and purpose is given, and a brief explanation of the cloaking problem and the main challenges addressed in the dissertation is proposed.
- In Chapter 2 an insight of the different cloaking methods and the current state of the art is presented, synthetically reviewing the principal findings present in literature.
- In Chapter 3 a deep analysis of the mantle cloaking problem and scattering reduction is carried out. In particular, an analysis of the scattered field in terms of harmonic composition is proposed considering both metallic cylinder coated by a dielectric layer, and metasurface coated cylinder. The analytical computation of the scattering coefficients associated to a cloaked cylinder is carried out, and the surface impedance boundary condition required to cancel one harmonic of the scattered field is expressed in a closed form solution, valid also beyond the quasi-static limit. Then, the focus is shifted on the cloaking of non electrically small structures, demonstrating the possibility to use a single layer homogeneous metasurface to partially reduce the scattered field also beyond the quasi-static limit.
- In Chapter 4 a realisable metasurface design, based on the previous analytical findings, is proposed for the cloaking of both electrically small and electrically large structures, analysing the effect of the metasurface on the scattered field absolute value and harmonic composition.
- Finally in Chapter 5 an inhomogeneous metasurface design is presented as a solution to increase the scattering reduction and cloaking bandwidth. Starting from the previous designed homogeneous metasurfaces, by modifying the unit cells dimension and by opportunely arranging them, an inhomogeneous coating layer is obtained, which improves the cloaking performances.

Chapter 2

Electromagnetic Cloaking: an introduction

Invisibility has always been a fascinating topic in the scientific community. The theoretical possibility to achieve invisibility was already studied and investigated in the past, as proven for example in [1] and [2] in which the concept of zero scattering object was proposed. In these two papers it was demonstrated that considering a dielectric object and covering it with an opportune dielectric coat, it is possible to strongly reduce the scattering of the whole structure by properly choosing the dielectric constants of the two objects.

However, the practical application of this concept remained unfeasible till recent years, in which the advent of metamaterial gave the possibility to implement actual cloaking coats and gave rise to different techniques and methods for the realisation of cloaking devices.

Therefore, in the literature of the last decade, numerous methods to obtain the cloaking effect have been proposed and realised. They can be grouped in different categories, depending on the concept and the followed approach. In particular, two significant groups emerge from this categorisation. The first is based on the transformation electrodynamics idea and comprises Transformation Optics and Carpet cloaking, while the second group includes all the methods which follow a scattering cancellation approach such as Plasmonic or Mantle cloaking.

In this thesis, the mantle cloaking approach is studied and deeply examined, nonetheless a brief summary of transformation methods and plasmonic cloaking is here exposed in order to better understand and contextualise the cloaking problem.

Moreover, before examining the cloaking methods, an introduction of metamaterials and their possible applications in electromagnetics is presented here, since metamaterials and especially metasurfaces (their two dimensional counterpart) are

used in the following to practically implement a cloaking device.

2.1 Metamaterials

Studies on metamaterials have gained a vast attention in recent years and they have become an interesting field in electromagnetics thanks also to their vast range of applications.

The name "metamaterials" was firstly introduced by Walser in [3] and, as the word "meta" suggests, it refers to materials which posses characteristics beyond the ones of natural material. Although currently the term metamaterial is used referring to a vast range of materials, it is possible to identify basic characteristics of metamaterials. They usually consist of a periodic (or quasi periodic) repetition of a basic unit cell, and their properties depends on the characteristics of the unit cells (material, shape, dimensions), as well as their spatial arrangement. Moreover they are specifically designed to obtain properties which are non common in natural material.

Indeed it is known that two fundamental parameters which describes electromagnetic properties of a material are the permittivity ε and the permeability μ. They characterize the material response to an applied electric and magnetic field, respectively. When a metamaterial is composed of the repetition of single elements which have a dimension much smaller than the wavelength of the incident field, the values of ε and μ of the single elements can be averaged and equivalent parameters can be defined to characterise the whole material.

When microwave frequencies are considered, the single unit cells of the metamaterials can be of the order of millimeters, and if their dimension is sufficiently smaller, the material can be homogenised and it can be described by an equivalent value of ε and μ.

By looking at the ε-μ diagram reported in Fig. 2.1, it can be seen that most natural materials posses a permeability equal to the void one, such that $\mu = \mu_0$, and a relative permittivity ε_r positive and greater than one, therefore belonging to the first quadrant of the $\varepsilon - \mu$ chart.

In the second quadrant, materials with negative ε and positive μ can be found, and they are defined as ENG (epsilon negative) materials. Some natural materials belongs to this category such as metals below plasma frequency.

Studies on metamaterials began from the artificial developing of ENG materials and LHM (left handed materials). This last category relies in the third quadrant of the $\varepsilon - \mu$ chart. This means that both ε and μ are negative. With this material type it is possible to realise negative refraction and backward wave propagation.

The possibility to have materials with both negative permittivity and permeability was already investigated by Veselago in [4] in 1968, however in last years numerous studied were carried out on ENG and LHM materials. In particular, in 1999 a paper by Pendry [5] used split ring resonators, a structure with two concentric metallic rings with a little gap, to achieve a vast range of permeability values which are not possible in nature, and in the next years, the split ring resonator was used to design a metamaterial which presented a negative value of permittivity and permeability simultaneously [6]. In the following years, different studies on negative index materials were proposed [7]–[10] and they we the basis for the development of metamaterials.

However, to the present days, metamaterials are not limited to negative index materials but are employed for a vast range of applications in order to exploit theirs unique characteristics of controlling and directing the electromagnetic waves propagation.

Moreover, during the years there was a shift from bulky three dimensional metamaterials to thin 2D metasurface layers. Metasurfaces follow the same principle of metamaterials, i.e. they are composed of the repetition of a specific unit cell. With respect to 3D metamaterials they are not defined by an equivalent value of permittivity and permeability, but they can be characterised by an equivalent value of surface impedance. In this thesis, metasurfaces are exploited as a cloaking layer and they are therefore modeled as a surface impedance boundary condition, at least in a first time.

Metamaterials and metasurfaces can be currently found in a vast range of applications such as the design of leaky wave antennas [11]–[13], absorbers [14]–[16], lenses [17], [18], polarization converters [19]–[22], while, here, they are studied as a cloaking device application.

2.2 Transformation Optics

The first cloaking method which is briefly examined is the Transformation Optics (TO) method. This exploits the coordinate transformation invariance of the Maxwell equations in order to cloak a desired object. In particular, the object is coated by a material with inhomogeneous and anisotropic permittivity and permeability designed in such a way to emulate a coordinate distortion of the space surrounding the object. In this way it is possible to bend and control the propagation of an incident wave such that an obscure region of the space can be created, in which the field does not propagate. Any object collocated in this region does not interact with the field and it is therefore invisible for an external observer.

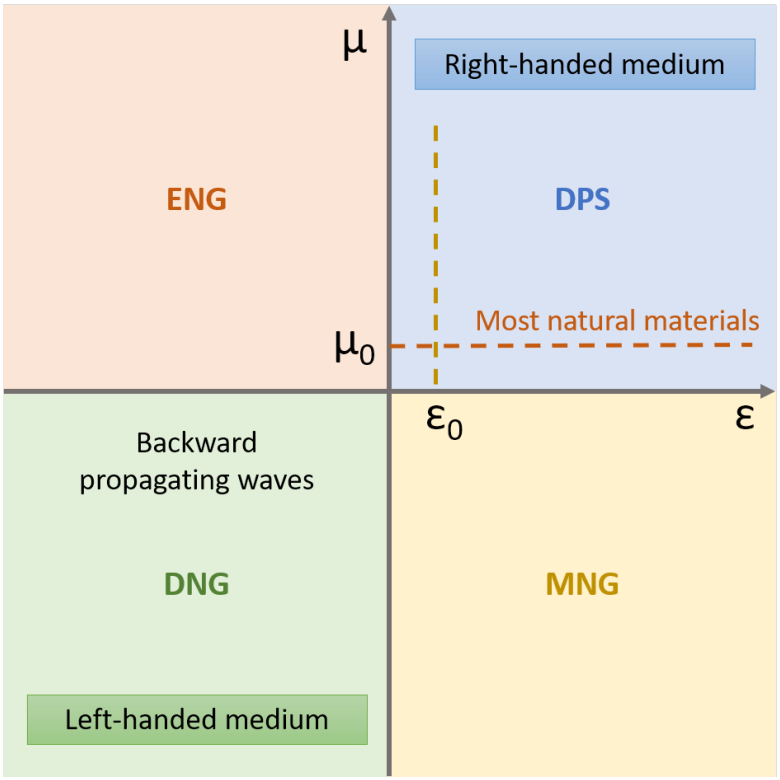

Figure 2.1: ε-μ diagram.

Although the basic concept of Transformation Optics and the connection between materials parameters and coordinate transformations was already studied in the half of 20th century [23], it became realisable only in recent years, thanks to the studies on metamaterials and left-handed materials. In fact, with this particular cloaking technique, the permittivity and permeability of the cloaking coat are required to be strongly anisotropic and they can also assume negative values. Therefore, the studies on metamaterials have been of crucial importance in the development of TO cloaking.

In 2006, two studies on transformation cloaking were presented simultaneously in two different papers by Pendry and Leonhardt [24], [25]. In [24] the concept of a spherical TO cloaking was proved: with the aim of cloaking a spherical object, the values of the permeability and permittivity tensor of the cloaking shell were computed. In the proposed design, the incident wave is channeled into the cloaking shell such to avoid the object on the inside, and the incident field pattern is restored beside the object, such that for an external observer the object is completely invisible. Following a similar concept, in [25] the author computed the opportune refractive index that the background medium should have to hide a spherical object

placed inside it.

After these firsts theoretical proofs of concept of TO, the first realisation of this type of cloaking device at microwave frequencies was proposed by Shuring in [26]. The authors proposed the design of a cloaking device for a conducting cylinder. After computing the required values of the permittivity and permeability tensors, the cloak was realised using ten different metamaterial cylindrical layers based on a split ring resonator unit cell which was already studied in different papers for its characteristics of realising a negative permeability [6]. The experimental measurements showed how the field propagates and it is compressed inside the cloaking layer, while it does not enter in the cloaked region in which the conductive cylinder is present. Moreover, in the region beyond the cylinder the wave fronts recompose as the cylinder were not present.

This method has the main advantage to produce a complete annulment of the field scattered by the object, at least theoretically. Furthermore, the cloaking design does not depend on the shape of the object to be hidden or on its size, therefore even electrically large object can be cloaked with this technique.

However, the practical realisation of this type of cloaking remains challenging due to several factors. First of all, the strong anisotropy required by the coating material parameters, which also needs to present equal electric and magnetic response such to match the background impedance, being a limitation in particular for optical frequencies. Moreover, the achievable bandwidth is usually narrow due to the superlumina propagation required inside the cloak. Indeed, the electromagnetic wave propagating in the cloaking coat requires to travel a longer path without showing phase variations.

A second method belonging to the category of TO is the carpet cloaking. This method has the same concept of TO cloaking but it is effective only for two dimensional cases. The method establishes that the object should be first covered by a Perfect Electric Conductor (PEC) layer and then hidden with a proper anisotropic medium such that the deformation created by the PEC layer appears flat.

Carpet cloaking was proposed in [27] which presented a quasi conformal mapping such to reduce the anisotropy required by the cloaking coat, and was later validated numerically and experimentally at both microwave [28] and optical frequencies [29], [30].

2.3 Electromagnetic Scattering

A second category of cloaking methods is based on scattering cancellation. Plasmonic and mantle cloaking belongs to this category, therefore, before detailing the

specific mechanisms of these two methods, it is opportune to briefly describe the scattering problem.

When an incident electric field impinges on an object (the scatterer), the field is partially absorbed and partially scattered around the object [31].

The field surrounding the object ($\boldsymbol{E}_{tot}$) can be therefore decomposed in two contributes: the incident field ($\boldsymbol{E}_i$), which is the field that would be present in the absence of the scatterer, and the scattered field ($\boldsymbol{E}_s$). Such that:

$$\boldsymbol{E}_{tot} = \boldsymbol{E}_i + \boldsymbol{E}_s \tag{2.1}$$

The scattered field can be defined in all points of the space external to the object and it depends on the geometry and the materials of the scatterer. In particular, the backward and the forward scattering can be defined. The first is a measure of the field reflected back in the same direction of the incident field, the second is the scatted field on the opposite side of the object with respect to the incident field direction. It should be noticed that, while in the half-plan in which the incident way lies, the scattering is determined as a reflection of the incident field itself, in the opposite half-plan, beyond the object, the scattering can be seen as a shadow region, in which the field is reduced.

An example is represented in Fig. 2.2. In this case, the scatterer object is metallic cylinder, while the incident field is a Transverse Magnetic (TM) polarised planewave, i.e. with the electric field vector parallel to the cylinder axis, with amplitude 1 V/m.

In Fig. 2.2 the real part of the incident, total and scattered field is represented. The incident field illuminates the scatterer from the left side. It can be seen that the presence of the cylinder strongly influences the surrounding field, distorting the field phase fronts and creating a shadow, a reduction of the field, on the opposite side of the cylinder with respect to the incident direction.

The right figure in Fig. 2.2 represents the real part of the scattered field. Since it is equal to the difference between the total and the incident field, in order to reproduce a situation in which the scatterer is not present, the scattered field should be annulled, such that $E_i = E_{tot}$. For this reason, a possible cloaking technique is based on the scattering cancellation.

Conversely to absorbing materials, a cloaking device should not only prevent the incident field to be reflected back, but also reduce the shadow region beyond the object such to minimize the object presence and in general to reduce (ideally to completely annul) the scattered field in all direction around the object. In this way, for an external observer (in any point of the background medium) the field phase and intensity should be the same as the object were not present.

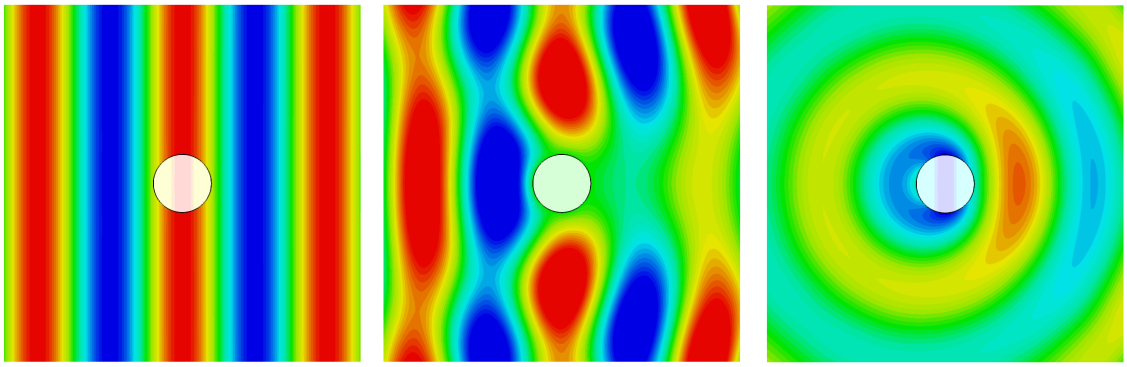

Figure 2.2: Real part of the incident, total and scattered field. The represented scatterer object is a conductive cylinder, and the incident field is a Transverse Magnetic polarised planewave.

2.4 Plasmonic Cloaking

As previously introduced, a different class of cloaking techniques includes plasmonic cloaking which was proposed in [32] and it is based on scattering cancellation. Therefore, the main idea is to cancel the field scattered by the target object, such that the total field surrounding the object resembles the incident field, concealing in this way the object presence.

Accordingly, the scattered field is decomposed in a sum of harmonics, and it can be proved that, if the scatterer is small compared to the wavelength of the illuminating wave, the scattered field is primarily composed by one dominating harmonic. Therefore, cancelling that harmonic it is possible to sensibly reduce the scattering.

Indeed, considering the scattering by a particle placed in a background medium with permittivity ε_0 and permeability μ_0, it is possible to write the scattered electric ($\boldsymbol{E}_s$) and magnetic ($\boldsymbol{H}_s$) field as in spherical coordinates as:

$$\begin{aligned}\boldsymbol{E}_s &= \sum_{n=1}^{\infty}\sum_{m=-n}^{n} c_n^{TM} a_{nm} \nabla\times\nabla\times(\hat{\boldsymbol{r}}\psi_n^m) - j\omega\mu_0 c_n^{TE} b_{nm} \nabla\times(\hat{\boldsymbol{r}}\psi_n^m)\\ \boldsymbol{H}_s &= \sum_{n=1}^{\infty}\sum_{m=-n}^{n} c_n^{TE} b_{nm} \nabla\times\nabla\times(\hat{\boldsymbol{r}}\psi_n^m) - j\omega\varepsilon_0 c_n^{TM} a_{nm} \nabla\times(\hat{\boldsymbol{r}}\psi_n^m)\end{aligned} \tag{2.2}$$

where ψ_n^m represents the spherical harmonics, with associate coefficients a_{nm} and b_{nm}, while c_n are the scattering coefficients.

In Eq. 2.2 the coefficients c_n^{TM} an c_n^{TE} quantify the amount of scattering related

to the n^{th} TM or TE harmonic, and their sum is directly proportional to the scattering cross-section, which is a measure of the total scattered power. Therefore, the idea of plasmonic cloaking is to cancel the scattered coefficients associated with the dominant harmonic.

To do so, the object is cloaked with a suitable material coat. In particular, in [32] it is demonstrated that, in order to cloak an object with a relative permittivity greater than one, as a common dielectric material, it is required a cloaking coat with relative permittivity lower than unity, from here derives the name Plasmonic. In this way, the polarizabilities of the object and the cloaking coat compensate each other, allowing to reach the total system invisibility.

Indeed in [32] it is demonstrated that the radius (a) and permittivity (ε) of the scatterer object and of the coating (a_c, ε_c) cannot assume arbitrary values but they should follow the rule:

$$\left(\frac{a}{a_c}\right)^3 = \frac{(\varepsilon_c - \varepsilon_0)(2\varepsilon_c + \varepsilon)}{(\varepsilon_c - \varepsilon)(2\varepsilon_c + \varepsilon_0)} \tag{2.3}$$

The main advantage of plasmonic cloaking with respect to TO, is that in this case the use of anisotropic materials is not required, but the cloaking coat can be homogeneous and isotropic and therefore easier to practically realise. Moreover, the thickness of the cloaking coat is reduced with respect to the Transformation Optics case.

An experimental realization was of plasmonic cloaking at microwave frequencies proposed in [33]. In order to realise a cloaking material with dielectric constant lower than ε_0 at microwave frequencies, a metamaterial is usually employed. For example in [34] a parallel-plate based metamaterial was used to implement this technique to numerically prove the cloaking of a 2D object, while in [35] the a parallel plate based coating is physically realised to cloak a finite length cylinder.

In the last decades different studies on plasmonic cloaking were conducted [36], [37], also to analyse the robustness of the method and its application to non ideal. finite length structures [38], [39] or the possibility of use multiple coating layer in order to achieve a greater bandwidth or multiple operational frequencies [40], [41].

2.5 Mantle Cloaking

Similar to plasmonic cloaking, mantle cloaking is based on the scattering cancellation approach, and it will be the main focus of this thesis. However, conversely to plasmonic cloaking, the scattering harmonic cancellation is not performed by using a bulk metamaterial coat, but a thin metasurface is employed.

Therefore, in this case, a 2D metasurface, composed of a periodic repetition of specifically designed unit cell, is used to cover the object such to modify the boundary conditions at the object-background interface.

Accordingly, the cloaking coat is characterised not by its value of dielectric constant, but instead by its equivalent value of surface impedance, and consequently, the metasurface is effectively modeled as a surface impedance boundary condition.

Given a metasurface layer, the surface impedance $\boldsymbol{Z}_s$ is a parameters that connects the average tangential electric field on the metasurface, $\boldsymbol{E}_{tan}$ with the average surface current density $\boldsymbol{J}_s$ induced on the metasurface by an incident wave. The surface current density is in turn proportional to the discontinuity of the averaged magnetic field across the metasurface boundary. Such that, on a homogeneous isotropic metasurface:

$$\boldsymbol{E}_{tan} = Z_s \boldsymbol{J}_s = Z_s \hat{\boldsymbol{r}} \times (\boldsymbol{H}_{tan}^{+} - \boldsymbol{H}_{tan}^{-}) \tag{2.4}$$

The use of a metasurface coat allows to control the interaction between the field and the object in such a way to control the field propagation.

Indeed, the surface impedance is a characteristic directly connected with the geometry and the materials parameters of the metasurface unit cell [42]. Hence, changing the geometry and the dimension of the metasurface unit cell it is possible to tune its equivalent value of surface impedance and therefore to control the intensity and phase of the scattered field.

As for plasmonic cloaking, the main advance of this method is that there is no necessity to employ an anisotropic cloaking layer. However, the main drawback of both mantle and plasmonic cloaking is the difficulty of cloaking electrically large objects. Indeed the harmonic orders n present in the scattered field increases with the object electrical dimension, such that $n \sim ka$ (where a is the object dimension and k the background medium wavenumber).

Mantle cloaking was proposed in [43] where the analysis of the cloaking of dielectric and conductive spheres by using a thin metasurface layer was carried out, presenting the computation of the required cloaking surface impedance.

After this analytical study, in later years, numerous papers were presented, which further investigated the mantle cloaking method, proposing different solutions and implementations, studying the cloaking design for spherical and cylindrical shapes of the scattered object [44] and different metasurface design [45], validating and measuring the efficiency of the proposed cloaking devices [46], [47] and proposing bilayer cloaking coats to enlarge cloaking bandwidth [48].

Cloaking has found applications in the coating of antennas in order to reduce

the mutual coupling between nearby antenna [49]–[52], or in the reduction of disturbance and interference due to the presences of obstacles in antenna proximity, which can be useful for example in implantable [53], or satellite applications [54] and more recently also to the development of intelligent antennas [55].

Mantle cloaking realization has been studied not only at microwave frequencies but also in the terahertz range where the use of graphene is largely employed [56]–[61].

Moreover, cloaking has found applications also beyond electromagnetics, extending and adapting the methods and analysis in other fields of study, such for example acoustic [62]–[64], or thermal [65]–[68] cloaking.

The two main difficulties of mantle cloaking are the increasing of the cloaking bandwidth, which due to the resonance nature of the cloaking is usually small, and the cloaking of electrically large structure.

To overcome this limitations different studied were proposed, to enlarge the cloaking bandwidth. For example in [69] the authors proposed to increase the cloaking bandwidth by tilting the object with respect to the incident field direction, and in [70] an elliptical metasurface was proposed to obtain a wideband antenna cloaking such to reduce the mutual coupling between nearby antennas. While in the terahertz range the use of an inhomogeneous graphene metasurface is vastly employed due to its tunability properties [71]–[73].

Also tunable and wideband cloaking were proposed which exploits metasurfaces with the presence of active elements [74]–[77].

Possible solutions to overcome the problem of cloaking electrically large structures were also proposed. An idea can be the use of a multilayer cloak [78]–[80]. Indeed, the use of a second cloaking layer allows to annul two harmonic of the scattered field at the same time, and therefore it is useful to further reduce the scattering by electrically large objects for which multiple harmonics are present in the scattering. Another idea is to use anisotropic metasurfaces [81], [82].

Nonetheless, the cloaking of objects beyond the low frequency region by employing a single layer passive metasurface, remains challenging. With this in mind, this thesis aims to study and investigate this problem, and to propose possible solutions to overcome it.

2.6 Cloaking and Anapole modes

An interesting development of the cloaking concept is the connection between the cloaking effect and a non-radiating source distributions, such for example

anapole modes. The concept of anapole modes can be explained by examining the scattering of a resonant particle in terms of multipoles decomposition. Indeed, the method of multiple decomposition theory allows to describe the scattering cross-section of a particle as a sum of electric and magnetic multipoles.

An arbitrary source distribution can be hence described as a sum of standard multipoles. Each multipole is connected with a specific charge-current distribution. The first two multipole families are the electric and magnetic dipole [83]. The electric dipole ($\boldsymbol{P}$) is associated with the radiation configuration of two opposite charges. The second multipole, the magnetic dipole ($\boldsymbol{M}$), is associated with a circular current. Finally, a third family of multipoles is the toroidal dipole ($\boldsymbol{T}$) which is produced by a poloidal current flowing around a torus meridian. In this way, a toroidal dipole moment manifests along the torus axis [84].

Following the multipoles decomposition, the scattering efficiency Q_{sca} of a particle is described as the combination of electric (a_E) and magnetic (a_M) scattering coefficients such that:

$$Q_{sca} = \frac{\pi}{k^2} \sum_{l=1}^{\infty} \sum_{m=-l}^{l} (2l+1)(|a_E(l,m)|^2 + |a_M(l,m)|^2) \tag{2.5}$$

A crucial point is that the electric and the toroidal dipole moment manifest similar radiation patterns, and under the condition $\boldsymbol{P} = -jk\boldsymbol{T}$, (where j is the imaginary unit and k is the background medium wavenumber) [85] they produce a destructive interference, and they mutually cancel each other, resulting into a non-radiating condition.

Therefore, the scattering induced by the toroidal dipole moment compensates the one related to the electric dipole moment, leading to the generation of a particular phenomenon, namely the anapole mode [85]. This consists into the destructive interference of the electric dipole moment by the toroidal one.

Moreover, the simultaneously presence of a magnetic dipole moment and anapole mode results into the annulment of the electric type radiation and consequently to the presence of an ideal magnetic dipole.

In [86] a cloaked structure based on a sinusoidally modulated metasurface is investigated for establishing a connection between the cloaking effect and the fulfilment of the anapole mode conditions. It is proven that at the cloaking frequency (i.e. the frequency at which the scattering is minimum), the condition $\boldsymbol{P} = -jk\boldsymbol{T}$ is fulfilled and therefore that the electric and toroidal dipoles compensate each other leading to the realisation of the anapole mode condition.

Moreover, near the cloaking frequency the magnetic dipole is the dominant one. Indeed, the normalised amplitude of the magnetic dipole $\boldsymbol{M}$ is two times higher

than the remaining electric and torodial dipoles and quadrupoles.

Consequently, the cloaking effect can be connected with the establishment of the anapole mode and the destructive interference between electric and toroidal dipole, which leads to the predominant presence of the magnetic dipole moment in the scattering response.

Chapter 3

Scattering by Cloaked Metallic Cylinders also Beyond the Quasi-static Limit

Part of the work described in this Chapter was also previously published in [87]–[89].

Starting from this Chapter, the reasoning and the main results achieved during the PhD years are illustrated, and in particular, this Chapter focuses on a deep analytical investigation of the cloaking mechanism and on the analysis of the field scattered by a cloaked metallic cylinder also beyond the quasi-static limit condition.

3.1 Introduction

As previously introduced, mantle cloaking consists into the reduction of the field scattered by an object illuminated by an electromagnetic wave. Therefore, the main purpose of mantle cloaking, and consequently of this dissertation, is first of all the study and analysis of the scattered field.

Hence, before addressing the problem of the design of a mantle cloaking layer, it is first necessary to understand the cloaking mechanism and to perform an analysis of the scattered field in terms of harmonic composition, and in particular, to examine how the presence of a coating layer can modify the scattering profile. For this reason, in this chapter, first, the scattered field of both dielectric and metasurface coated metallic cylinders is studied and secondly the design of a proper metasurface able to minimize the scattering is proposed.

3.2 Bare metallic cylinders

As a starting point, the harmonic analysis of the field scattered by a bare Perfect Electric Conductor (PEC) cylinder is considered, since it is the basis and the reference for the successive analysis of cloaked structures. The cylinder is assumed to be infinitely long and to be illuminated by a TM polarised plane wave, i.e., with the electric field vector parallel to the cylinder axis. However, the following considerations can be similarly adjusted for a Transverse Electric (TE) polarization.

Hence, the proposed set up is represented in Fig. 3.1.

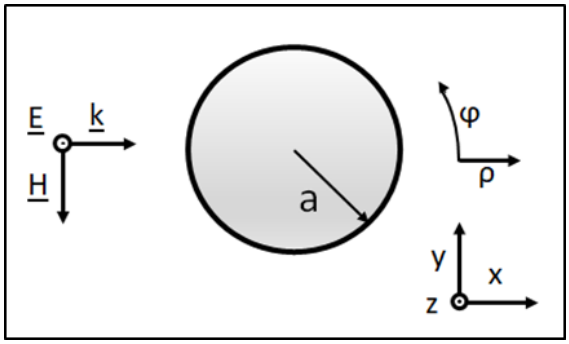

Figure 3.1: Transverse section of the considered problem. A bare conductive cylinder is illuminated by a TM polarised planewave.

Considering the geometry of the problem, it is convenient to express the total electric field in the background medium $\boldsymbol{E}_{tot}$ in cylindrical coordinate system as a sum of harmonics [90]:

$$\boldsymbol{E}_{tot}(\rho,\varphi) = \hat{\boldsymbol{z}} E_0 \sum_{n=-\infty}^{\infty} j^{-n}[J_n(k_0\rho) + c_n H_n^{(2)}(k_0\rho)]e^{jn\varphi} \tag{3.1}$$

where n is the harmonic order, c_n represents the scattering coefficients (of order n), J_n and $H_n^{(2)}$ are the Bessel and Hankel functions of second order, k_0 is the wavenumber in the background medium (here free space), ρ and φ are the radial and azimuthal cylindrical coordinates, respectively.

The total field is therefore equal to a first contribution related to the incident field, represented by the Bessel functions J_n, and a second part correspondent to the scattered field, represented by the Hankel functions of second order $H_n^{(2)}$ and the scattering coefficients c_n.

In particular, the scattering coefficients c_n are of fundamental importance because they denote the weight of the associated harmonic in the scattering composition, and therefore they are a measure of the contribute of the harmonic to the total scattering.

Accordingly, the scattered field $\boldsymbol{E}_s(\rho, \varphi)$ is expressed as:

$$\boldsymbol{E}_s(\rho, \varphi) = \hat{\boldsymbol{z}} E_0 \sum_{n=-\infty}^{\infty} j^{-n} c_n H_n^{(2)}(k_0 \rho) e^{jn\varphi} \tag{3.2}$$

The unknown scattering coefficients c_n can be computed considering the boundary condition of the system, i.e. the annulment of the total tangential electric field on the cylinder surface $\boldsymbol{E}_{tot}(a, \varphi) = 0$, such that:

$$\hat{\boldsymbol{z}} E_0 \sum_{n=-\infty}^{\infty} j^{-n} [J_n(k_0 a) + c_n H_n^{(2)}(k_0 a)] e^{jn\varphi} = 0 \tag{3.3}$$

where a is the cylinder radius.

Imposing the boundary condition, it is found that, in the considered case of a bare metallic cylinder, the scattering coefficient associated with the n^{th} harmonic is equal to [90]:

$$c_n = -\frac{J_n(k_0 a)}{H_n^{(2)}(k_0 a)} \tag{3.4}$$

and recalling that the Hankel functions of second order are a combination of the Bessel and Neumann functions (Y_n) such that [91]:

$$H_n^{(2)}(x) = J_n(x) - jY_n(x) \tag{3.5}$$

the coefficients can be equivalently expressed as:

$$c_n = -\frac{J_n(k_0 a)}{J_n(k_0 a) - jY_n(k_0 a)} \tag{3.6}$$

From Eq. 3.6 it can be noticed that, the modulus of the scattering coefficients annuls in correspondence of the zeros of the Bessel functions of first kind $J_n(k_0 a)$, while it reaches its maximimum value, i.e. $|c_n| = 1$, when the Neumann functions $Y_n(k_0 a)$ go to zero.

In Fig. 3.2 the modulus of the scattering coefficients associated to the harmonics with modal index $n = 0{:}10$ are represented for different radii of the cylinder.

As expected, when the cylinder electrical dimension increases, a higher number of harmonics is presents in the scattered field, while when the radius is much smaller than the wavelength of the incident field, i.e. in a low frequency regime condition, the number of harmonics which contributes to the scattering is limited, and the scattering is primarily dominated by the first harmonic with modal index $n = 0$.

Indeed, as outlined in Fig. 3.2, for a normalized cylinder radius $a/\lambda = 0.1$, where λ is the wavelength of the incident field, only the coefficients c_0 and c_1 are

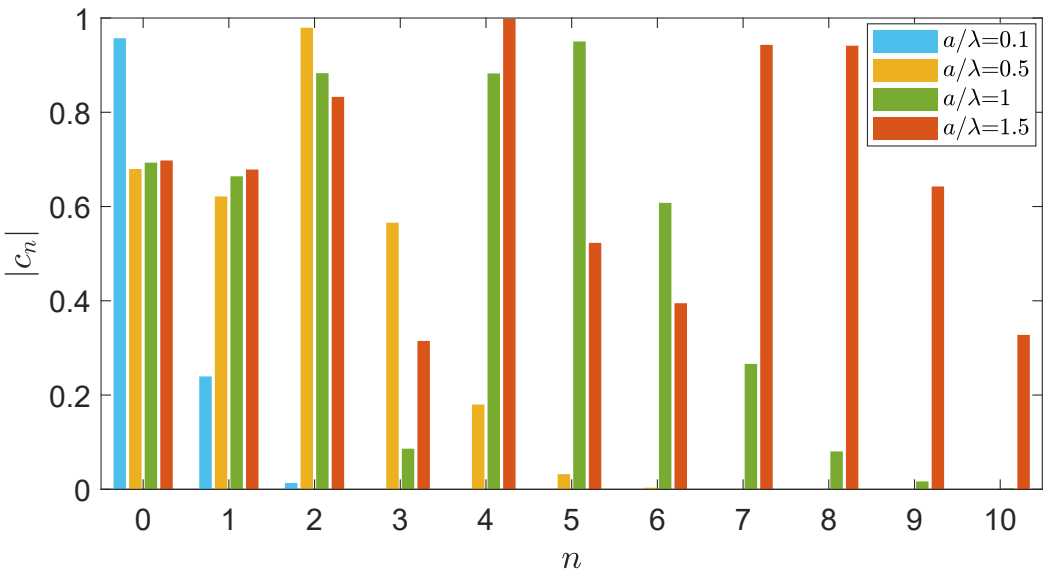

Figure 3.2: Modulus of the scattering coefficients considering a bare conductive cylinder for different values of the cylinder radius with respect to the wavelength of the incident field [87] ©2020 Optical Society of America.

non-null, while for $a/\lambda = 1$ the harmonics with modal order from $n = 0$ to $n = 9$ are present.

It is also important to underline that in Fig. 3.2 only the non negative harmonic indexes are represented. This is due to the parity relation of the Bessel functions [91]:

$$J_{-n}(x) = (-1)^n J_n(x) \tag{3.7}$$
$$Y_{-n}(x) = (-1)^n Y_n(x) \tag{3.8}$$

so that the value of the scattering coefficients c_{-n} is equal to c_n as can be evinced from Eq. 3.6. However, in the scattered field, the harmonics with both positive and negative modal index are present, as expressed by Eq. 3.2.

The increasing number of harmonics represents the main obstacle for achieving the cloaking of non-electrically small cylinders. In fact, as it will be detailed in the following, considering a mantle cloaking problem, each harmonic requires a specific value of surface impedance (and therefore of metasurface geometry) to be annulled. Hence, for electrically small cylinders, in order to reduce the scattered field, a possible strategy is to cancel the first dominant harmonic. However, when the

normalised cylinder radius (with respect to the background wavelength) increases, also the number of harmonics that contributes to the scattering increases, and moreover, it is not possible to identify a dominant component. For this reason, achieving an important scattering reduction with a homogeneous metasurface is challenging for non-electrical small structures.

In Fig. 3.3 the field profile (absolute value, real and imaginary part) of the scattered field $\boldsymbol{E}_s(\rho, \varphi)$ and of the different harmonics which compose the total scattering is shown, for $a/\lambda = 0.1$. Therefore the quantity $E_n = j^{-n} c_n H_n^{(2)}(k_0\rho) e^{jn\varphi}$ is represented. Only the indexes n = -1, 0, 1 are considered because they correspond to the only non-null coefficients. Indeed, since the coefficients c_1 and c_{-1} are significantly lower than c_0, the scale in the n = 1, -1 plots is reduced such to appreciate the correspondent fields.

3.3 Dielectric coated metallic cylinders

Mantle cloaking exploits the use of a thin metasurface layer as a cloaking coat. This is usually composed of a specific periodic metallic pattern, and, if the object to be cloaked is made of conductive material, the metallic pattern is printed on a spacer dielectric layer which is in turn bend on the object external surface. The presence of the dielectric layer is necessary such to avoid short circuits between the metallic metasurface pattern and the object itself. In case the object is not conductive, the dielectric layer can be avoided such to reduce the coat thickness to (almost) zero.

Since here the cloaking of conductive cylinders is considered, before studying a cloaked structure and the effect of a metasurface coating on the scattering, it is interesting to analyse the field scattered by a conductive cylinder coated by a dielectric layer, as illustrated in Fig. 3.4.

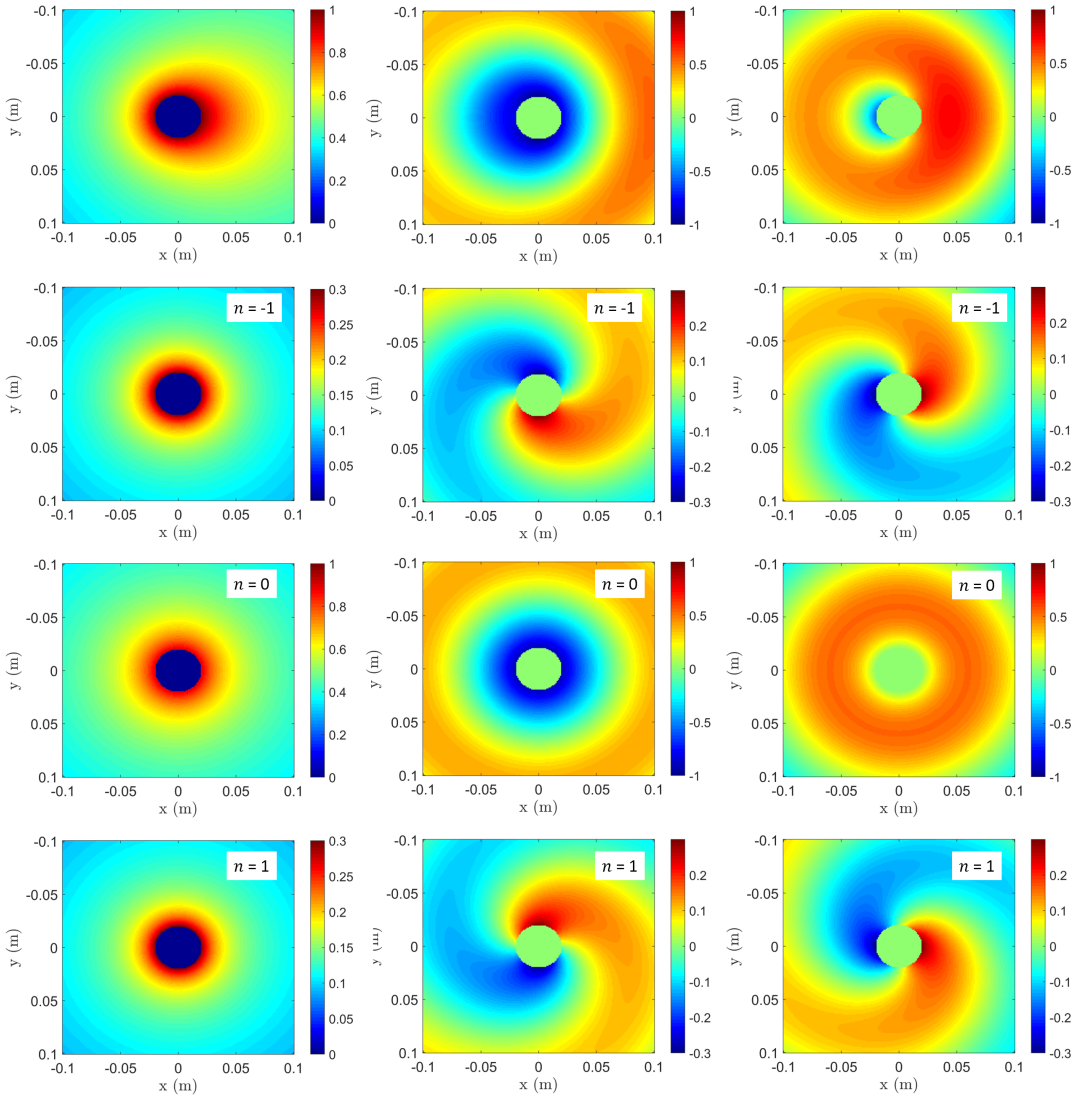

Figure 3.3: Field profile of the different harmonics (total scattered field first row, n = -1 second row, $n = 0$ third row, $n = 1$ last row) present in the field scattered by a metallic cylinder with normalised radius $a/\lambda = 0.1$, illumined by a TM polarised planewave. Absolute value (left column), real (center) and imaginary (rigth) part.

Thus, considering a metallic cylinder with radius a, and a dielectric coating layer with relative permittivity ε_r and thickness $t = b - a$, illuminated by a TM planewave, it is possible to write the electric and magnetic fields in the different media (PEC cylinder $\boldsymbol{E}_{PEC}$, dielectric $\boldsymbol{E}_{diel}$, $\boldsymbol{H}_{diel}$ and surrounding background $\boldsymbol{E}_{back}$, $\boldsymbol{H}_{back}$) as:

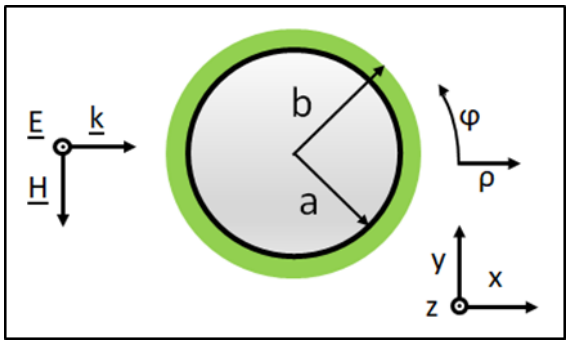

Figure 3.4: Transverse section of the considered problem. A bare conductive cylinder coated by a dielectric layer is illuminated by a TM polarised planewave.

$$\boldsymbol{E}_{PEC} = 0 \tag{3.9}$$

$$\boldsymbol{E}_{diel}(\rho,\varphi) = \hat{\boldsymbol{z}} E_0 \sum_{n=-\infty}^{\infty} j^{-n}\Big[a_n J_n(k_d\rho) + b_n Y_n(k_d\rho)\Big] e^{jn\varphi} \tag{3.10}$$

$$\boldsymbol{E}_{back}(\rho,\varphi) = \hat{\boldsymbol{z}} E_0 \sum_{n=-\infty}^{\infty} j^{-n}\Big[J_n(k_0\rho) + c_n H_n^{(2)}(k_0\rho)\Big] e^{jn\varphi} \tag{3.11}$$

$$\boldsymbol{H}_{diel}(\rho,\varphi) = \hat{\boldsymbol{\varphi}} E_0 \frac{k_d}{j\omega\mu_d} \sum_{n=-\infty}^{\infty} j^{-n}\Big[a_n J_n'(k_d\rho) + b_n Y_n'(k_d\rho)\Big] e^{jn\varphi} \tag{3.12}$$

$$\boldsymbol{H}_{back}(\rho,\varphi) = \hat{\boldsymbol{\varphi}} E_0 \frac{k_0}{j\omega\mu_0} \sum_{n=-\infty}^{\infty} j^{-n}\Big[J_n'(k_0\rho) + c_n H_n'^{(2)}(k_0\rho)\Big] e^{jn\varphi} \tag{3.13}$$

where k_d is the wavenumber in the dielectric, μ_d and μ_0 are the dielectric and background permeability, and the symbol $(')$ denote the derivative of the function with respect to the whole argument $(k\rho)$.

With respect to previous case, here it is necessary to take into account the fields in the dielectric coat (expanded in a sum of harmonics as well as the external field), which are denoted by the functions J_n and Y_n weighted by the coefficients a_n and b_n (not to be confused with the cylinder radius a and the cylinder plus dielectric radius b).

Hence, to find a solution for the fields, it is necessary to compute the three unknown coefficients sets: a_n, b_n and c_n. To do so, the boundary conditions of the system need to be evaluated which consist in the continuity of the tangential fields, both at the metal-dielectric interface $(\rho = a)$ and at the dielectric-background interface $(\rho = b)$, such that:

$$\begin{cases} \boldsymbol{E}_{PEC}(a,\varphi) = \boldsymbol{E}_{diel}(a,\varphi) \\ \boldsymbol{E}_{diel}(b,\varphi) = \boldsymbol{E}_{back}(b,\varphi) \\ \boldsymbol{H}_{diel}(b,\varphi) = \boldsymbol{H}_{back}(b,\varphi) \end{cases} \tag{3.14}$$

Therefore, the following system of equations is obtained.

$$\begin{cases} \sum\limits_{n=-\infty}^{\infty} j^{-n}\Big[a_n J_n(k_d a) + b_n Y_n(k_d a)\Big]e^{jn\varphi} = 0 \\ \sum\limits_{n=-\infty}^{\infty} j^{-n}\Big[a_n J_n(k_d b) + b_n Y_n(k_d b)\Big]e^{jn\varphi} = \sum\limits_{n=-\infty}^{\infty} j^{-n}\Big[J_n(k_0 b) + c_n H_n^{(2)}(k_0 b)\Big]e^{jn\varphi} \\ \frac{k_d}{j\omega\mu_d}\sum\limits_{n=-\infty}^{\infty} j^{-n}\Big[a_n J_n'(k_d b) + b_n Y_n'(k_d b)\Big]e^{jn\varphi} = \\ \qquad\qquad \frac{k_0}{j\omega\mu_0}\sum\limits_{n=-\infty}^{\infty} j^{-n}\Big[J_n'(k_0 b) + c_n H_n'^{(2)}(k_0 b)\Big]e^{jn\varphi} \end{cases} \tag{3.15}$$

Projecting all the equations on exponential functions $\exp(jn\varphi)$, and exploiting the orthogonality of the exponential functions, a system of three equations valid for each harmonic is derived:

$$\begin{cases} a_n J_n(k_d a) + b_n Y_n(k_d a) = 0 \\ a_n J_n(k_d b) + b_n Y_n(k_d b) = J_n(k_0 b) + c_n H_n^{(2)}(k_0 b) \\ \frac{k_d}{j\omega\mu_d}\Big[a_n J_n'(k_d b) + b_n Y_n'(k_d b)\Big] = \frac{k_0}{j\omega\mu_0}\Big[J_n'(k_0 b) + c_n H_n'^{(2)}(k_0 b)\Big] \end{cases} \tag{3.16}$$

Considering the boundary equations system in matrix form, an expression of the scattering coefficients c_n can be found as the ratio of two matrix determinants, such that:

$$c_n = \frac{\det C}{\det A} \tag{3.17}$$

where

$$C = \begin{pmatrix} J_n(k_d a) & Y_n(k_d a) & 0 \\ J_n(k_d b) & Y_n(k_d b) & J_n(k_0 b) \\ \frac{k_d}{j\omega\mu_d} J_n'(k_d b) & \frac{k_d}{j\omega\mu_d} Y_n'(k_d b) & \frac{k_0}{j\omega\mu_0} J_n'(k_0 b) \end{pmatrix} \tag{3.18}$$

and

$$A = \begin{pmatrix} J_n(k_d a) & Y_n(k_d a) & 0 \\ J_n(k_d b) & Y_n(k_d b) & -H_n^{(2)}(k_0 b) \\ \frac{k_d}{j\omega\mu_d} J_n^{'}(k_d b) & \frac{k_d}{j\omega\mu_d} Y_n^{'}(k_d b) & -\frac{k_0}{j\omega\mu_0} H_n^{'(2)}(k_0 b) \end{pmatrix} \tag{3.19}$$

For simplicity, the permeability of the dielectric is considered equal to the background one such that $\mu_d = \mu_0 = \mu$, since materials without a megnetic response are considered.

Solving the determinant of the matrix C it is obtained:

$$\begin{aligned} \det(C) = J_n(k_d a)\left(\frac{k_0}{j\omega\mu} J_n^{'}(k_0 b) Y_n(k_d b) - \frac{k_d}{j\omega\mu} Y_n^{'}(k_d b) J_n(k_0 b)\right) \\ - Y_n(k_d a)\left(\frac{k_0}{j\omega\mu} J_n^{'}(k_0 b) J_n(k_d b) - \frac{k_d}{j\omega\mu_d} J_n^{'}(k_d b) J_n(k_0 b)\right) \end{aligned} \tag{3.20}$$

For brevity, the following definitions are introduced:

$$\frac{k_0}{j\omega\mu} = k \tag{3.21}$$

$$\frac{k_d}{j\omega\mu} = k\sqrt{\varepsilon_r} \tag{3.22}$$

such that the determinant of C can be written as:

$$\begin{aligned} \det(C) = kJ_n(k_d a) J_n^{'}(k_0 b) Y_n(k_d b) - k\sqrt{\varepsilon_r} J_n(k_d a) Y_n^{'}(k_d b) J_n(k_0 b) \\ - kY_n(k_d a) J_n^{'}(k_0 b) J_n(k_d b) + k\sqrt{\varepsilon_r} Y_n(k_d a) J_n^{'}(k_d b) J_n(k_0 b) \end{aligned} \tag{3.23}$$

which is in turn equal to:

$$\begin{aligned} \det(C) = kJ_n^{'}(k_0 b)\Big(J_n(k_d a) Y_n(k_d b) - Y_n(k_d a) J_n(k_d b)\Big) \\ + kJ_n(k_0 b)\sqrt{\varepsilon_r}\Big(-J_n(k_d a) Y_n^{'}(k_d b) + Y_n(k_d a) J_n^{'}(k_d b)\Big) \end{aligned} \tag{3.24}$$

Finally it is obtained,

$$\det C = kJ_n^{'}(k_0 b) p_n - k\sqrt{\varepsilon_r} J_n(k_0 b) q_n \tag{3.25}$$

where:

$$p_n = J_n(k_d a)Y_n(k_d b) - Y_n(k_d a)J_n(k_d b) \tag{3.26}$$

and

$$q_n = J_n(k_d a)Y_n^{'}(k_d b) - Y_n(k_d a)J_n^{'}(k_d b) \tag{3.27}$$

are the Bessel functions products as defined by [91].

The determinant of A can be derived from $\det C$ substituting the term $J_n(k_0 b)$ by $-H_n^{(2)}(k_0 b)$ such that:

$$\det A = -kH_n^{'(2)}(k_0 b)p_n + k\sqrt{\varepsilon_r}H_n^{(2)}(k_0 b)q_n \tag{3.28}$$

Therefore, substituting Eq. 3.25 and Eq. 3.28 in Eq. 3.17, the scattering coefficients c_n will be equal to:

$$c_n = \frac{kJ_n^{'}(k_0 b)p_n - k\sqrt{\varepsilon_r}J_n(k_0 b)q_n}{-kH_n^{'(2)}(k_0 b)p_n + k\sqrt{\varepsilon_r}H_n^{(2)}(k_0 b)q_n} \tag{3.29}$$

Finally, the scattering coefficients related to a dielectric coated metallic cylinder can be computed as:

$$c_n = -\frac{J_n^{'}(k_0 b)p_n - \sqrt{\varepsilon_r}J_n(k_0 b)q_n}{H_n^{'(2)}(k_0 b)p_n - \sqrt{\varepsilon_r}H_n^{(2)}(k_0 b)q_n} \tag{3.30}$$

In order to understand how the dielectric coating modifies the scattering coefficients with respect to the bare cylinder case, in Fig. 3.5 the modulus of the scattering coefficients $c_{0,1,2}$ is represented for different dielectric permittivity i.e. ε_r = 2, 5, 10 (a, b, c) and the metallic cylinder radius with respect to the incident field wavelength and compared with the coefficients associated to the bare cylinder. It is apparent that with respect to the bare cylinder, the trend of the scattering coefficients is significantly modified as the dielectric constant of the coat increases.

Moreover, since three coefficients are not sufficient for describe the scattered field for higher cylinder radius, Fig. 3.6 shows the modulus of the complete set of non-null scattering coefficients c_{0-15} for different ε_r and dielectric thickness and for a normalised cylinder radius from $a/\lambda = 0.1$ to $a/\lambda = 1.5$.

3.4 Cloaked cylinder

After the studying of the filed scattered by a dielectric coated metallic cylinder, in this section a cloaked cylinder is considered, investigating how the cloaking coat can modify and reduce the scattering of the structure.

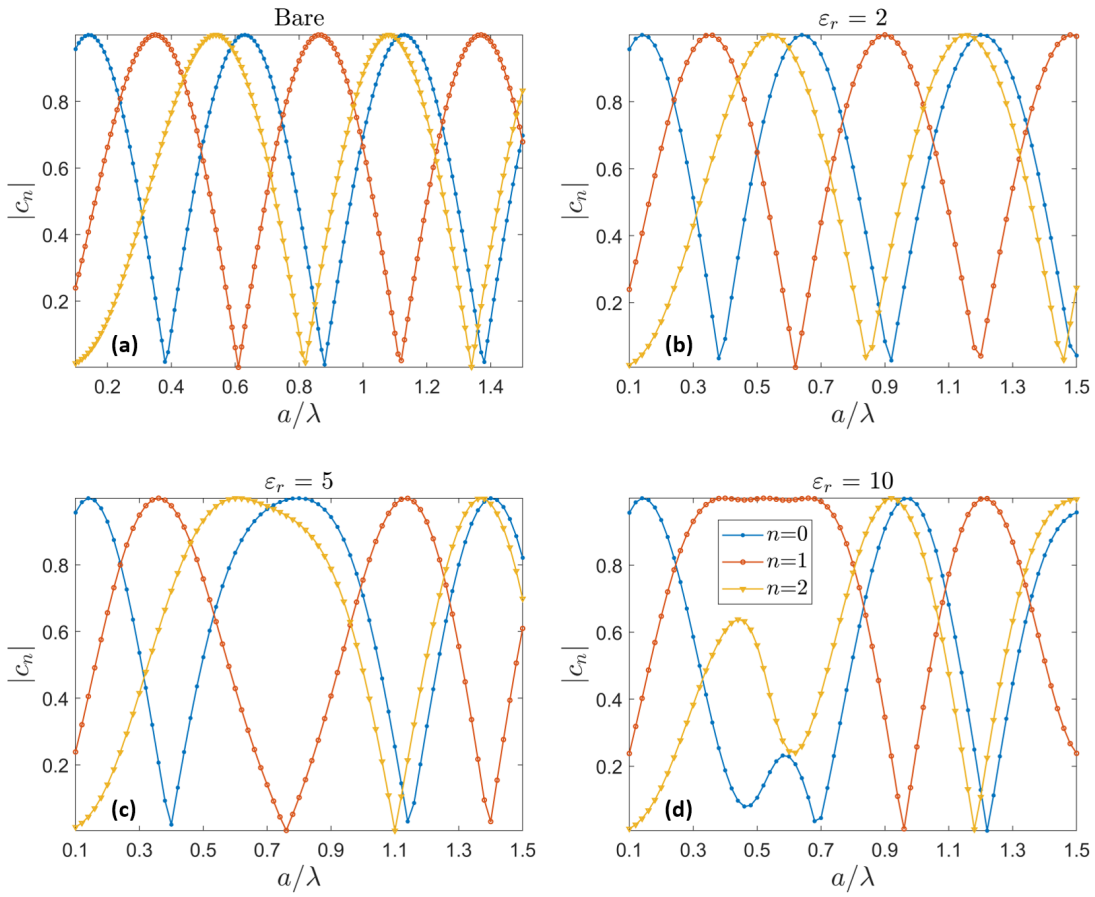

Figure 3.5: Modulus of the scattering coefficients c_0, c_1 and c_2 with respect to the cylinder normalised radius a/λ, for $a = 2$ cm, $b = 1.15a$ and $\varepsilon_r = 10$, and comparison with the coefficients associated to the bare cylinder [87] ©2020 Optical Society of America.

As seen before, in the mantle cloaking technique, the object to be concealed (in this case a metallic cylinder) is covered with an opportune metasurface in order to reduce its scattering. In literature, different unit cells shapes and designs are considered, such for example metallic patches, strips or crosses [44]–[46], [70], [92]. However, before discussing the design of a practical metasurface layer, it is necessary to analytically study the field scattered by a mantle cloaked cylinder. Thus, for this purpose, the metasurface is modeled as a surface impedance boundary condition at the interface between the dielectric layer and the background medium.

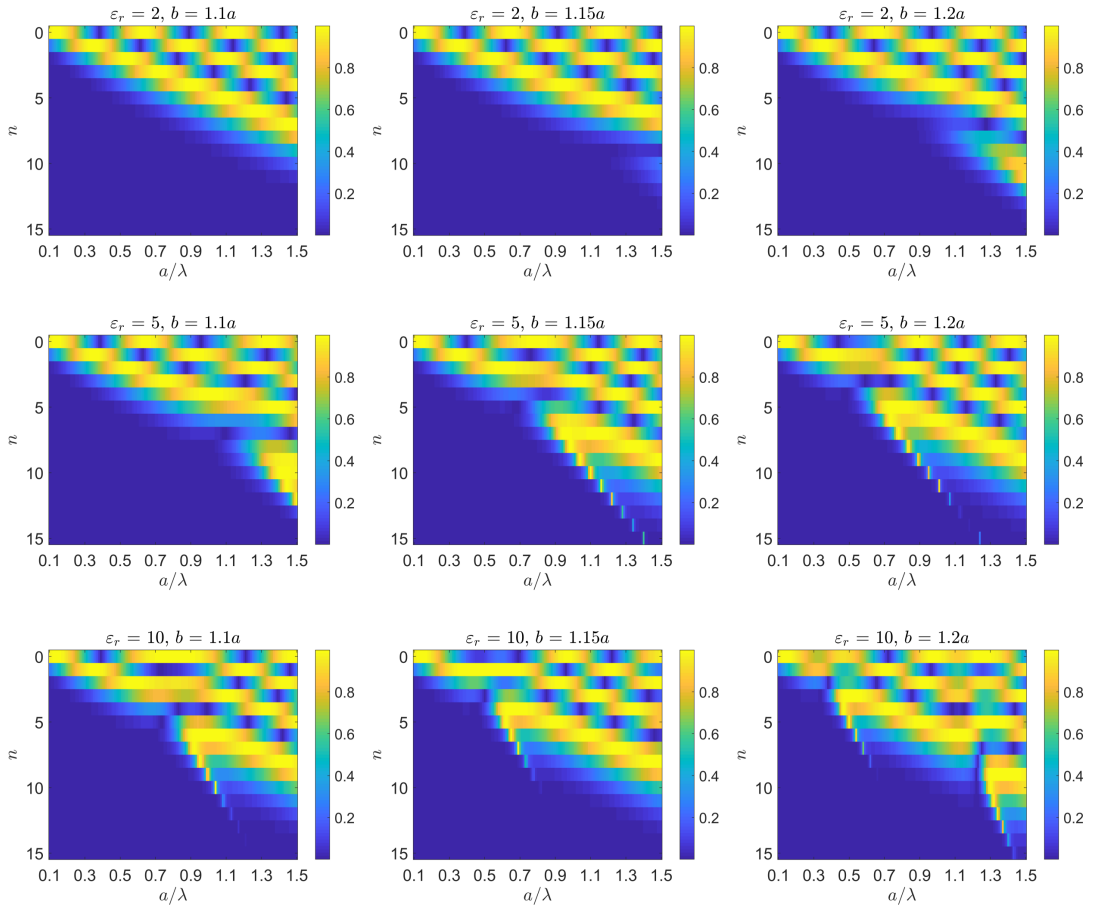

Figure 3.6: Modulus of the scattering coefficients c_{0-15} with respect the cylinder radius for different values of dielectric permittivity and thickness [87] ©2020 Optical Society of America.

3.4.1 Scattering coefficients computation

Similarly to previous cases, to understand how the surface impedance influences the field scattered by the cylinder it is possible to analyse the field in the dielectric layer and in the background medium. Also in this case it is possible to write the expression of the electric and magnetic fields inside the dielectric and in the background, and by applying the continuity and the surface impedance boundary condition a closed form solution for the scattering coefficients can be obtained.

Therefore, the fields are described by Eq. 3.13 presented previously. Then, the continuity boundary conditions at the media interface should be considered, and in particular, the surface impedance condition should be imposed between the

dielectric layer and the background medium.

The surface impedance is a parameter which relates the average tangential electric field on the object surface boundary with the surface current density induced on the considerate surface. The latest, in turn, is equal to the jump of the average magnetic field on the two sides of the surface. Here, a homogeneous and passive metasurface is considered such that its characteristic surface impedance can be expressed as a single surface impedance value:

$$Z_s(\varphi) = Z_s = jX_s \tag{3.31}$$

With respect to previous case, the boundary condition at the interface between the dielectric layer and the background medium is now modified in order to take into account the surface impedance boundary condition and the last equation of the system Eq. 3.14 is accordingly substituted by:

$$\boldsymbol{E}(b,\varphi) = Z_s \times \hat{\boldsymbol{\rho}} \times (\boldsymbol{H}_{back}(b,\varphi) - \boldsymbol{H}_{diel}(b,\varphi)) \tag{3.32}$$

Such that the following system is obtained:

$$\begin{cases} a_n J_n(k_d a) + b_n Y_n(k_d a) = 0 \\ a_n J_n(k_d b) + b_n Y_n(k_d b) = J_n(k_0 b) + c_n H_n^{(2)}(k_0 b) \\ a_n J_n(k_d b) + b_n Y_n(k_d b) = Z_s \frac{k_0}{j\omega\mu_0}\left[J_n'(k_0 b) + c_n H_n'^{(2)}(k_0 b)\right] \\ \qquad\qquad\qquad\qquad -Z_s \frac{k_d}{j\omega\mu_d}\left[a_n J_n'(k_d b) + b_n Y_n'(k_d b)\right] \end{cases} \tag{3.33}$$

Similarly to dielectric coating, writing the boundary conditions system in matrix form, it is possible to obtain an expression of the scattering coefficients as a ratio of two matrix determinants. By solving the determinants, a closed form to express the scattering coefficients is then computed, which, in this case, depends also on the considered surface impedance. From this formulation is therefore possible to write the surface impedance (or admittance, as it will be considered in the following) that causes the total annulment of one scattering harmonic.

Therefore, following the same procedure introduced previously, from the boundary conditions system it is obtained:

$$c_n = \frac{\det F}{\det D} \tag{3.34}$$

where:

$$F = \begin{pmatrix} J_n(k_d a) & Y_n(k_d a) & 0 \\ J_n(k_d b) & Y_n(k_d b) & J_n(k_0 b) \\ J_n(k_d b) + \frac{k_d}{j\omega\mu_d} J_n^{'}(k_d b) Z_s & Y_n(k_d b) + \frac{k_d}{j\omega\mu_d} Y_n^{'}(k_d b) Z_s & \frac{k_0}{j\omega\mu_d} J_n^{'}(k_0 b) Z_s \end{pmatrix} \tag{3.35}$$

and

$$D = \begin{pmatrix} J_n(k_d a) & Y_n(k_d a) & 0 \\ J_n(k_d b) & Y_n(k_d b) & -H_n^{(2)}(k_0 b) \\ J_n(k_d b) + \frac{k_d}{j\omega\mu_d} J_n^{'}(k_d b) Z_s & Y_n(k_d b) + \frac{k_d}{j\omega\mu_d} Y_n^{'}(k_d b) Z_s & -\frac{k_0}{j\omega\mu_d} H_n^{'(2)}(k_0 b) Z_s \end{pmatrix} \tag{3.36}$$

So that the determinant of F matrix is computed as:

$$\begin{aligned} &\det(F) = \\ &J_n(k_d a)\left(\frac{k_0}{j\omega\mu} J_n^{'}(k_0 b) Y_n(k_d b) Z_s - J_n(k_0 b) Y_n(k_d b) - \frac{k_d}{j\omega\mu} Y_n^{'}(k_d b) J_n(k_0 b) Z_s\right) \\ &- Y_n(k_d a)\left(\frac{k_0}{j\omega\mu} J_n^{'}(k_0 b) J_n(k_d b) Z_s - J_n(k_0 b) J_n(k_d b) - \frac{k_d}{j\omega\mu_d} J_n^{'}(k_d b) J_n(k_0 b) Z_s\right) \end{aligned} \tag{3.37}$$

As before, $k = \frac{k_0}{j\omega\mu}$ is introduced for brevity, and therefore:

$$\begin{aligned} \det(F) = {} & k J_n(k_d a) J_n^{'}(k_0 b) Y_n(k_d b) Z_s - J_n(k_d a) J_n(k_0 b) Y_n(k_d b) \\ & - k\sqrt{\varepsilon_r} J_n(k_d a) Y_n^{'}(k_d b) J_n(k_0 b) Z_s - k Y_n(k_d a) J_n^{'}(k_0 b) J_n(k_d b) Z_s \\ & + Y_n(k_d a) J_n(k_0 b) J_n(k_d b) + k\sqrt{\varepsilon_r} Y_n(k_d a) J_n^{'}(k_d b) J_n(k_0 b) Z_s \end{aligned} \tag{3.38}$$

Dividing both terms by $Z_s = 1/Y_s$:

$$\begin{aligned} \frac{\det(F)}{Z_s} = {} & k J_n(k_d a) J_n^{'}(k_0 b) Y_n(k_d b) - J_n(k_d a) J_n(k_0 b) Y_n(k_d b) Y_s \\ & - k\sqrt{\varepsilon_r} J_n(k_d a) Y_n^{'}(k_d b) J_n(k_0 b) - k Y_n(k_d a) J_n^{'}(k_0 b) J_n(k_d b) \\ & + Y_n(k_d a) J_n(k_0 b) J_n(k_d b) Y_s + k\sqrt{\varepsilon_r} Y_n(k_d a) J_n^{'}(k_d b) J_n(k_0 b) \end{aligned} \tag{3.39}$$

$$\begin{aligned}\frac{\det(F)}{Z_s} =& -Y_s J_n(k_0 b)\Big(J_n(k_d a)Y_n(k_d b) - Y_n(k_d a)J_n(k_d b)\Big) \\ &+ kJ_n^{'}(k_0 b)\Big(J_n(k_d a)Y_n(k_d b) - Y_n(k_d a)J_n(k_d b)\Big) \\ &- k\sqrt{\varepsilon_r}J_n^{'}(k_0 b)\Big(J_n(k_d a)Y_n^{'}(k_d b) - Y_n(k_d a)J_n^{'}(k_d b)\Big)\end{aligned} \tag{3.40}$$

Then, considering the Bessel functions products p_n, q_n it is obtained:

$$\frac{\det(F)}{Z_s} = -Y_s J_n(k_0 b)p_n + kJ_n^{'}(k_0 b)p_n - k\sqrt{\varepsilon_r}J_n(k_0 b)q_n \tag{3.41}$$

The determinant of D is derived from $\det(F)$ substituting $J_n(k_0 b)$ by $-H_n^{(2)}(k_0 b)$.

Therefore:

$$\frac{\det(D)}{Z_s} = Y_s H_n^{(2)}(k_0 b)p_n - kH_n^{'(2)}(k_0 b)p_n + k\sqrt{\varepsilon_r}H_n^{(2)}(k_0 b)q_n \tag{3.42}$$

Finally, substituting Eq. 3.41 and 3.42 into Eq. 3.34, a closed form solution to express the scattering coefficients is obtained:

$$c_n = \frac{-Y_s J_n(k_0 b)p_n + kJ_n^{'}(k_0 b)p_n - k\sqrt{\varepsilon_r}J_n(k_0 b)q_n}{Y_s H_n^{(2)}(k_0 b)p_n - kH_n^{'(2)}(k_0 b)p_n + k\sqrt{\varepsilon_r}H_n^{(2)}(k_0 b)q_n} \tag{3.43}$$

which is equal to:

$$c_n = \frac{p_n k J_n(k_0 b)\left(-\frac{Y_s}{k} + \frac{J_n^{'}(k_0 b)}{J_n(k_0 b)} - \frac{\sqrt{\varepsilon_r}q_n}{p_n}\right)}{p_n k H_n^{(2)}(k_0 b)\left(\frac{Y_s}{k} - \frac{H_n^{'(2)}(k_0 b)}{H_n^{(2)}(k_0 b)} + \frac{\sqrt{\varepsilon_r}q_n}{p_n}\right)} \tag{3.44}$$

Remembering that $k = \frac{k_0}{j\omega\mu} = -jY_0$ it can be therefore expressed:

$$\frac{Y_s}{k} = jY_s/Y_0 = j\hat{Y}_s \tag{3.45}$$

where Y_0 is the background admittance.

Consequently, Eq. 3.44 can be written as:

$$c_n = \frac{J_n(k_0 b)\left(-j\hat{Y}_s + \frac{J_n^{'}(k_0 b)}{J_n(k_0 b)} - \frac{\sqrt{\varepsilon_r}q_n}{p_n}\right)}{H_n^{(2)}(k_0 b)\left(j\hat{Y}_s - \frac{H_n^{'(2)}(k_0 b)}{H_n^{(2)}(k_0 b)} + \frac{\sqrt{\varepsilon_r}q_n}{p_n}\right)} \tag{3.46}$$

Finally, the scattering coefficients associated with the metasurface coated cylinder are computed as:

$$c_n = -\frac{J_n(k_0 b)}{H_n^{(2)}(k_0 b)} \left(\frac{j\hat{Y}_s - \frac{J_n'(k_0 b)}{J_n(k_0 b)} + \frac{\sqrt{\varepsilon_r} q_n}{p_n}}{j\hat{Y}_s - \frac{H_n^{'(2)}(k_0 b)}{H_n^{(2)}(k_0 b)} + \frac{\sqrt{\varepsilon_r} q_n}{p_n}} \right) \tag{3.47}$$

Looking at Eq. 3.47 it can be noticed that when Y_s approaches infinity, the coefficients c_n becomes:

$$c_n(Y_s \to \infty) = -\frac{J_n(k_0 b)}{H_n^{(2)}(k_0 b)} \tag{3.48}$$

which is equal to the expression of the scattering coefficients associated to a bare cylinder with radius b is considered. This is perfectly consistent because considering an infinite surface admittance boundary conditions it is equivalent to cover the cylinder with a conductive layer and therefore to have a conductive cylinder of radius b.

3.4.2 Surface impedance to annul one scattering harmonic

Previously it has been illustrated that in order to cloak the cylinder, it is necessary to reduce its scattering (ideally to completely annul it). Therefore, the scattering coefficients should be imposed equal to zero.

From the scattering coefficients expressed in Eq. 3.47 it is possible to obtain an expression of the surface admittance that leads to the annulment of one harmonic of the scattered field. Therefore, imposing $c_n = 0$ it is obtained:

$$Y_s(c_n = 0) = \frac{1}{Z_s(c_n = 0)} = k \left(\frac{J_n'(k_0 b)}{J_n(k_0 b)} - \sqrt{\varepsilon_r} \frac{q_n}{p_n} \right) \tag{3.49}$$

In Fig. 3.7 the surface reactance that annuls the single harmonics with modal index from $n = 0$ to $n = 10$ is represented, with respect to the cylinder normalised radius. and a dielectric layer with $b = 1.15a$ and $\varepsilon_r = 10$.

In Fig. 3.7d the behaviour of Y_s is shown for low frequency regime. It can be seen that, in this particular case, the values of Y_s follow a monotonic behaviour at the increasing of both a/λ and the index n. In this case only harmonics indexes n = 0, 1, 2 are considered because they are the only present in the scattering.

This can be an obstacle for increasing the cloaking bandwidth when using passive metasurfaces. Indeed, the reactance of a passive metasurface monotonically increases with the frequency. as stated by the Foster's reactance theorem, and

therefore the same harmonic cannot be annulled at different frequency at the same time.

It is important to notice that the value of Y_s is associated to the harmonic order n and that, with a homogeneous metasurface, and therefore a homogeneous value of surface impedance it is possible to completely cancel only one harmonic at one frequency. Indeed, it should be underlined that, once fixed the cylinder radius, different harmonics require different values of surface impedances to be cancelled. As already discussed, this is the principal limitation to cloaking cylinders with a radius not much smaller than the wavelength of interest, because, beyond the quasi-static limit, different harmonics order are present in the scattered field, and the associated scattering coefficients cannot be annulled at the same time by using a homogeneous surface impedance.

It should be also noticed that, to compute Eq. 3.49 no approximation was made on the cylinder electrical dimension and this formulation is therefore valid also beyond the quasi-static limit, so that it can be applied also to non electrically small structures, as it will be successively demonstrated in Ch. 4.

3.5 Cloaking and scattering reduction

In order to perform a quantitative analysis of the cloaking performances, a measure of the scattering reduction should be taken into account. Here, the Scattering Width (SW) is considered as a figure of merit. Indeed, the SW corresponds to the ratio of the scattered and the incident powers, thus minimizing the scattered field is equivalent to minimize the SW.

Hence, the SW can be computed as [90], [93]:

$$SW = \lim_{\rho \to \infty} 2\pi\rho \left[\frac{|\boldsymbol{E}_s|^2}{|\boldsymbol{E}_i|^2} \right] \tag{3.50}$$

Assuming a far field condition ($k_0\rho \to \infty$) it is possible to approximate the Hankel functions (for large argument) as:

$$H_n^{(2)}(k_0\rho \to \infty) = \sqrt{\frac{2}{\pi k_0 \rho}} \exp\left(-j(x - \frac{n\pi}{2} - \frac{\pi}{4}) \right) \tag{3.51}$$

which can be written as:

$$H_n^{(2)}(k_0\rho \to \infty) = \sqrt{\frac{2j}{\pi k_0 \rho}} j^n \exp(-jk_0\rho) \tag{3.52}$$

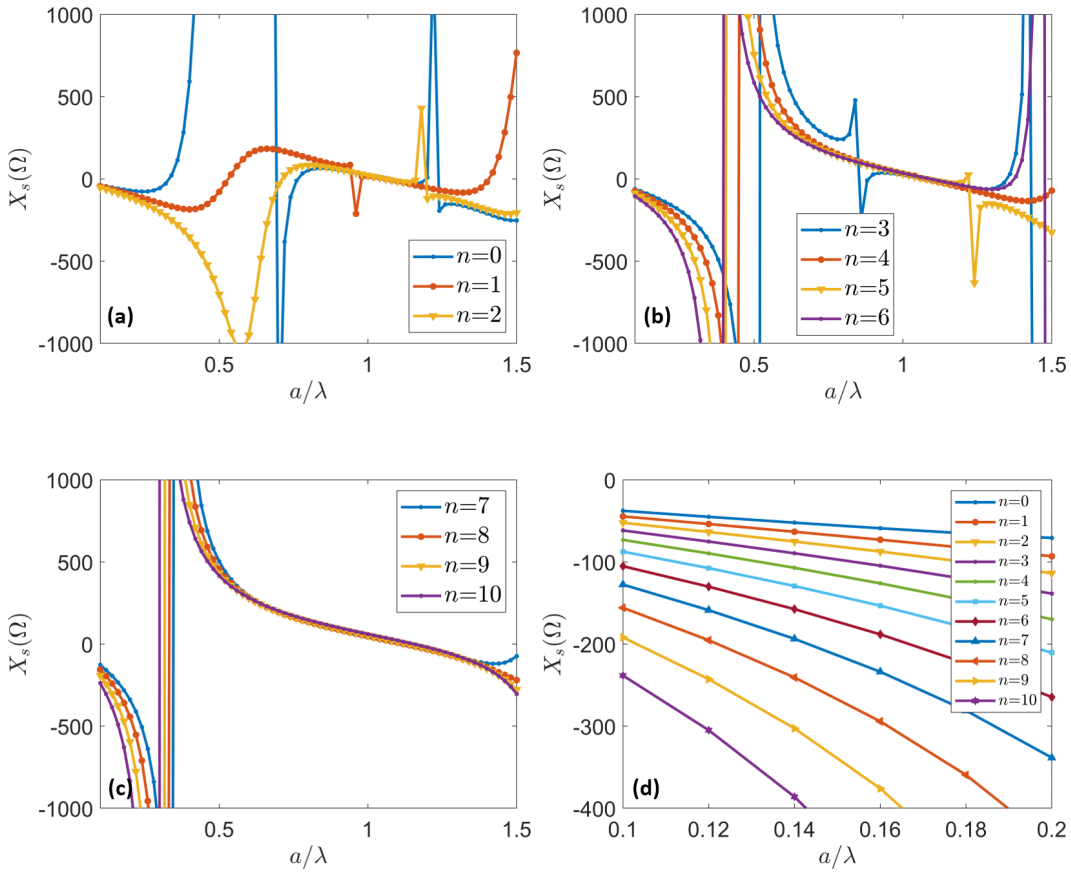

Figure 3.7: Surface reactance that annuls the harmonic n = 0,1,2 (a), n = 3,4,5,6 (b), n = 7,8,9 (c) with respect to the cylinder normalised radius. Detail for low frequency regime (d). The dielectric layer characteristics are b =1.15a, ε_r = 10 [87] ©2020 Optical Society of America.

Remembering that the scattered field $\boldsymbol{E}_s(\rho,\varphi)$ is equal to:

$$\boldsymbol{E}_s(\rho,\varphi) = \hat{\boldsymbol{z}} E_0 \sum_{n=-\infty}^{\infty} j^{-n} c_n H_n^{(2)}(k_0\rho)\exp(jn\varphi) \tag{3.53}$$

and substituting the far field approximation of the function $H_n^{(2)}(k_0\rho)$ into the scattered field equation, it is obtained:

$$\boldsymbol{E}_s(\rho,\varphi) = \hat{\boldsymbol{z}} E_0 \sum_{n=-\infty}^{\infty} j^{-n} c_n \left[\sqrt{\frac{2j}{\pi k_0\rho}} j^n \exp(-jk_0\rho)\right] \exp(jn\varphi) \tag{3.54}$$

$$\boldsymbol{E}_s(\rho,\varphi) = \hat{\boldsymbol{z}} E_0 \sqrt{\frac{2j}{\pi k_0 \rho}} \exp(-jk_0\rho) \sum_{n=-\infty}^{\infty} j^{-n} c_n j^n \exp(jn\varphi) \tag{3.55}$$

Finally,

$$\boldsymbol{E}_s(\rho,\varphi) = \hat{\boldsymbol{z}} E_0 \sqrt{\frac{2j}{\pi k_0 \rho}} \exp(-jk_0\rho) \sum_{n=-\infty}^{\infty} c_n \exp(jn\varphi) \tag{3.56}$$

Therefore, in far field, the ratio between the scattered and the incident field absolute values is expressed as:

$$\frac{|\boldsymbol{E}_s|}{|\boldsymbol{E}_i|} \rightarrow \frac{|E_0 \sqrt{\frac{2j}{\pi k_0 \rho}} \exp(-jk_0\rho) \sum_{n=-\infty}^{\infty} c_n \exp(jn\varphi)|}{|E_0 \exp(-jk_0\rho)|} \tag{3.57}$$

$$\frac{|\boldsymbol{E}_s|}{|\boldsymbol{E}_i|} \rightarrow \sqrt{\frac{2}{\pi k_0 \rho}} \left| \sum_{n=-\infty}^{\infty} c_n \exp(jn\varphi) \right| \tag{3.58}$$

So that the SW reads as:

$$SW = \frac{4}{k_0} \left| \sum_{n=-\infty}^{\infty} c_n \exp(jn\varphi) \right|^2 = \frac{2\lambda}{\pi} \left| \sum_{n=-\infty}^{\infty} c_n \exp(jn\varphi) \right|^2 \tag{3.59}$$

Therefore, the SW is a function of the angular coordinate φ, and here it is chosen to consider $\varphi = 0$ to evaluate the SW. This is because for $\varphi = 0$ the field scattered by the bare cylinder reaches is maximum value [90].

Therefore, for $\varphi = 0$:

$$SW = \frac{2\lambda}{\pi} \left| \sum_{n=-\infty}^{\infty} c_n \right|^2 \tag{3.60}$$

Once defined the method of evaluation of the cloaking performance, the surface impedance which offers the best cloaking result and therefore minimises the SW for the given scatterer object should be evaluated.

With Eq. 3.49 the proper surface admittance required to annul a specific harmonic of the scattered field has been computed. However, as seen before, when non-electrical small structures are considered, different harmonics are present into the scattering and a dominant harmonic component cannot be identified. Moreover, also in the quasi static limit case, when the scattering is primarily dominated by the harmonic with modal index $n = 0$, it can be demonstrated [88] that the annulment of this predominant harmonic could be not the best option.

This is due to the face that the imposition of the surface impedance boundary

condition affects all the harmonics. Therefore, even if one harmonic is suppressed, other harmonics can be enhanced.

As an example in Fig. 3.8 the scattering coefficients of a cloaked cylinder with a normalised radius $a/\lambda = 0.13$, are reported considering two surface impedances: the first annuls the coefficient c_0, while the second correspond to a minimum of the SW. The considered dielectric layer has a thickness $b = 1.15a$ and a relative permittivity $\varepsilon = 2$.

In the first case, for X_s = -46.54 Ω it can be noticed that although c_0 is completely annulled, c_1 and c_2 are increased with respect to the base case, while for X_s = -51 Ω no coefficient is totally cancelled, however both c_0 and c_1 are decreased leading to a stronger reduction of the SW with respect to previous case, and consequently a minimum of the scattering.

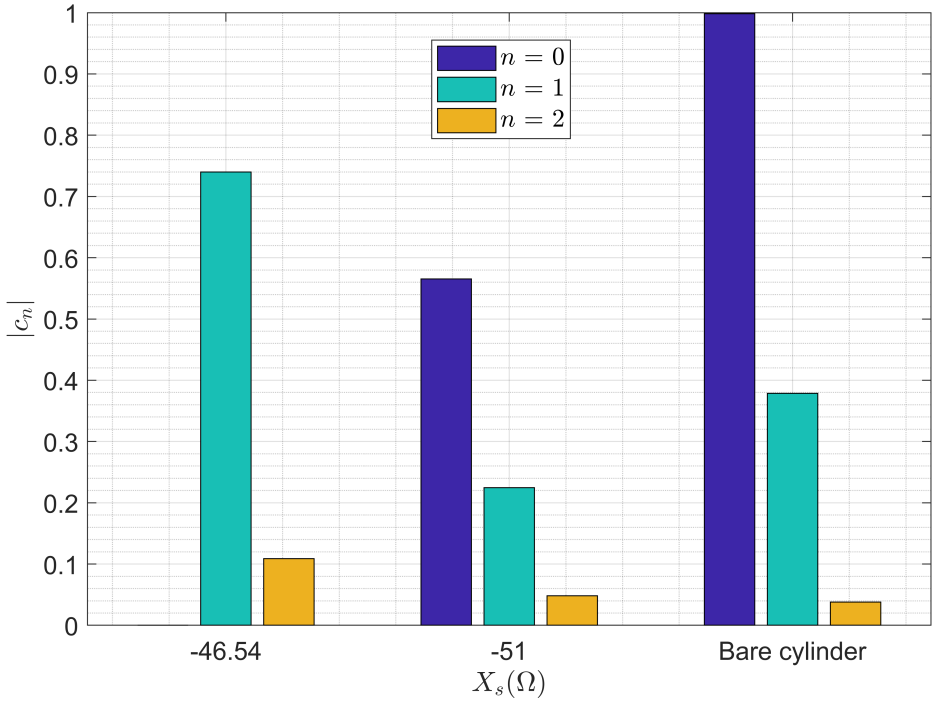

Figure 3.8: Absolute value of the scattering coefficients for different surface impedances when $a/\lambda = 0.13$ compared to the bare case (on the right). On the left the impedance which annuls the the dominant harmonic $n = 0$ is considered, while in the center the impedance which minimise the scattering is imposed [88] ©2017 IEEE.

Therefore, in the following a parameter sweep is performed with the aim of compute the surface reactance value, from now on identified as X_{opt}, which causes

a minimum of the scattered field at the varying of the cylinder electrical dimension.

In Fig. 3.9 the SW reduction (the difference between the SW of the bare cylinder and the cloaked cylinder) for different surface reactances and normalised cylinder radius is reported, for the dielectric layer characteristics $b = 1.2a$ and $\varepsilon_r = 10$.

For electrically small cylinders, a minimum of the SW is obtained for capacitive surface impedances, as also confirmed in [45], where it is shown that the cloaking metasurface should realise a capacitive surface impedance for cloaking metallic cylinders, while an inductive impedance in case of dielectric scatters.

However, when the thickness of the dielectric increases and reaches the values of $t = \lambda_d/4$, where λ_d is the wavelength in the dielectric layer, the surface impedance changes sign becoming positive. This means that, when frequency regimes over the quasi-static limit are examined, and in general when $t > \lambda_d/4$, also positive values of X_s need to be considered as a possible solution for cloaking a metallic cylinder.

Indeed, the input impedance of the cloaked cylinder is equal to the parallel of the grounded dielectric layer, and the surface impedance boundary condition. In order to annul the scattering, the input impedance of cloaked cylinder needs to be equal to the background medium impedance.

Therefore, when the dielectric thickness t becomes greater than a quarter of the wavelength in the dielectric, the input impedance of the grounded dielectric layer, and consequently X_s, changes signs. This behaviour is shown in Fig. 3.9, which represents the difference of the SW between the bare and cloaked cylinder, for a value of a/λ varying from 0.1 to 1.5 considering both negative and positive values of X_s.

As illustrated by Fig. 3.9, the minima of the SW show a periodic tendency. Indeed, the SW minima occur in correspondence of negative values of X_s for low values of the cylinder normalised radius a/λ. Specifically, in the considered case, till $a/\lambda = 0.4$. However, Fig. 3.9 reveals that for a/λ comprised between 0.4 and 0.8, a SW reduction can be obtained by considering positive values of X_s. This periodic trend is present also with the increasing of a/λ even if due to the higher cylinder dimension, an increasing number of harmonics is present in the scattered field, resulting in a lower SW reduction.

This results is further analyzed in Fig. 3.10 which illustrates the optimum cloaking surface reactances X_{opt} with respect to different cylinder normalised radius a/λ and dielectric coating properties. It can be noticed the resonant nature of X_{opt} and the transition from capacitive to inductive values.

Furthermore, in Fig. 3.10c, d the SW values corresponding to X_{opt} are shown and compared to the bare cylinder results. The SW of the cloaked structure is

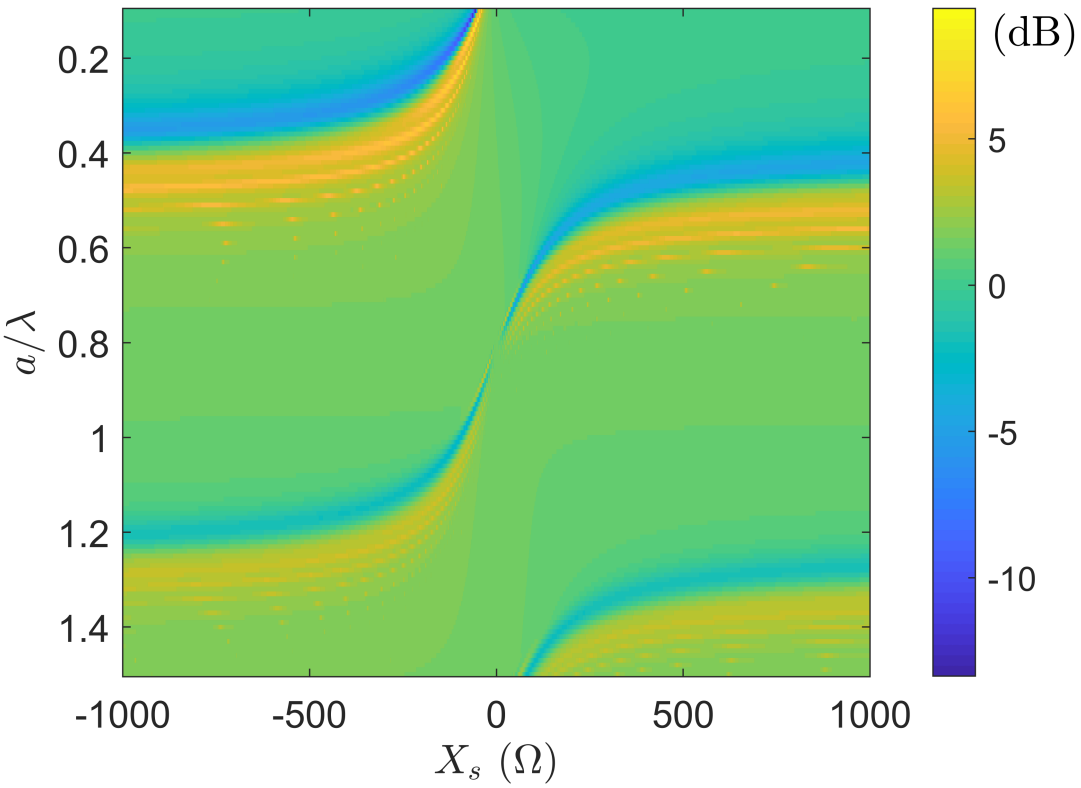

Figure 3.9: *SW* of a cloaked conductive cylinder with respect to the cylinder radius and the cloaking metasurface reactance. The dielectric layer characteristics are $b = 1.20a$, $\varepsilon_r = 10$ [87] ©2020 Optical Society of America.

compared with the one of the bare cylinder, taking as a reference a reduction of 3 dB from the bare level.

The results indicate that a considerable reduction of the *SW* can be obtained for a cylinder radius much smaller than the wavelength of the incident field, by employing a negative surface reactance. While, as the cylinder dimension increases, the *SW* reduction becomes significantly smaller. However, for a cylinder radius comparable to the wavelengths it is still possible to identify a second cloaking zone in which a local minimum of the *SW* is obtained in correspondence of positive values of X_{opt} if appropriate values of b and ε_r are chosen.

Indeed, examining Fig. 3.10 it can be noticed that a minimum of the *SW* is reached for a normalised radius of a/λ equal to 0.68 and 0.92, considering a dielectric layer with relative permittivity $\varepsilon_r = 10$ and a total radius $b = 1.2a$ and $1.15a$ respectively. In this two cases, the *SW* is reduced by 5.4 dB and 4 dB with

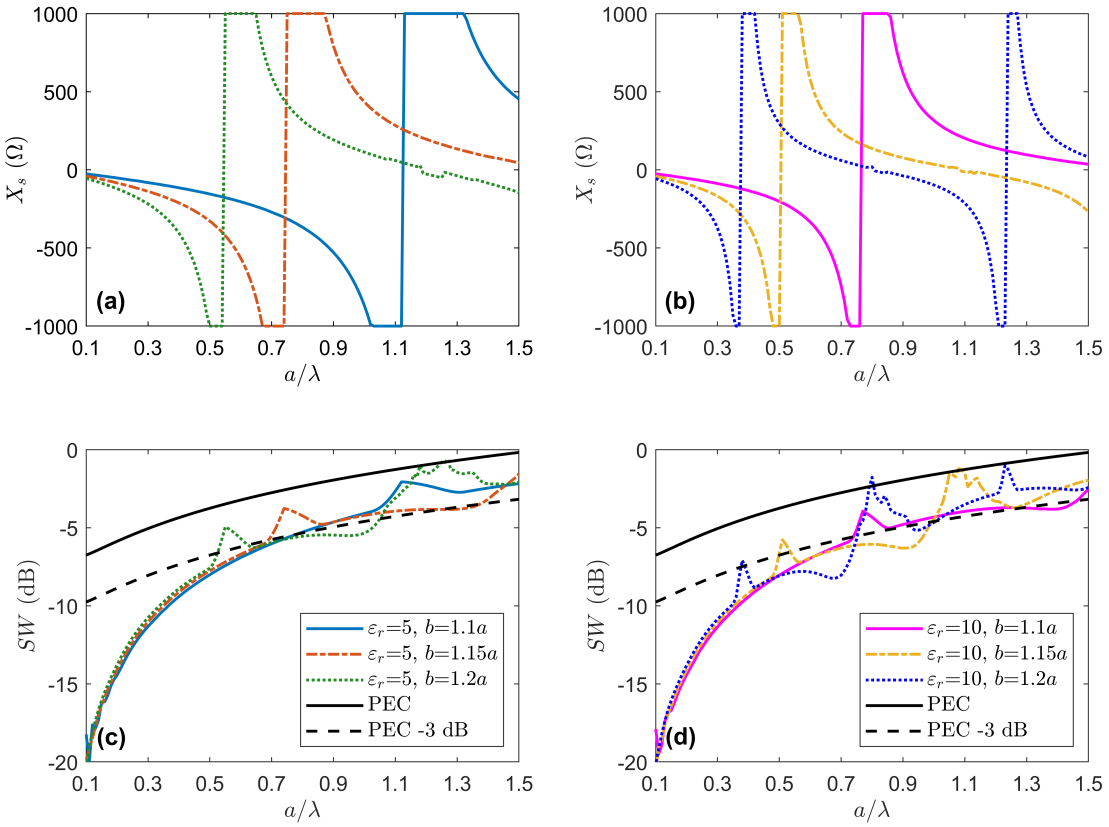

Figure 3.10: Optimum surface reactances (a, b) and associated SW (b, c) for cloaking a conductive cylinder, with respect to the cylinder normalised radius, considering different thickness and permittivity of the dielectric coating. It can be seen that beyond the quasi-static limit, a local minimum of the SW is present [87] ©2020 Optical Society of America.

a surface reactance X_s equal to 73 Ω and 68 Ω.

Moreover, a comparison between the optimum surface reactance and the surface reactance which annuls a specific harmonic is performed. Indeed, Fig. 3.11 represents the surface reactance which annuls the harmonics with modal index n = 0, 1, 2 and the surface impedance which leads to a minimum of the SW, namely X_{opt} in a low frequency condition. It can be seen that for this frequency range the X_{opt} value is comprised between the impedances that annuls the coefficients c_0 and c_1.

As an example of the possibility of reducing the scattered field of an electrically large cylinder with the using of a positive surface reactance is reported in Fig. 3.12

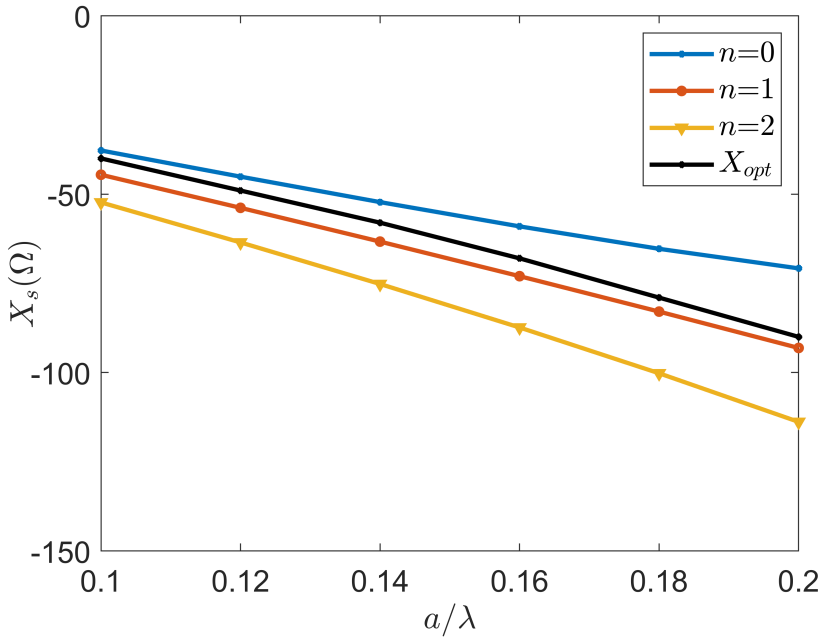

Figure 3.11: Comparison between the optimum surface impedance and the surface impedance which annuls the scattering coefficients c_0, c_1, and c_2.

which shows the scattered field of a cylinder with normalised radius $a/\lambda = 0.8$ and compared with the scattering by the bare cylinder and the cloaked cylinder considering a dielectric layer with $b = 1.25a$, $\varepsilon_r = 5$ and a surface reactance $X_s = 110\Omega$. The structure is supposed to be illuminated by an incident planewave with amplitude 1 V/m. It can be clearly seen that the scattered field is reduced with respect to the bare cylinder even if the cylinder radius is comparable with the incident wavelength.

Moreover, in Fig. 3.13 the scattering coefficients related to the bare and cloaked cylinder are reported. Although the coefficients c_0 and c_2 are increased in the cloaked case, the rest of the coefficients is reduced, leading to a lower scattered field.

The results obtained with the use of a positive surface reactance are than compared to previous works present in literature. Indeed, authors which addressed the problem of cloaking below low frequency regime have used different strategies to achieve this goal by using a homogeneous metasurface.

For example in [94] the authors propose to use a low thickness of the dielectric coating. In this way they demonstrated that different harmonic orders require similar surface impedance values to be annulled.

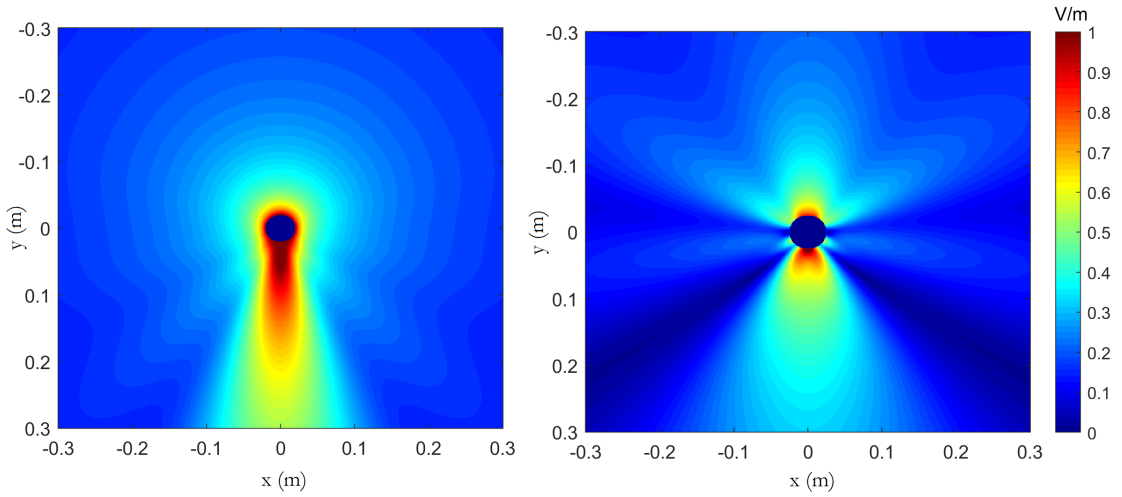

Figure 3.12: Field scattered by a metallic cylinder with normalized radius ($a/\lambda = 0.8$) in the bare case (a) and in the cloaked case (b) considering $X_s = 110\ \Omega$ [89] ©2017 IEEE.

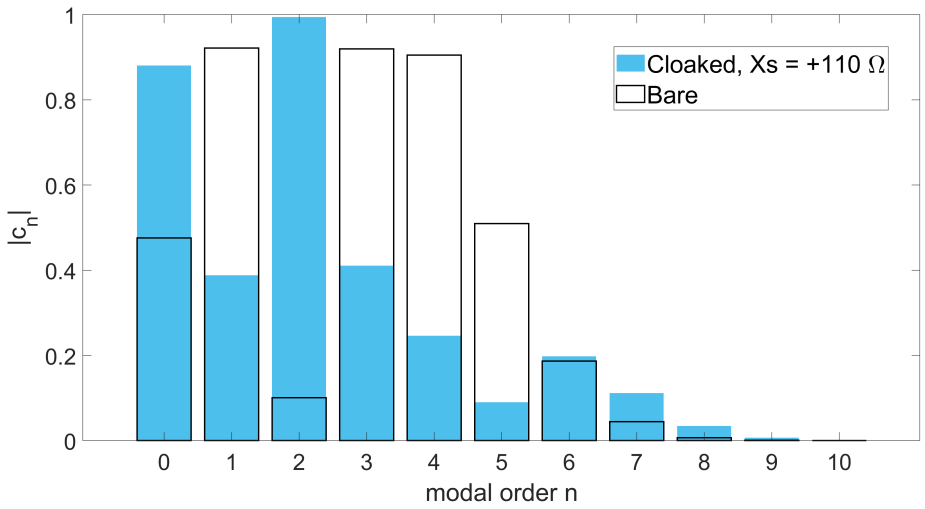

Figure 3.13: Modulus of the scattering coefficients c_n for a bare and cloaked ($X_s = 110\ \Omega$) cylinder with $a/\lambda = 0.8$ [89] ©2017 IEEE.

Applying this method, the proposed cloaking device was able to achieve a SW reduction of 4.8 dB for a cylinder radius equal to $a/\lambda = 0.5$ and a reduction of 3.3 dB for $a/\lambda = 0.67$. Here, as can be noticed in Fig. 3.10, with the use of a positive surface reactance, it is possible to achieve a reduction of 5.4 dB for a normalised cylinder radius $a/\lambda = 0.68$.

A different approach was used in [95] to cloak a cylinder with dimension $a/\lambda = 1.425$. With the proposed cloak design, the SW reduction was equal to 2 dB. Here, looking at Fig. 4.9, it is possible to see that a reduction of 3.3 dB can be achieved for a normalised radius $a/\lambda = 1.38$ by using a dielectric layer with a thickness equals to just the 10% of the bare cylinder radius and a permittivity of $\varepsilon_r = 10$.

Chapter 4

Design of a Practical Mantle Cloaking Metasurface

Part of the work described in this Chapter was also previously published in [87], [96].

In the previous chapter, the theoretical study of the cloaking problem has been carried out and an analysis with particular focusing on the scattering harmonic composition of the appropriate surface impedance boundary condition to cloak metallic cylinders has been proposed, especially considering the challenges in the cloaking of non electrically small structures.

The next step to design an appropriate cloaking device, consists into the choice of the metasurface which realises the proper surface impedance boundary condition studied in the analytical formulation of the problem. Depending on the material and geometrical parameter of the object and the dielectric layer, and on the frequency of operation, a metasurface with specific shape and dimensions is required. Therefore, it is necessary to have a connection between the surface impedance value and the metasurface geometric and material parameters.

4.1 Electrically small cylinders

4.1.1 Scattering harmonic analysis

In this section, two practical mantle cloaking metasurfaces will be examined considering objects with different electrical dimensions.

First, the cloaking of an electrically small metallic cylinder is considered. Therefore, the cylinder radius is set to $a = \lambda/10$. Considering the cylinder illuminated by a TM polarised planewave, the scattered field harmonic composition is analytically

computed following Eq. 3.6 and it is represented on the right side of Fig. 4.1. It can be seen that in this case, only the harmonics with modal index $n = 0$ and $n = 1$ are present in the scattering, and it is possible to identify $n = 0$ as the dominant one.

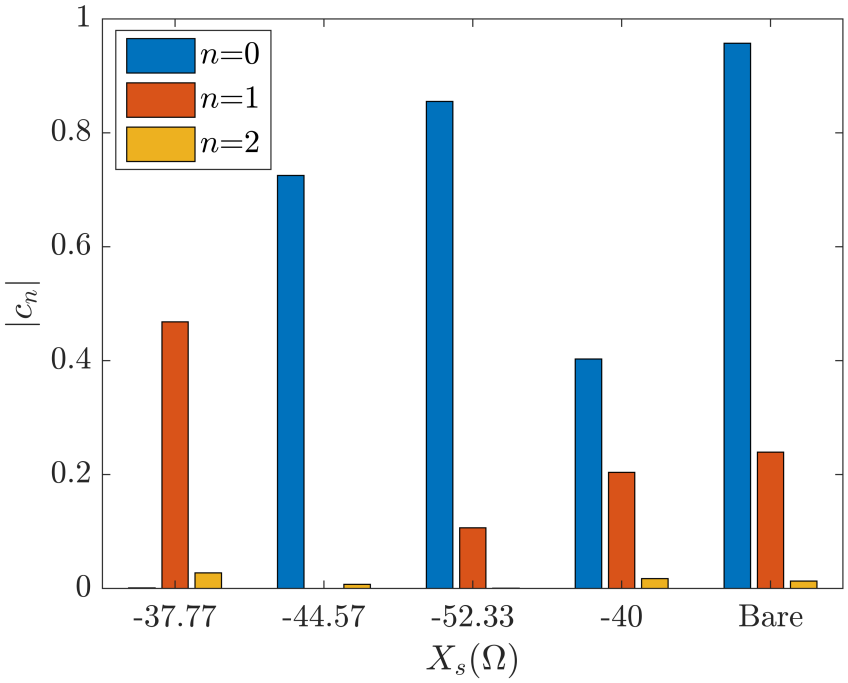

Figure 4.1: Scattering coefficients associated with a metallic cylinder of normalised radius $a/\lambda = 0.1$, coated by a dielectric layer of thickness $t = 0.15a$ and relative permittivity $\varepsilon_r = 10$, considering differing surface reactances X_s.

In this example it is decided to use a dielectric coating with permittivity ε_r=10 for both the electrically small and large cylinder.

A first analysis is then performed to evaluate the minimum SW which is possible to achieve with the use of different dielectric thicknesses, and the correspondent surface impedance value which is required to minimize it. The result of this analysis is detailed in Fig. 4.2.

As can be noticed, a minimum can be achieved for $b = 1.08a$ imposing a surface impedance of X_s = -20 Ω. However, for this value of b the SW response strongly fluctuates with small variations of b, therefore here it is chosen to use a dielectric thickness such that $b = 1.15a$ and a correspondent surface impedance X_s = -40 Ω since around that value the SW curve shows less fluctuation at the varying of b and the design is therefore more robust against manufacturing imperfections.

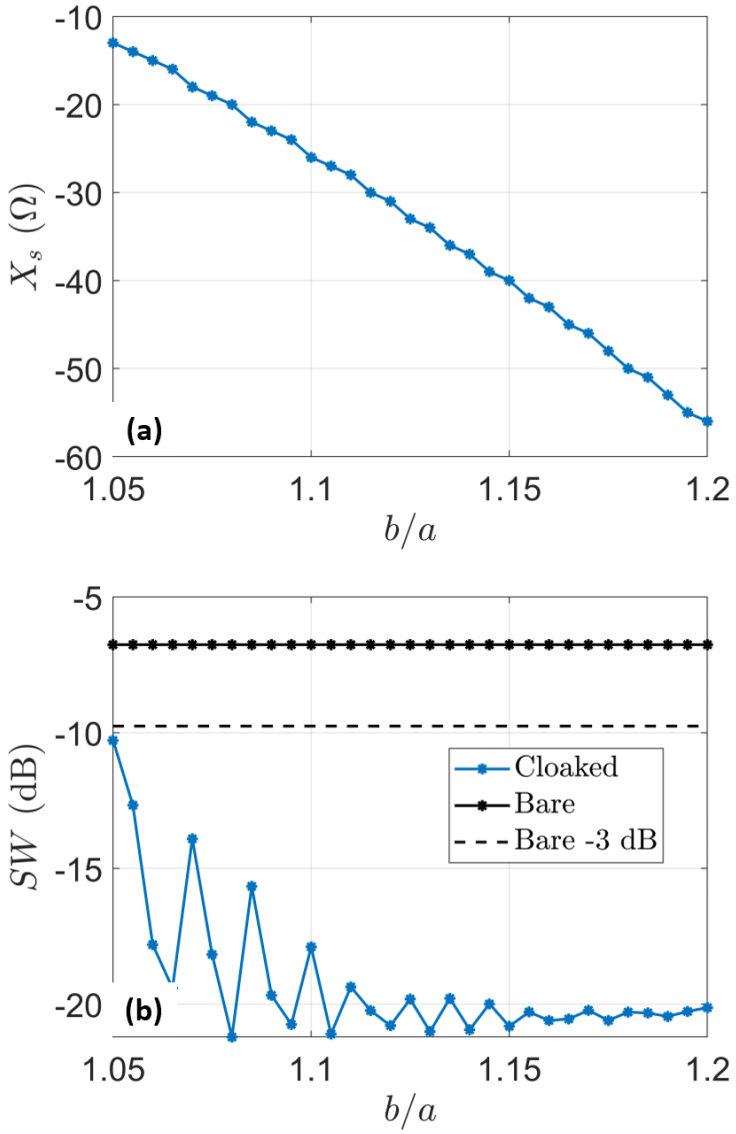

Figure 4.2: Optimum surface reactance (a) and correspondent SW (b) for a metallic cloaked cylinder with radius $a/\lambda = 0.1$, with respect to the dielectric coating layer thickness, considering a relative permittivity of the coating $\varepsilon_r = 10$.

Moreover, it is possible to compare the surface impedance values that minimize the scattering with the ones that annul the different harmonics. Indeed, following Eq. 3.49, it is found that to cancel the harmonics with modal index $n = 0$ and $n = 1$ a surface reactance X_s = -37.77 Ω and X_s = -44-57 Ω is required, respectively. The harmonic composition of the scattered field for the different surface impedances is

reported in Fig. 4.1.

Although the harmonic with modal index $n = 0$ is the principal component of the scattered field, it can be noticed that when c_0 is annulled, c_1 is increased with respect to the bare case. For this reason, the scattering is not minimised. Instead, for X_s = -40 Ω, no harmonic is completely cancelled, however the scattered field is minimized.

Moreover, also the coefficients a_n and b_n (with $n = 0, 1, 2$) which are associated with the field in the dielectric layer are computed and are reported in Fig. 4.3. In particular, a comparison between the cloaked cylinder and a dielectric coated one (without considering the surface impedance boundary condition) is performed. It is found that in the first case (cloaked structure) the coefficients are significantly higher than in the second situation. This proves that, due to the surface impedance cloaking, the field is confined in the dielectric layer, in which therefore there is a strong field presence, reducing in this way the scattering.

Furthermore, in Fig. 4.4 the scattered field for the different surface impedances is shown, namely X_s = -37.77 Ω corresponding to $c_0 = 0$ and X_s = -40 Ω corresponding to a minimum SW, and compared with the scattering by the bare cylinder. This comparison shows first of all the significant scattering reduction with respect to the bare cylinder case, and second it gives a further proves that the annulment of the dominant harmonic does not necessary imply a minimum of the scattered field.

4.1.2 Metasurface design

Once defined the dielectric thickness, permittivity and the surface impedance boundary condition, the metasurface has to be designed.

In literature, different approaches are present which allow to derive the surface impedance of a specific metasurface geometry. For example, in [42] analytical formulas to compute the surface impedance of square patch and metallic strips based metasurfaces for different angle of the incident field are reported.

It must be underlined that this formulation is based on the hypothesis of an infinite periodic and planar metasurface. Therefore, here, the approximation of a planar metasurface is firstly considered in order to compute the geometrical parameters of the metasurface unit cell, and in a second step, the effect of the cylinder curvature is analysed.

In this case it is decided to use as metasurface unit cell a metallic square patch which requires few design parameters, but it is effective and vastly used in literature [45], [47], [94], [95]. The cylinder radius is set to a = 20 mm, therefore $b = 1.15a$ = 23 mm. The operational frequency is set to f = 1.5 GHz such that $a = \lambda/10$,

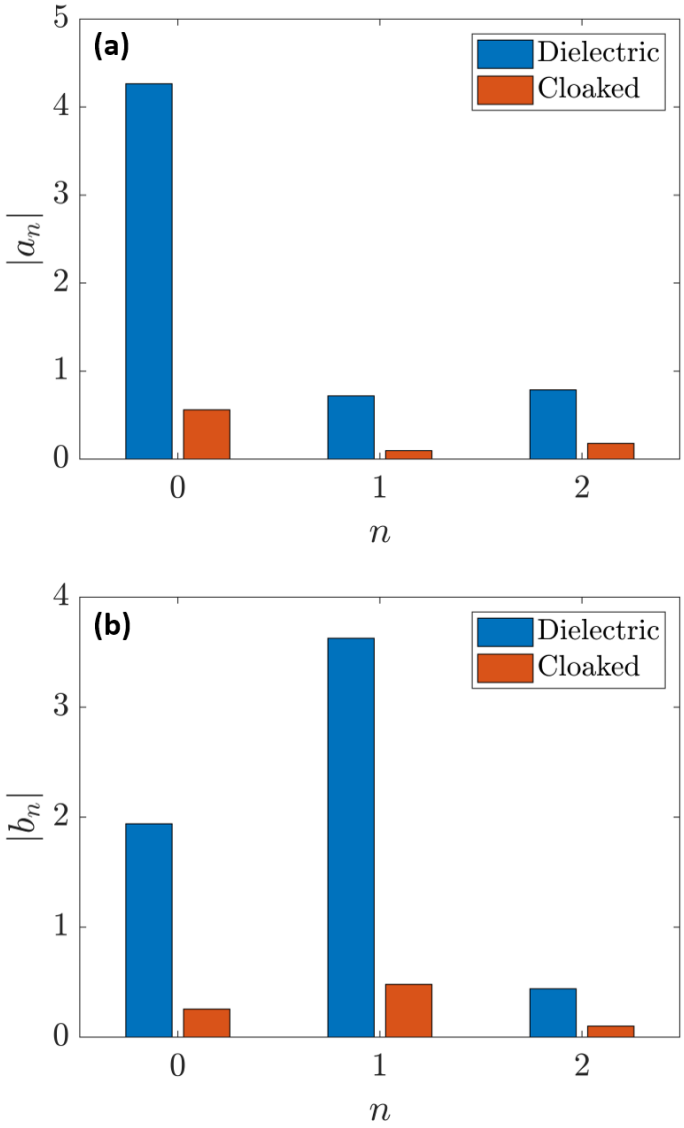

Figure 4.3: Coefficients a_n and b_n related to the field in the dielectric layer. Comparison between a dielectric coated cylinder (without the metasurface) and a cloaked cylinder with X_s = -40 Ω.

respecting the low frequency regime.

Therefore, in order to retrieve the surface impedance value of the metasurface, the square patch unit cell is simulated with CST Studio Suite. In particular, a planar unit cell is taken into account, which is composed of a grounded dielectric layer with a printed metallic square patch. To simulate an infinite periodic surface,

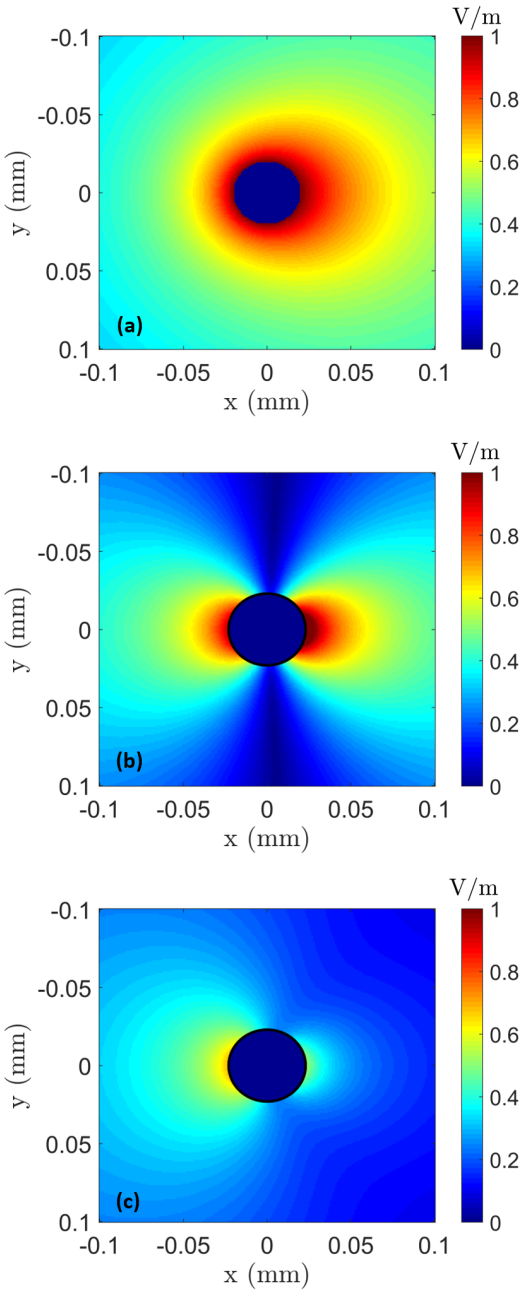

Figure 4.4: Comparison of the scattered fields from the bare (a) and the cloaked (b, c) cylinder. In (b) the surface impedance which annuls the dominant scattering coefficient c_0 is considered, while in (c) the impedance which leads to a minimum of the scattering is employed.

periodic boundary conditions are set on the unit cell sides.

The structure can be modeled as a Transmission line problem and its equivalent circuit is shown in fig 4.5. It consists of a short-circuited transmission line, which models the grounder dielectric layer, in parallel with the unknown surface impedance. The input impedance of the circuit Z_{in} is retrieved with the numerical simulation while the short-circuited line impedance, Z_{sc}, is computed as:

$$Z_{sc} = Z_d j \tan(k_d t) \tag{4.1}$$

where $t = 3$ mm represents the dielectric thickness, $Z_d = Z_0/\sqrt{\varepsilon_r}$ and $k_d = k_0\sqrt{\varepsilon_r}$ are the characteristic impedance and wavenumber of the dielectric layer, respectively, Z_0 being the background medium impedance, and $\varepsilon_r = 10$ is the dielectric relative permittivity.

By expressing the problem in terms of admittances, the input admittance Y_s is computed as the sum of the short-circuited line admittance, Y_{sc} and the surface admittance Y_s. Therefore, it can be written:

$$Y_{in} = Y_s + Y_{sc} \rightarrow Y_s = Y_{in} - Y_{sc} \tag{4.2}$$

Such that:

$$Z_s = \frac{Z_{in} Z_{sc}}{Z_{sc} - Z_{in}} \tag{4.3}$$

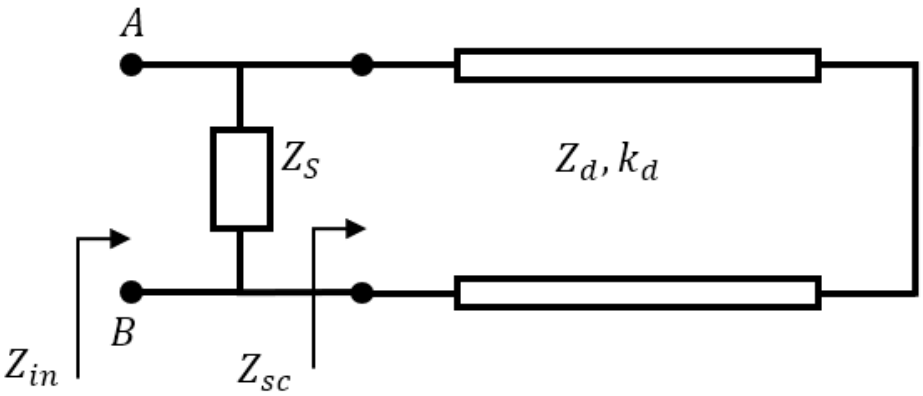

Figure 4.5: Equivalent circuit of the planar metasurface [96].

Now, the design parameters of the metasurface unit cell should be computed. Since a square patch unit cell is proposed as can be seen in Fig. 4.6, two parameters

needs to be considered, namely the unit cell lengths D and w, which corresponds to the distance between two metallic patches.

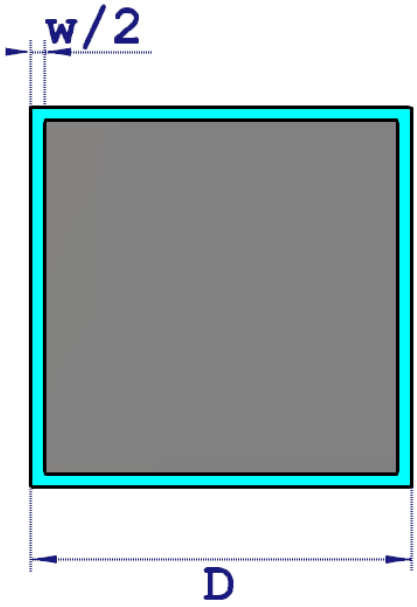

Figure 4.6: Square patch cell.

In order to compute the opportune values of D and w, the first thing to consider is that an integer number of unit cells has to be present in the azimuthal direction on the cylinder boundary, so that the length of the unit cell must follow the rule $D = 2\pi b/N$, where N is the numbers of unit cell repetitions. Moreover, a even number of N is considered to ensure the symmetry of the structure.

It should be also noticed that, in order compute an equivalent surface impedance and to consider the metasurface as a homogeneous surface, a sufficient number of repetitions on the cylinder boundary should be implemented.

Therefore, here it is considered $N = 8$ and $N = 10$ which corresponds to a unit cell period $D = 18$ mm and $D = 14.5$ mm, respectively. With this parameters, different w are taken into account, to achieve a surface reactance $X_s = 40\ \Omega$ for $f = 1.5$ GHz, and the results are shown in Fig. 4.7.

The computed surface impedance is plotted in Fig. 4.7 for different lengths w of the metallic patch. To ensure the value of X_s = -40 Ω , the length of the metallic patch has to be set to $w = 0.2$ mm. It can be noticed that if $N = 10$ is considered, to have $X_s = 40\ \Omega$, a value of $w < 0.5$ should be used, while by setting $N = 8$, it is required that $w = 0.2$ mm. Therefore, in order to not have a separation between

two adjacent metallic patches too small, it is decided that $N = 8$, $D = 18$ mm and $w = 0.2$ mm.

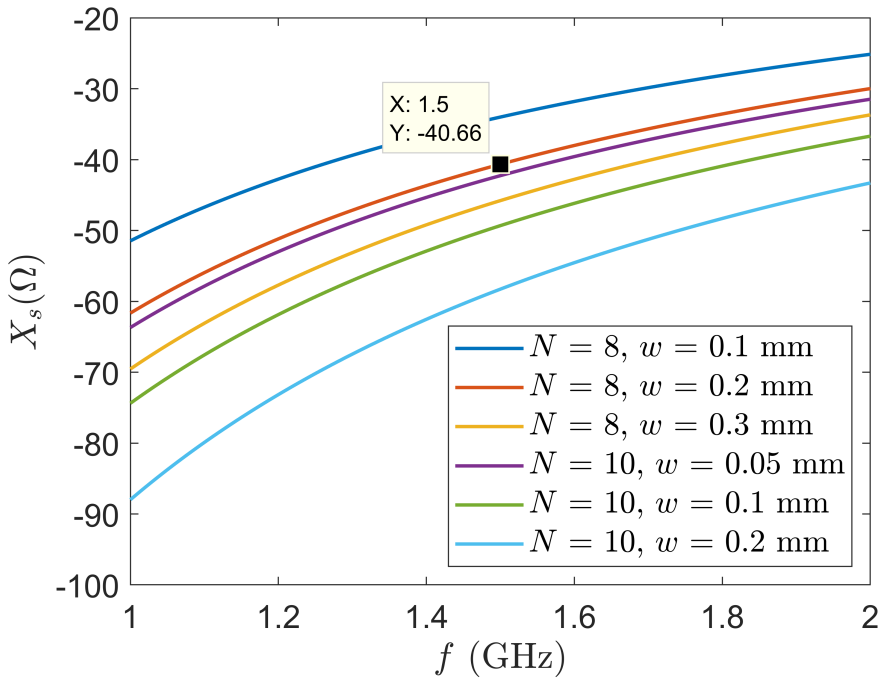

Figure 4.7: Surface reactance of the square patch metasurface for different design parameters.

A full wave simulation of the coated cylinder is performed with CST Studio Suite, and the proposed design is detailed in Fig. 4.8. It can be seen that the square patch metasurface is bent around the cylinder and the whole structure is illuminated by a TM polarised planewave. To simulate an infinitely long cylinder, electric boundary conditions are imposed on the top and bottom face of the cylinder, while open boundaries are set in the other directions.

The resulting SW for the bare and the cloaked cases at different frequencies are reported in Fig. 4.9. As can be noticed, the cloaking frequency, i.e. the frequency at which the scattering is minimum, results to be $f = 1.44$ GHz. The difference with respect to the design frequency of 1.5 GHz is likely to be searched in the cylindrical configuration, and therefore it is due to the effect of the curvature on the metasurface surface impedance.

It is supposed that a larger curvature will give rise to a reduced difference between the expected and calculated values.

In Fig. 4.10 the real part of the total electric field resulting from the numerical

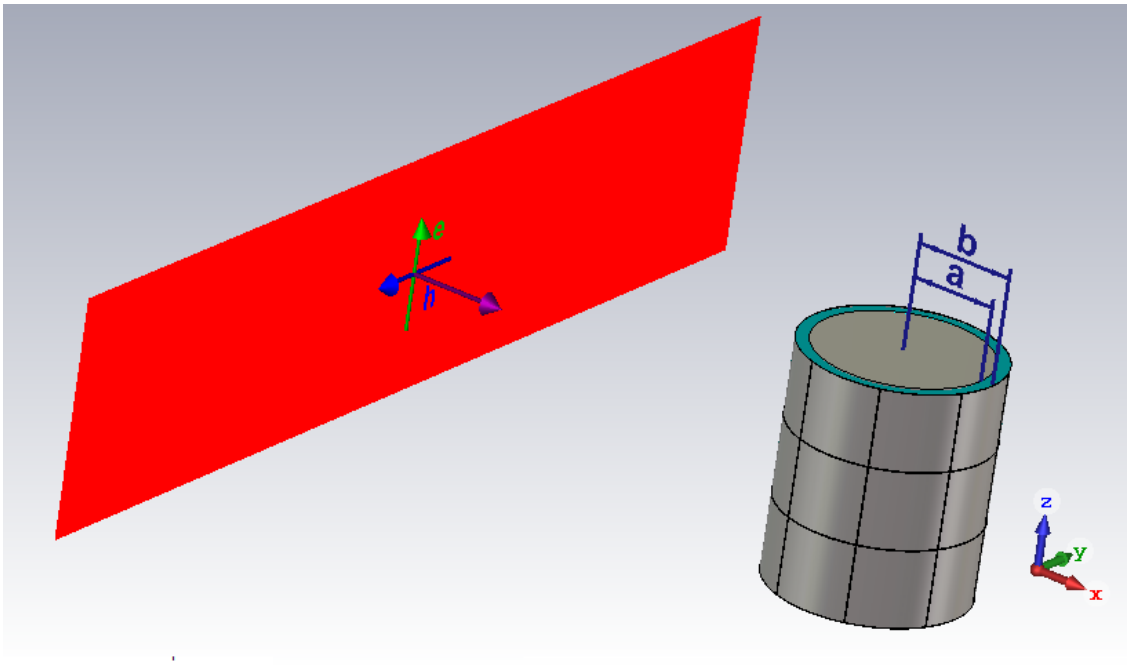

Figure 4.8: Representation of the proposed metasurface cloaked cylinder.

simulation surrounding the bare cylinder and the cylinder cloaked by the square patch metasurface layer are represented. As a reference, the incident planewave is also reported. It can be noticed that, considering the bare cylinder, the field is strongly distorted by the object presence and a shadow can be clearly seen on the back side of the cylinder. However, in the cloaking case, the total field resembles the incident planewave in all directions around the object and the filed phase fronts are reconstructed.

4.1.3 Curvature effect

To compute the surface impedance of the proposed metasurface. a planar surface was considered. However, here the metasurface needs to be bent around the cylinder, having a conformal shape. Therefore, in order to understand the effect of the metasurface curvature on the scattered field, the harmonic composition of the field is examined, and the scattering coefficients are retrieved from the scattered field computed from the full wave simulation of the cylinder.

In fact, recalling that the scattered field in cylindrical coordinates (ρ,φ,z) is expressed as:

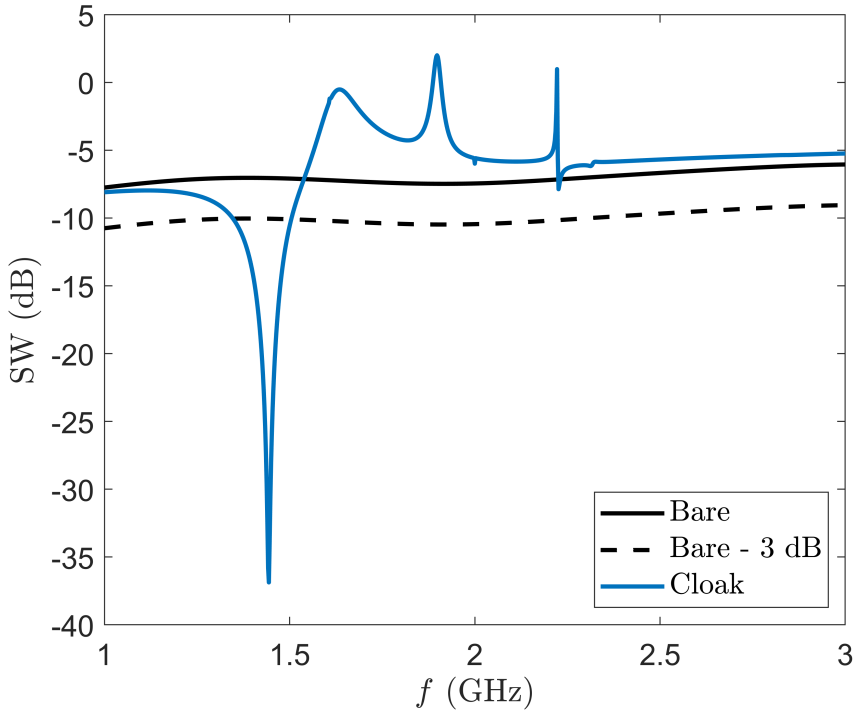

Figure 4.9: SW of the cylinder cloaked with the proposed patch based metasurface, compared with the bare cylinder SW. The resulting cloaking frequency is $f = 1.44$ GHz.

$$\hat{\boldsymbol{z}} E_s(\rho, \varphi) = \hat{\boldsymbol{z}} \sum_{n=-\infty}^{\infty} j^{-n} c_n H_n^{(2)}(k_0 \rho) \exp(jn\varphi) \tag{4.4}$$

it is possible to project $E_s(\rho, \varphi)$ on the exponential functions $\exp(-jl\varphi)$ such that:

$$< E_s(\rho, \varphi), \exp(jl\varphi) > = < \sum_{n=-\infty}^{\infty} j^{-n} c_n H_n^{(2)}(k_0 \rho) \exp(jn\varphi), \exp(jl\varphi) > \tag{4.5}$$

Remembering that:

$$\int_0^{2\pi} \exp(jn\varphi) \exp(-jl\varphi)\, d\varphi = \begin{cases} 0 & n \neq l \\ 2\pi & n = l \end{cases} \tag{4.6}$$

it is obtained:

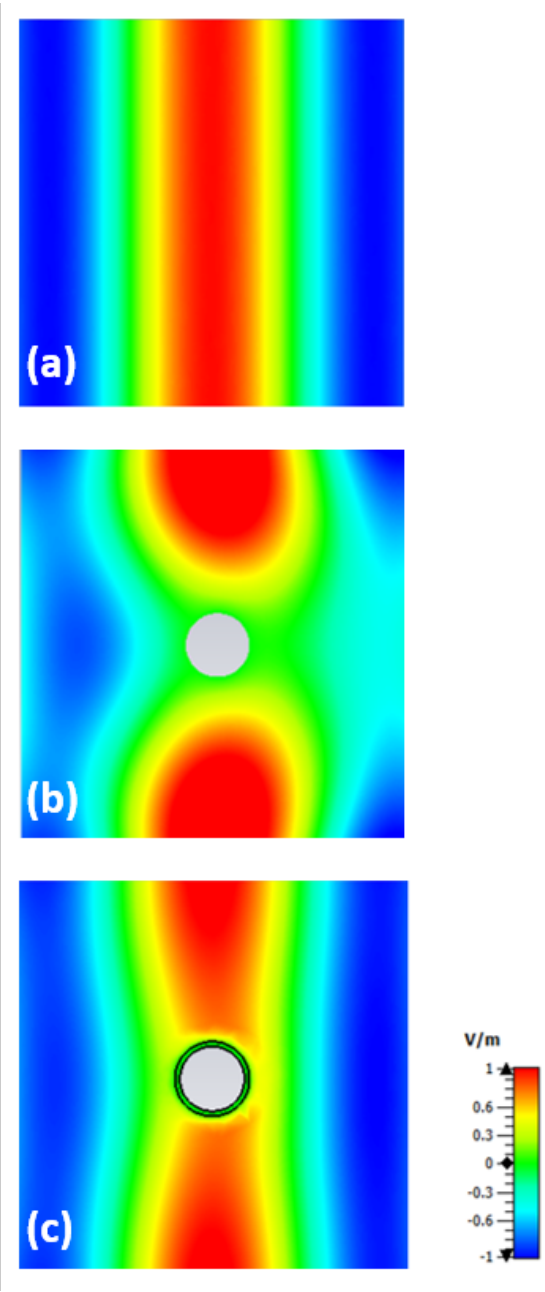

Figure 4.10: Real part of the total electric field surrounding the cylinder. (a) incident planewave (no object is present); (b) bare cylinder; (c) cloaked cylinder.

$$< E_s(\rho,\varphi), \exp(jl\varphi) >= \begin{cases} 0 & n \neq l \\ j^{-l} c_l H_l^{(2)}(k_0\rho) 2\pi & n = l \end{cases} \tag{4.7}$$

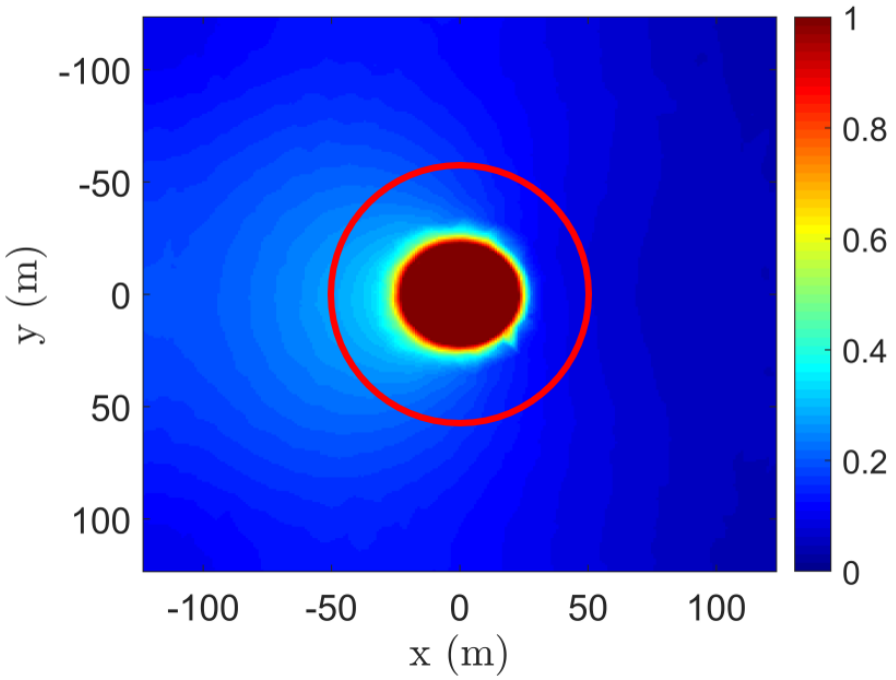

Figure 4.11: Representation of the points of measurements of the scattered field, to retrieve the scattering coefficients (the measurement unit is V/m).

such that the scattering coefficients can be retrieved from the scattered field and they are computed as:

$$c_l = \frac{< E_s(\rho, \varphi), \exp(jl\varphi) >}{j^{-l} H_l^{(2)}(k_0\rho) 2\pi} \tag{4.8}$$

where $E_s(\rho, \varphi)$ is the scattered field, here simulated with CST Studio Suite, computed on an arbitrary circumference around the cylinder as shown in Fig. 4.11. Moreover Fig. 4.11 also reports the absolute value of the electric field scattered by the metasurface cloaked cylinder simulated with CST studio suite at the cloaking frequency $f = 1.44$ GHz.

The consistence of the method is proved first of all by computing the scattering coefficients of a bare conducting cylinder and comparing them with the analytical result. Therefore, the scattered field values evaluated on an arbitrary circumference around the cylinder are retrieved from the simulation, and the scattering coefficients are computed by following Eq. 4.8.

In Fig. 4.12 the results of the scattering coefficients for a bare cylinder with $a = 0.1\lambda$ and $a = 0.5\lambda$ are shown. In particular, different radius of the circumference

in which the scattered field is examined are considered, to prove that the resulting coefficients are independent of the chosen value of the circumference radius. As can be notices, the scattering coefficients retrieved from the full wave simulation with the projection method, are in perfect consistence with the analytical ones.

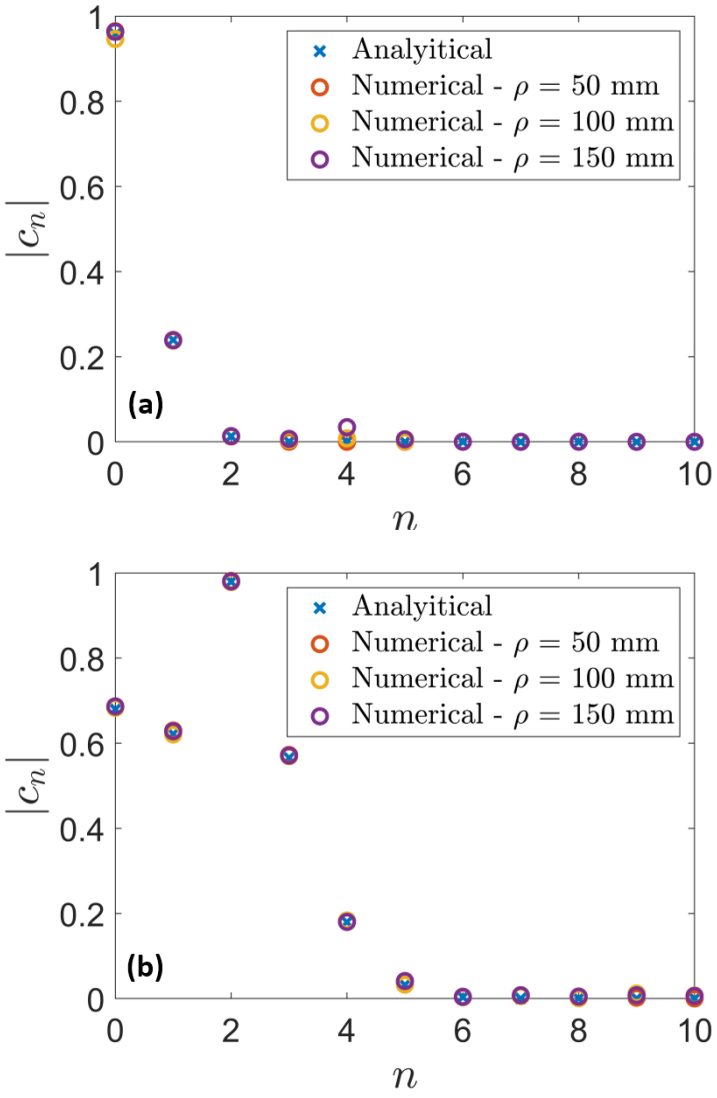

Figure 4.12: Scattering coefficients associated to a bare cylinder with radius $a/\lambda = 0.1$ (a) and $a/\lambda = 0.5$ (b). Comparison between the analytical results and the numerical results computed by using the projection method. Different values of ρ are considered to prove the stability of the results.

A further comparison is shown in Fig. 4.13. In this case, the cloaked cylinder is

considered, however the metasurfaces is substituted by an ideal surface reactance X_s = -40 Ω. The structure is simulated with CST and the coefficients are retrieved form the scattered field at the cloaking frequency and they are compared with their analytical counterpart. Also in this case the results are in perfect agreement.

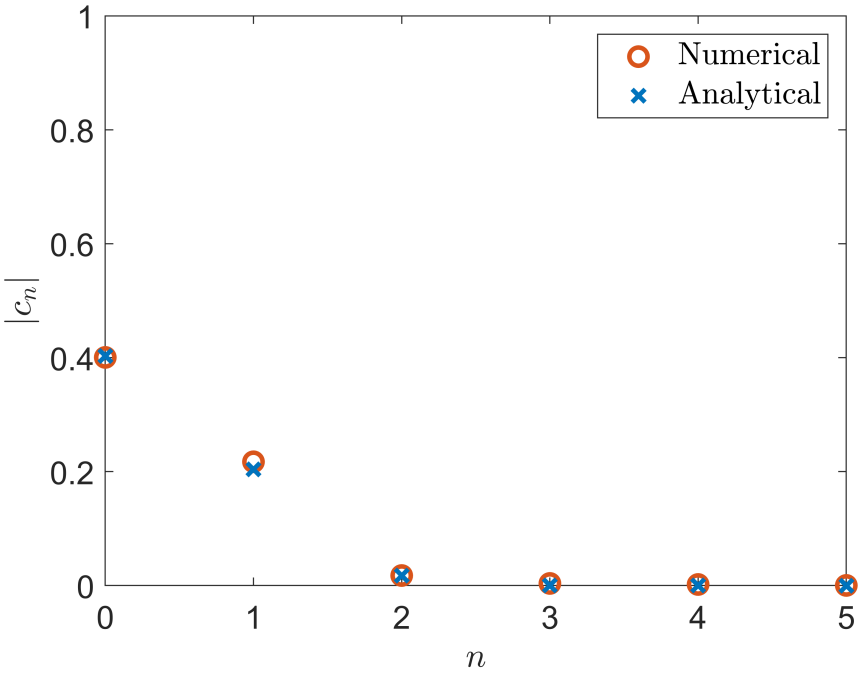

Figure 4.13: Scattering coefficients associated to a cylinder cloaked by an ideal homogeneous surface impedance layer with X_s = -40 Ω. Comparison between the analytical results and the numerical results computed by using the projection method.

Hence, the same analysis is performed considering now the full wave simulation of the scattered field of the cloaked cylinder and the results are reported in Fig. 4.14 In this case, the scattering coefficients derived from the numerical simulation are compared with the ones computed analytically considering a surface impedance of Z_s= -j40 Ω, as designed. As shown in Fig 4.14, while the coefficient c1 has the same absolute value of the analytical prediction, interestingly, it can be seen that the coefficient c0 is lower than analytically predicted. The cause of this mismatch should be searched in the effect of cylindrical curvature of the metasurface.

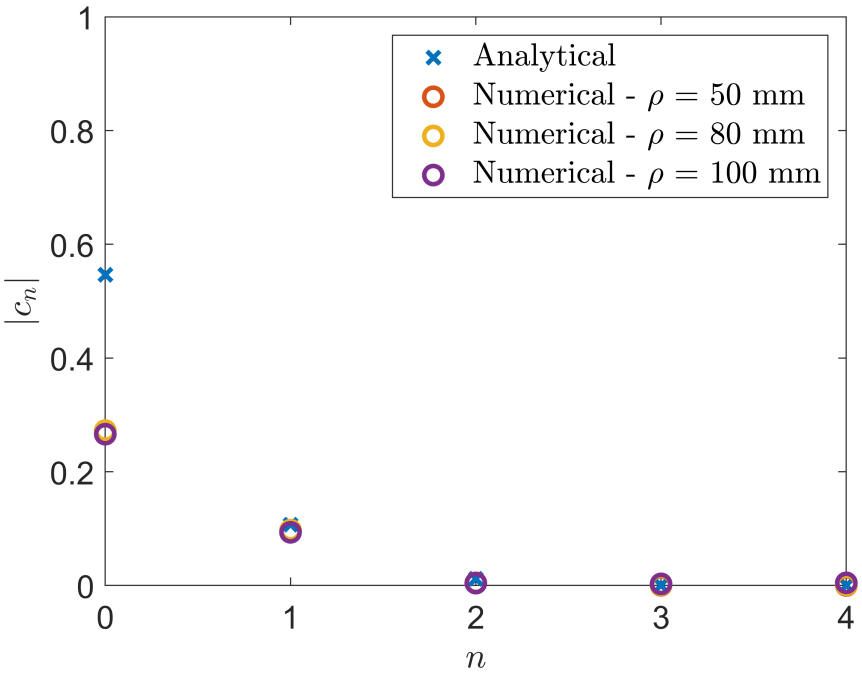

Figure 4.14: Scattering coefficients associated to a cylinder cloaked with the proposed patch metasurface. Comparison between the analytical results considering an ideal surface reactance X_s = -40 Ω and the numerical results computed by using the projection method. Different values of ρ are considered to prove the stability of the results.

4.2 Beyond quasi-static limit

In this section a similar analysis of previous case of study is performed considering the same cylinder at a higher operational frequency.

By looking at the graph in Fig. 3.10, it can be noticed that using a dielectric layer with thickness $t = b - a = 0.15a$ and $\varepsilon_r = 10$ it is possible to obtain a local minimum of the SW when $a/\lambda = 0.92$. In this case, considering $a = 20$ mm, this results in a cloaking frequency $f = 13.8$ GHz.

The scattering coefficients corresponding to the bare cylinder at this frequency are reported in Fig. 4.15. With respect to the previous case, here, a higher number of harmonics composes the scattering. Moreover, the harmonic with $n = 0$ is not the dominant one, but the higher scattering coefficients result to be c_4 and c_1. Moreover, in Fig. 4.16 the surface reactance condition which annuls the different scattering coefficients is shown.

Regarding the cloaking condition, from Fig. 3.10 it can bee seen that the

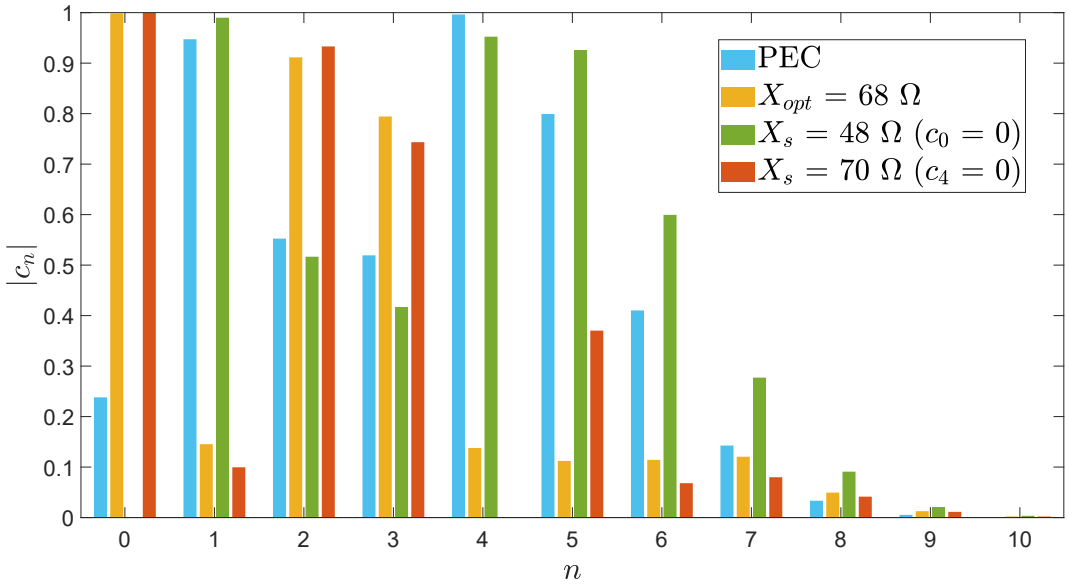

Figure 4.15: Modulus of the scattering coefficients c_n associated to the bare and cloaked cylinders considering different surface impedances values [87] ©2020 Optical Society of America.

required surface reactance to obtain the minimum SW should assume a positive value equal to $X_s = 68\ \Omega$.

In this case, the cloaking surface reactance, $X_s = 68\ \Omega$ is close to the reactance which annuls the scattering coefficient c_4. As a reference also the scattering coefficients obtained by using the reactance which annuls c_0 are shown. This corresponds to $X_s = 48\ \Omega$, much lower than the optimum solution, proving that which an electrically large cylinder is considered, the use of this surface impedance should not be considered as a performing solution to achieve the cloaking effect.

Therefore, in order to achieve the positive surface reactance value $X_s = 68\ \Omega$, for this second case, the metasurface is chosen to be composed of a periodical repetition of metallic striplines [45].

The metasurface unit cell is hence composed by a metallic stripline of width w printed on a dielectric substrate, and periodically repeated with period D.

In this case, the number of unit cell is set to $N = 36$ such that $D = 2\pi b/N = 4.01$ mm.

A parameter sweep is then performed to compute the value of w such that the metasurface impedance is $X_s = 68\ \Omega$ at the design frequency $f = 13.8$ GHz. As illustrated before, the metasurface unit cell is simulated with CST studio suite and the obtained value of X_s are reported in Fig. 4.17. Therefore, to have a value of

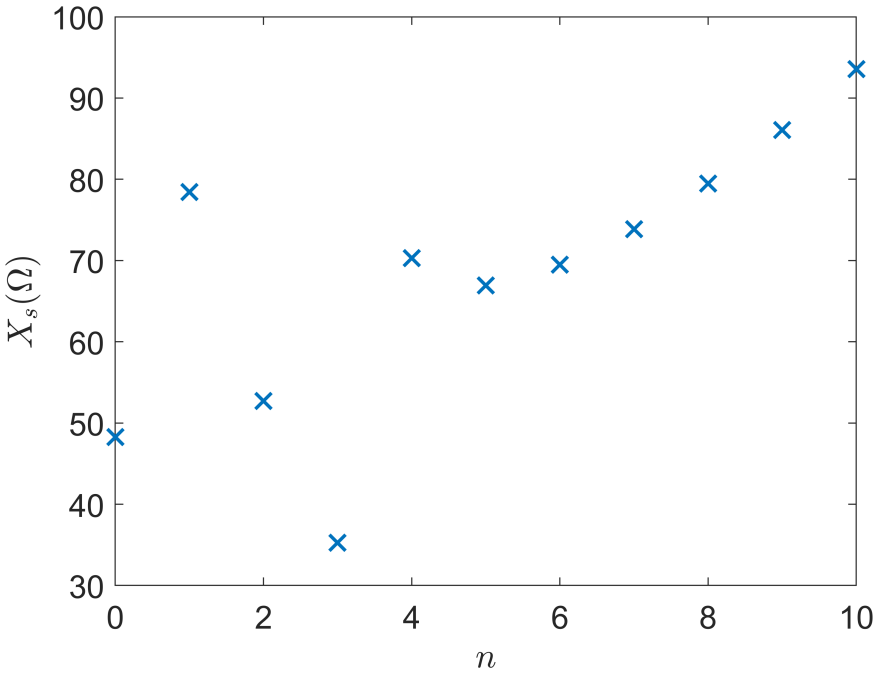

Figure 4.16: Surface reactance that cancel the different scattering coefficients of the proposed cylinder.

$X_s = 68\ \Omega$ it is chosen a stripline width $w = 1.07$ mm and a unit cell length of $D = 4.01$ mm, such that $N = 36$ strips are present on the total surface bent around the cylinder.

In Fig.4.18 the CAD model of the cylinder with the metasurface coat is represented.

The structure is simulated with CST Studio Suite, considering as incident field a TM polarised planewave, and the SW results are reported in Fig. 4.19 comparing them with the SW of a bare cylinder. As it can be noticed, a minimum of the SW it is obtained at a frequency $f = 13.75$ GHz, corresponding to a value of $a/\lambda = 0.917$, and a 4 dB reduction of the SW with respect to the bare value is achieved at the cloaking frequency.

In order to further validate this result, the SW resulting from the numerical simulations is compared with the analytical results for both the bare and the cloaked cylinders.

Regarding the cloaked cylinder, the scattered field is analytically computed following Eq. 3.47 and Eq. 3.2 by considering in the place of Z_s the surface impedances obtained from the numerical simulation of the single unit cell (reported

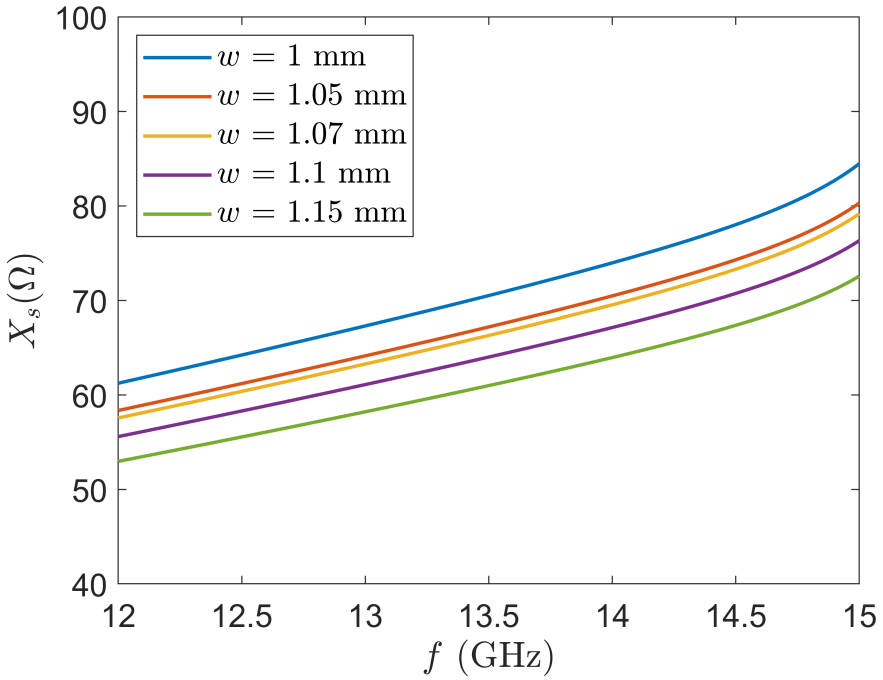

Figure 4.17: Surface reactance of the stripline based metasurface for different design parameters.

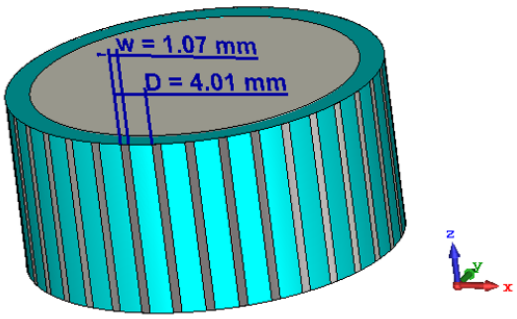

Figure 4.18: CAD model of the cylinder cloaked with the metallic strips based metasurface [87] ©2020 Optical Society of America.

in Fig. 4.17). For this reason, the resulting SW is called semi-analytical.

While, for the bare cylinder, the scattered field is analytically computed firstly evaluating the scattering coefficients (also reported in Fig. 4.15) from Eq. 3.6, than computing the scattered field following Eq. 3.2. Finally the scattered field is placed in Eq. 3.60 to obtain the resulting SW.

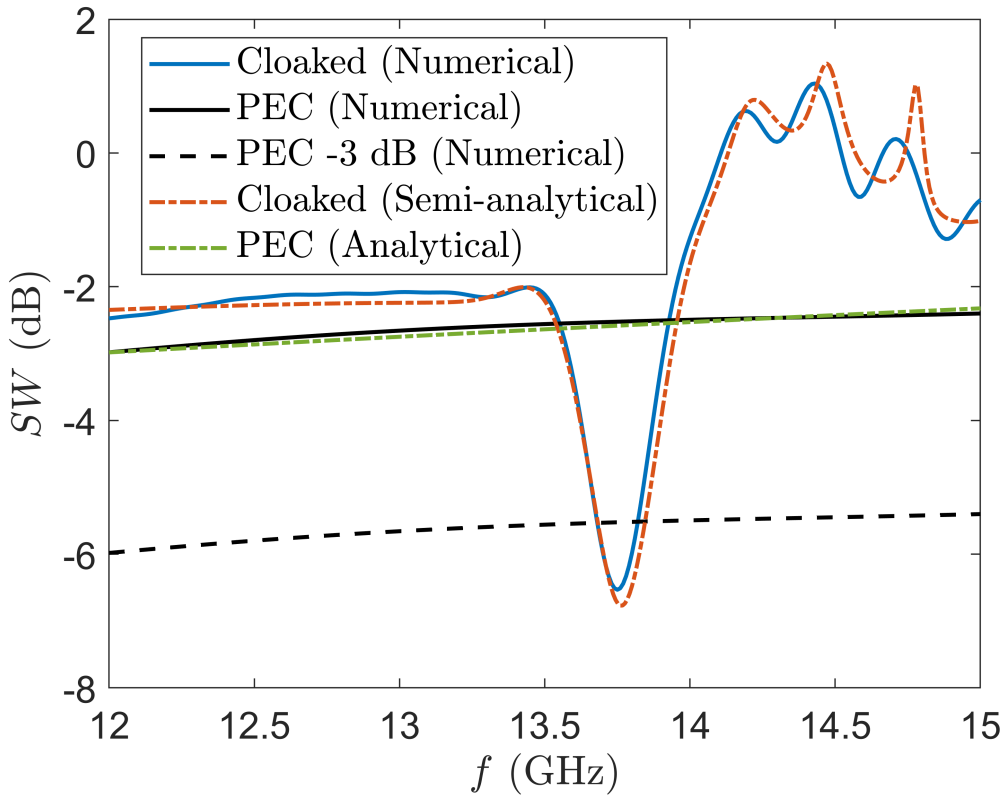

Figure 4.19: Simulated SW of the bare and cloaked cylinders. Comparison of the numerical and the (semi-) analytical results [87] ©2020 Optical Society of America.

It should also be underlined that for both the cloaked and the bare structure the SW is computed considering in Eq. 3.2 a value of $\rho = 150$ mm.

The comparison between (semi-)analytical and numerical results shows that they are in excellent agreement as it can be seen in Fig. 4.19, proving the validity of the theoretical analysis performed in Ch. 3.

Furthermore, the absolute value of the scattered field resulting from the numerical simulations is show in Fig. 4.20 for the bare and the cloaked cases at the cloaking frequency $f = 13.75$ GHz. Even if due to the cylinder diameter, the scattered field of the cloaked cylinder is higher than the one of the quasi-static case, the reduction with respect to the bare cylinder can be clearly noticed.

An additional analysis of the scattering harmonic composition is performed. Therefore, the scattering coefficients are numerically retrieved from the scattered field at the cloaking frequency $f = 1.45$ GHz, following the previously presented approach.

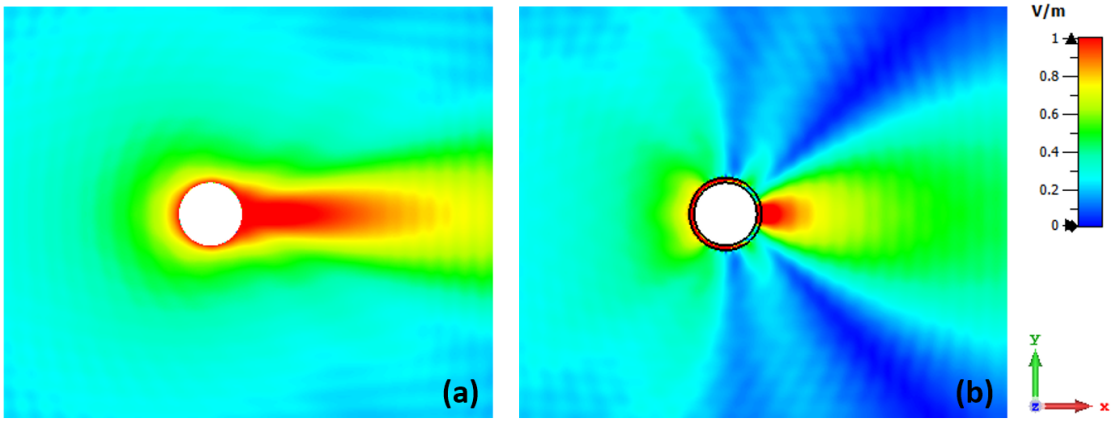

Figure 4.20: Absolute value of the scattered electric fields resulting from the numerical simulation. Comparison of the bare case (a) and the cloaked cylinder (b), with the proposed stripline metasurface, at the cloaking frequency $f = 13.75$ GHz [87] ©2020 Optical Society of America.

The comparison between the numerically retrieved coefficients and the analytical ones is shown in Fig. 4.21. It can be noticed that in this case the results are in excellent agreement and the mismatch is negligible.

This is due to the fact that the curvature of the cylinder is now higher with respect to the incident field wavelength and the metasurface can be therefore well approximated by a planar structure.

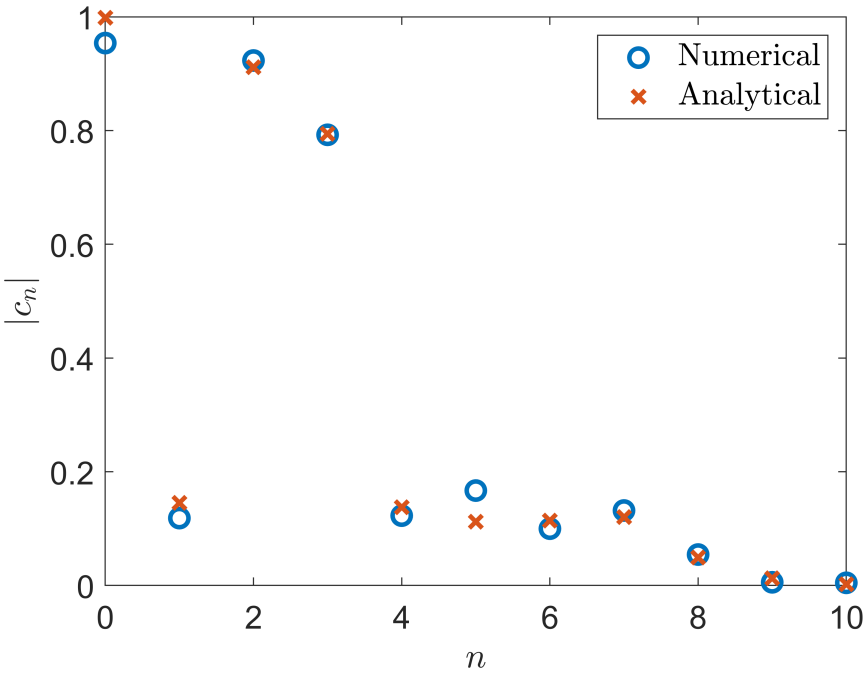

Figure 4.21: Comparison between the scattering coefficients of the cloaked cylinder with the stripline based metasurface. Comparison between numerical and analytical values. It can be seen that in this case the results are in excellent agreement due to the higher curvature radius of the cylinder with respect to the incident field wavelength.

Chapter 5

Inhomogeneous surface impedance

Part of the work described in this Chapter was also previously published in [97].

5.1 Introduction

In the last Chapter, the cloaking of metallic cylinders by using homogeneous metasurfaces has been examined and it has been explained how to design a proper metasurface to reduce the field scattered by the cylinder. However, the limitation of a homogeneous metasurface were discussed. In particular, it was demonstrated that the use of a homogeneous metasurface can cancel only one harmonic of the scattered field and therefore it offers limited cloaking effect in case of electrically large structures, for which the scattered field has a richer harmonic composition, even if a partial reduction of the scattering can be obtained by properly designing the metasurface.

To overcome these limitations, different approaches can be followed. One of the simplest strategy to adopt is to use multiple cloaking coats. Indeed, the inclusion of a second cloaking layer introduces an additional degree of freedom, giving the possibility to annul two different harmonics order at the same frequency. Another option is the use of active elements, which allows to have control on the surface impedance dispersion of the employed metasurface.

However, in the first case, the cloaking layer dimension becomes important, increasing the total dimension of the structure, while in the second case, the cloaking design would be more complex and expensive.

Therefore, in this chapter the use of inhomogeneous passive metasurfaces is proposed. This method consists into the use of a metasurface realised with a semi-periodical pattern of unit cells, this means that the unit cells have different dimensions one from another.

In particular, the metasurface is considered inhomogeneous on the azimuthal direction, while the unit cells are repeated periodically in the longitudinal direction.

5.2 Electrically small cylinders

The first proposed structure is based on a square patch metasurface which in previous chapter has been used to cloak an electrically small cylinder with normalised radius a/λ=0.1.

To design the inhomogeneous metasurface, the design proposed in Sec. 4.1 is taken as a starting point. In that case, the metasurface was homogeneous and consisted in a periodic repetition of identical metallic square patches printed on a dielectric layer.

In this inhomogeneous case is therefore decided to combine two patches with different lengths. In particular, the metasurface is composed of the repetition of a macro unit cell, which is in turn composed of the combination of two sub unit cells, namely cell A and cell B.

In a first case, the macro cell consists of one cell A and one cell B, place adjacently. Therefore, the complete metasurface is formed by the alternating repetition of one cell A and one cell B as reported in Fig. 5.1.

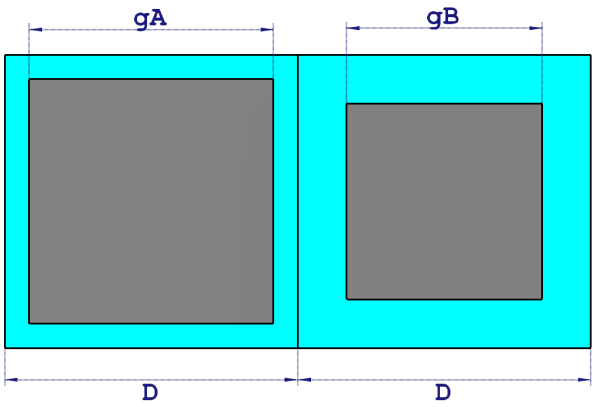

Figure 5.1: Macro cell of the proposed inhomogeneous metasurfaces. [97].

The two sub unit cells have the same length of the dielectric layer, such that $D_A = D_B = D = 18$ mm for both the two cells, while for cell A the length of the metallic patch is fixed to $g_A = D - w_A = 17.8$ and the one of cell B, $g_B = D - w_B$ is varied and a parameter sweep is performed to understand the effect on the scattered field.

In Fig 5.2 the SW results for different w_B are shown, comparing them with both the bare cylinder and the homogeneous metasurface. As can be noticed, in this case there are no significant improvements in the SW response with respect to the homogeneous structure neither in term of SW reduction or cloaking bandwidth.

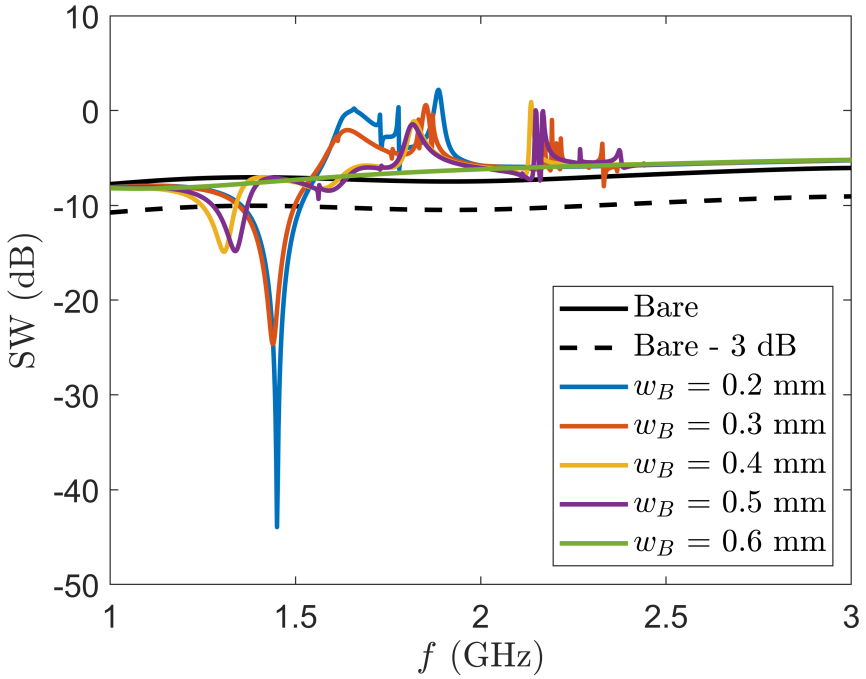

Figure 5.2: SW results considering the proposed inhomogeneous metasurface design for different values of w_B.

Therefore, it is decided to increment the period of the two sub unit cells, such that the macro-cell is composed by two subsequent unit cells of type A and two unit cells of type B, and it is reported in Fig. 5.3. Also for this second structure, w_A is fixed to 2 mm, while w_B varies from 0.2 mm to 1 mm.

The obtained SW with this inhomogeneous cloaking is reported in Fig. 5.4. In this case it is evident the presence of a second minimum of the SW around 2.2 GHz, which is more pronounced as the value of w_B increases. Moreover, the first cloaking frequency, gradually shifts towards 1.6 GHz as w_B increases (and consequently the length of the metallic patch of cell B decreases).

Therefore, the use of an inhomogeneous metasurface allows to achieve two different cloaking frequencies, without the addition of a second cloaking layer and can be an optimum solution for dual-band applications.

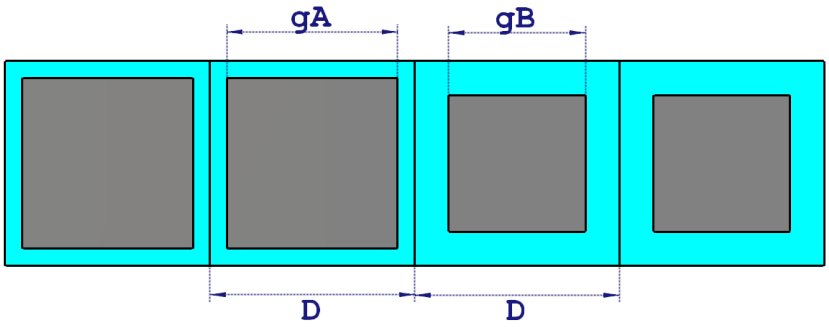

Figure 5.3: Macro cell of the proposed inhomogeneous metasurfaces. [97].

5.3 Beyond quasi-static limit

Following the approach of previous section, as a second case of study, the square patch is applied to a non electrically small cylinder and its performances are compared to the ones of a homogeneous metasurface in terms of scattering reduction and cloaking bandwidth.

Similarly to previous examples, the cloaked cylinder has a radius of $a = 20$ mm and the dielectric coat has a thickness of $t = 0.15a$, leading to a total radius of the cloaked cylinder equal to $b = 1{,}15a = 23$ mm, while the relative permittivity of the dielectric layer is now considered $\varepsilon_r = 2$.

In order to have and integer number of unit cells on the azimuthal direction it is decided to use N= 12 cells. In this way the total length of a unit cell is equal to $D = 2\pi b/N = 12.04$ mm.

First, the homogeneous case is taken into account, and the separation between two metallic patches is fixed to $w_1 = 2$ mm, such that the metallic patch length is set to $g_1 = D - w_1 = 10.04$ mm. The SW of the homogeneous structure is reported in Fig. 5.5 (blue curve). It can be noticed that the correspondent cloaking frequency is $f_1 = 6$ GHz, such that ratio between the cylinder radius and the free space wavelength corresponds to $a/\lambda_1 = 0.4$.

Than, in order to further increase the cloaking bandwidth and the SW reduction, following the approach presented previously, it is decided to employ an inhomogeneous metasurface combining two different sub unit cells, namely cell A and cell B, such that a combination of the two sub-unit cells compose a macro-cell, which is turn periodically repeated to compose the total metasurface.

In this case, it is decided to use a different arrangement of the two patches such to have a macro cell composed by three cells of type A followed by three cells of

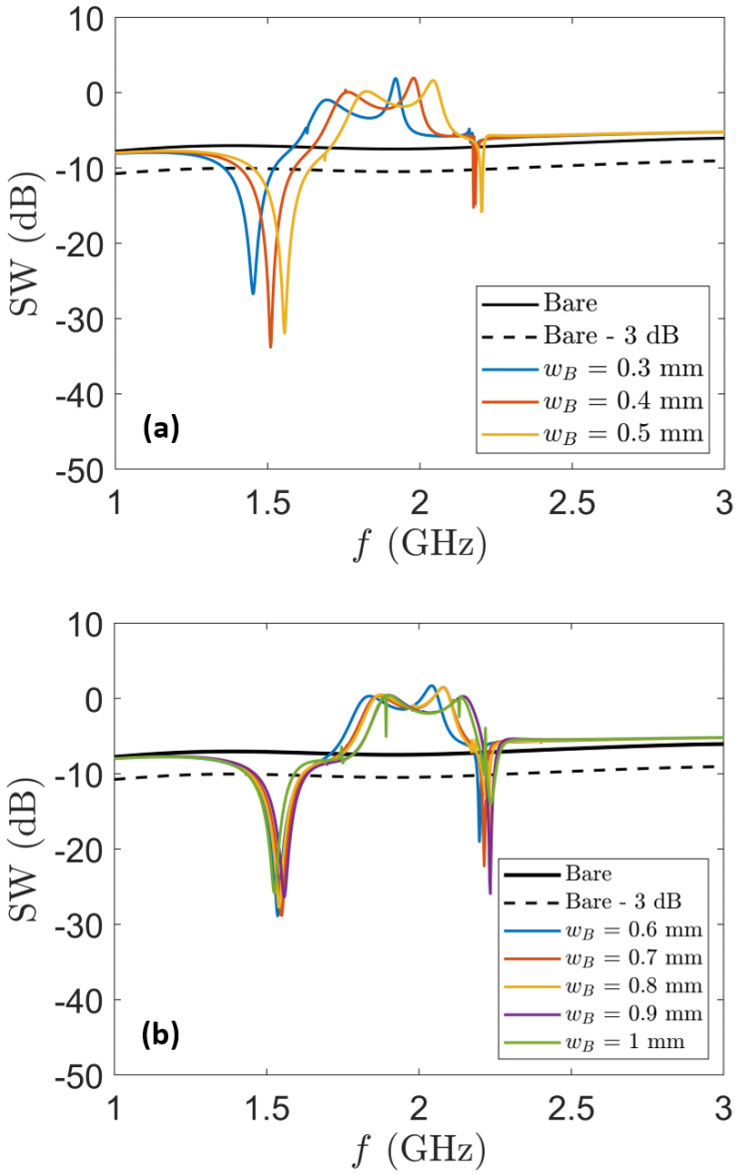

Figure 5.4: SW results considering the proposed inhomogeneous metasurface design for different values of w_B.

type B so that the macro cell will be the one represented in Fig. 5.6.

Regarding cell A, $D - w_A = g_A$ is fixed to the constant value $g_A = g_1 = 2$mm. Then, a parameter sweep of w_B is performed, starting from $w_B = 2$mm (homogeneous case), to $w_B = 5$ mm and the SW resulting from the parameter sweep are

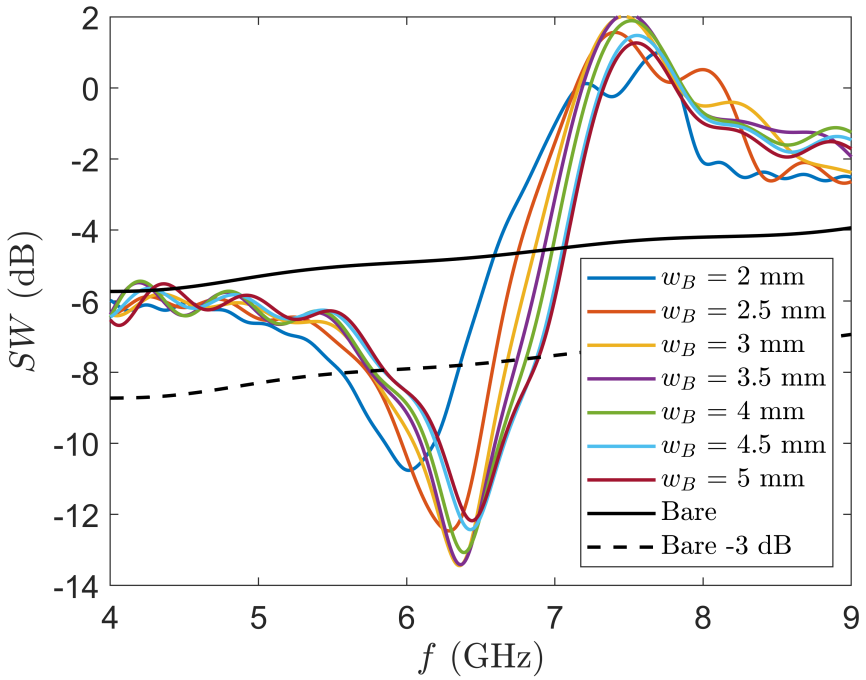

Figure 5.5: SW results considering the proposed inhomogeneous metasurface design for different values of w_B.

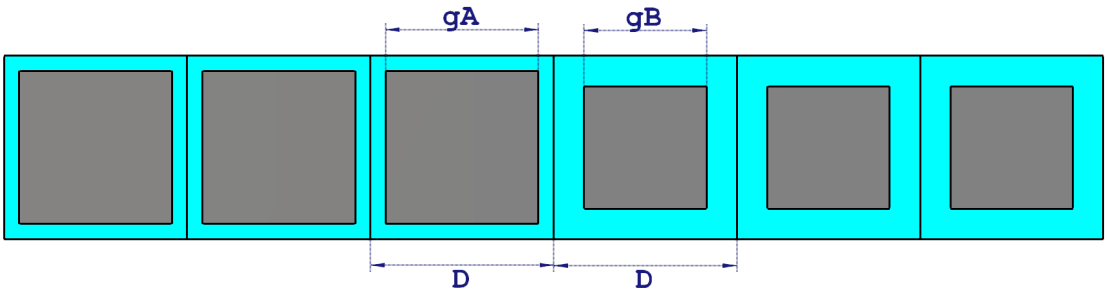

Figure 5.6: Macro cell of the proposed inhomogeneous metasurfaces [97] ©2020 IEEE

reported in Fig. 5.5. It can be noticed that the increasing of w_B has the effect of increasing the SW reduction and the cloaking bandwidth, with a slightly shift of the cloaking frequency toward 6.4 GHz.

Furthermore, by looking at the SW results in Fig. 5.5 it is noticed that the optimum value of w_B which leads to both a greater SW reduction and cloaking bandwidth is $w_B = 4$ mm.

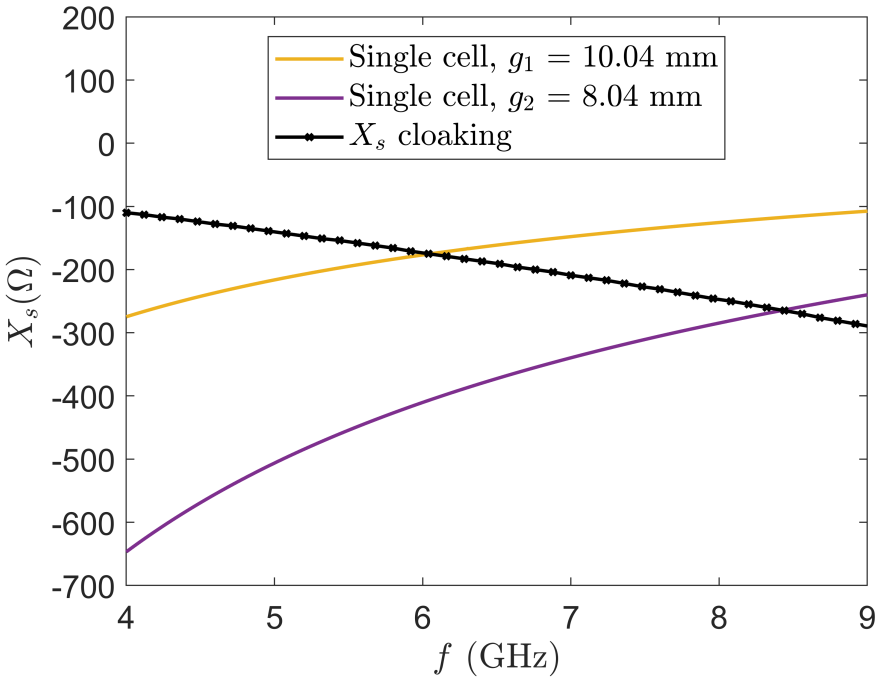

Figure 5.7: Intersection between the optimum cloaking reactance and the homogeneous metasurface reactance.

Moreover, the surface reactance of the inhomogeneous metasurface considering $w_1 = 2$ mm and $w_2 = 4$ mm are reported inf Fig. 5.7. Also the optimum cloaking surface reactance is shown, and it can be seen that it intersect the metasurface reactance curve at the two cloaking frequencies.

Therefore, the cloaking performance of the inhomogeneous metasurface composed by the macro-cell represented in Fig. 5.6 are reported in Fig. 5.8 comparing the SW with the one obtained with a homogeneous metasurface considering w_1 =2 mm and $w_2 = 4$ mm, respectively.

It can be seen that, in the inhomogeneous case, the cloaking effect is increased, and the SW is further reduced with respect the use of a single homogeneous cell, reaching a reduction of 8.2 dB with respect to the bare case the frequency $f =$ 6.4 GHz which corresponds to a normalised cylinder radius $a/\lambda = 0.43$, while in the homogeneous case, the SW reduction was equal to 5.85 dB. Furthermore, the cloaking bandwidth is also increased, reaching a value of 16.4%.

Moreover, the absolute value of scattered field at the three cloaking frequencies, $f_A = 6$ GHz, $f_B = 8.1$ GHz (homogeneous metasurfaces) and $f = 6.4$ GHz (inhomogeneous metasurface), is represented in Fig. 5.9. It can be clearly seen

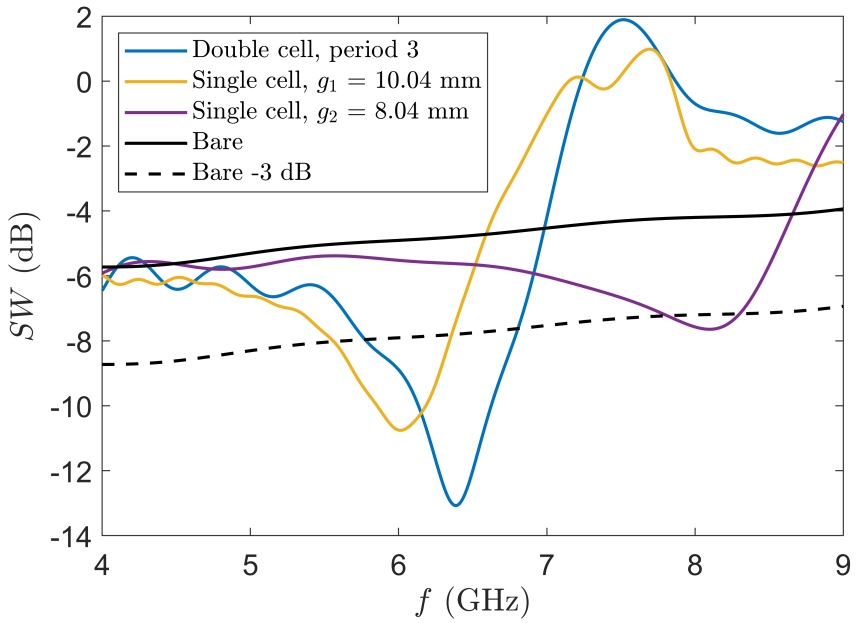

Figure 5.8: SW of the cloaked structures for different metasurface configurations, compared to the bare metallic cylinder results. With the double cell configuration the scattering reduction and the bandwidth are increased [97] ©2020 IEEE.

that with the use of the inhomogeneous metasurface, the scattered field is further reduced with respect to the homogeneous case, improving the cloaking effect.

Furthermore, an harmonic analysis of the scattered field is performed. Therefore, the scattering coefficients are retrieved from the numerical simulation of the scattered, evaluated on an arbitrary circumference around the cylinder, following the procedure explained in section 4.1.

The scattering coefficients associated to both the bare cylinder and the cloaked one are computed at the three cloaking frequencies: $f = 6$ GHz and $f = 8.1$ GHz, corresponding to the homogeneous structure with $w_1 = 2$ mm and $w_2 = 4$ mm, respectively, and $f = 6.4$ GHz, corresponding to the inhomogeneous metasurface.

For the bare case, the numerically retrieved coefficients are compared to the analytically ones, computed following Eq. 3.6 and, as can be noticed in Fig 5.10 they are in perfect agreement. In particular, the scattering coefficients up to c_5 are present and, the harmonics with index $n = 1$ and $n = 2$ dominates in the first case for which $w_1 = 2$ mm and $f = 6$ GHz, wile $n = 0$, $n = 2$, $n = 3$, in the second ($w_2 = 4$ mm, $f = 8.1$ GHz).

The coefficients associated with the cloaked structures are computed only numerically, and different values of the circumference radius on which the scattered

field is evaluated, in order to examine the stability of the results. Indeed, it can be seen that the resulting scattering coefficients are independent on the chosen circumference, and, more interestingly, it appears that, for the inhomogeneous case, the modulus of all the scattering coefficients it is lowered under 0.5.

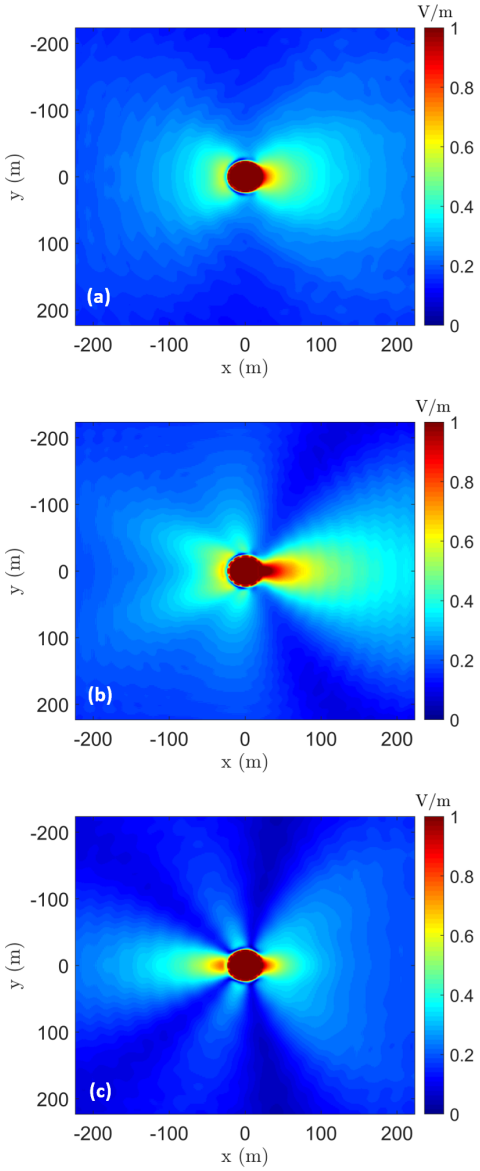

Figure 5.9: Scattered field with the homogeneous square patch metasurface at f_1 = 6 GHz (a), f_2 = 8.1 GHz (b) and with the inhomogeneous metasurface at f = 6.4 GHz (c).

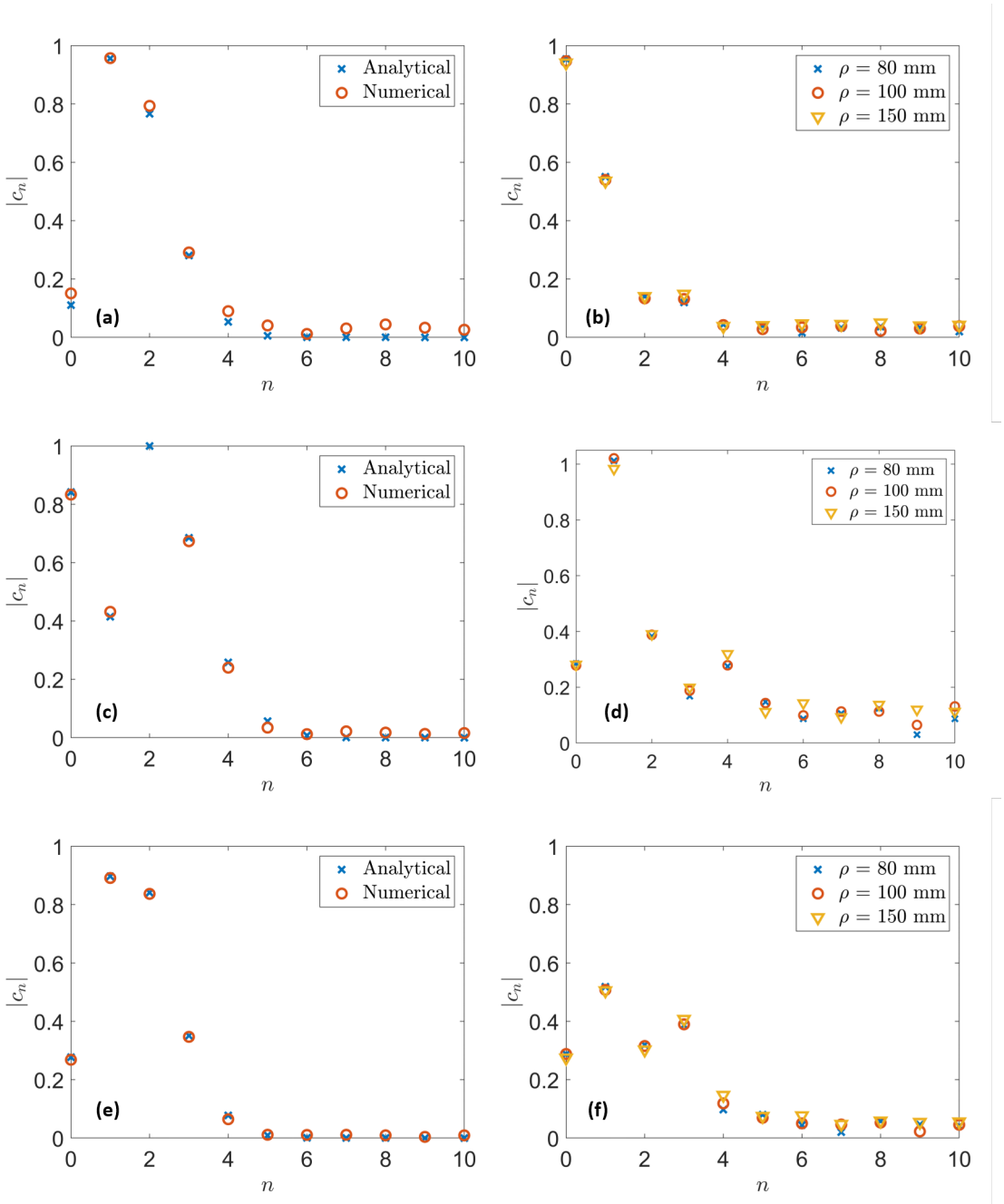

Figure 5.10: Scattering coefficients associated to the bare (a, c, e) and the cloaked (b, d, f) cylinder, at the cloaking frequencies $f_1 = 6$ GHz (a, b), $f_2 = 8.1$ GHz (c, d) considering homogeneous metasurface, and $f = 6.4$ GHz (e, f), with the inhomogeneous metasurface. The bare results are computed both analytically and numerically, the cloaked ones are computed only numerically considering different values of ρ.

The only limitation in this case is that with the use of this inhomogeneous metasurface, the SW results depend on the direction of incidence of the illuminating planewave. Indeed, in Fig. 5.11 the SW is reported considering a shift of 90 degrees of the incident field on the plane normal to the cylinder axis (the incident field is still parallel to the cylinder axis).

It can be noticed that in this case the cloaking effect is not present and the maximum SW reduction is equal to 2 dB when $f = 8.75$ GHz.

However, this is not a problem for all the applications in which the incidence angle of the illuminating field is known, for example if a fixed obstacle is present in the proximity of an antenna.

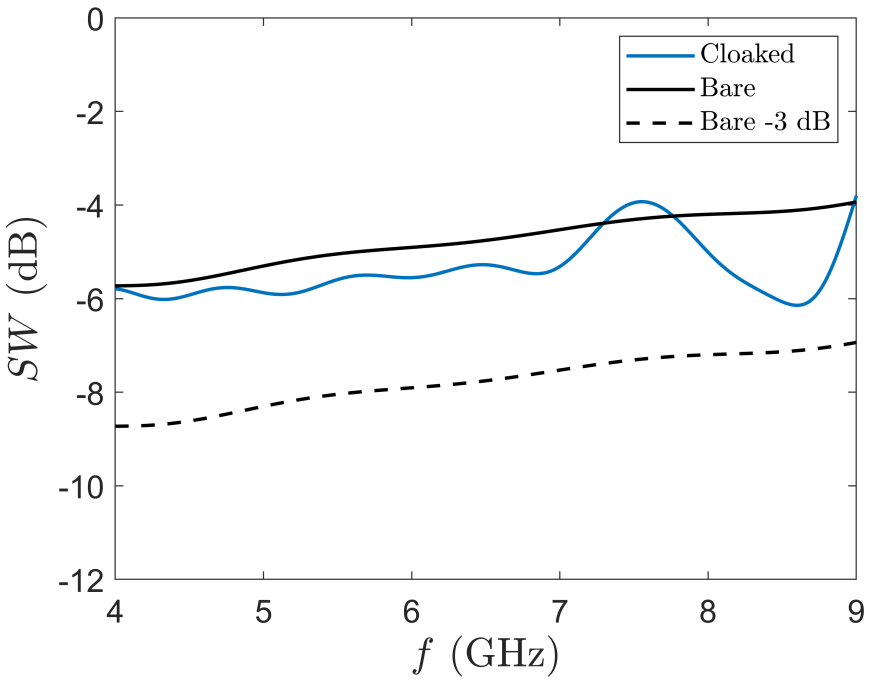

Figure 5.11: SW of the cylinder cloaked by the inhomogenous metasurface for a 90 degree shift of the incident field.

A second example of the use of an inhomogenous metasurface beyond the quasi-static limit is proposed,starting from the design of the stripline unit cell presented in Sec. 4.2.

Indeed, it was shown that with the homogeneous configuration, based on the stripline metasurface is possible to partially reduce the scattering when the cylinder radius is comparable with the wavelength of the incident field.

It is now decided to modify the proposed metasurface and to use striplines with

different width such to increase the scattering reduction.

In the homogeneous configuration, $N = 36$ repetition of the unit cell in the azimuthal direction the cylinder boundary was employed. Now, based on the results obtained previously, it is decided to alternate nine striplines of width w_A and nine of width w_B, such to have also in this case a total number of strips $N = 36$.

The value of w_A is fixed as in the homogeneous structure at $w_A = 1.07$ mm, while a parameter sweep of w_B is performed and w_B is varied from 1.2 mm to 1.7 mm. The SW results for different w_B are reported in Fig. 5.12

It can be seen that there is an improvement in the scattering reduction with respect to the homogeneous case, combined to a slight increase of the cloaking frequency. The lower SW is obtained for $w_B = 1.4$ mm. Indeed, with this value, the SW reduction with respect to the bare case of equal to 9.4 dB at the cloaking frequency $f = 13.9$ GHz, which corresponds to a normalized cylinder radius $a/\lambda = 0.93$.

This is a strong improvement with respect to the 4 dB reduction obtained with the homogeneous case.

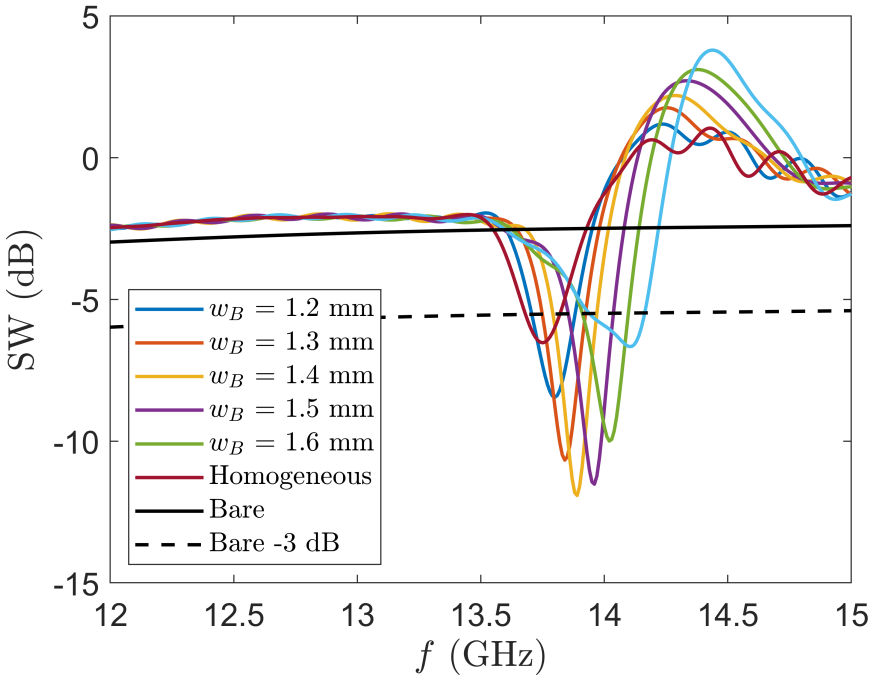

Figure 5.12: SW results considering the proposed inhomogeneous metasurface design for different values of w_B.

The absolute value of the scattered electric field at the cloaking frequency $f =$

13.9 GHz, obtained with the use of the inhomogeneous metasurface considering w_B = 1.4 mm is reported in Fig. 5.13. The comparison with the corresponding bare result shows a significant reduction of the scattering.

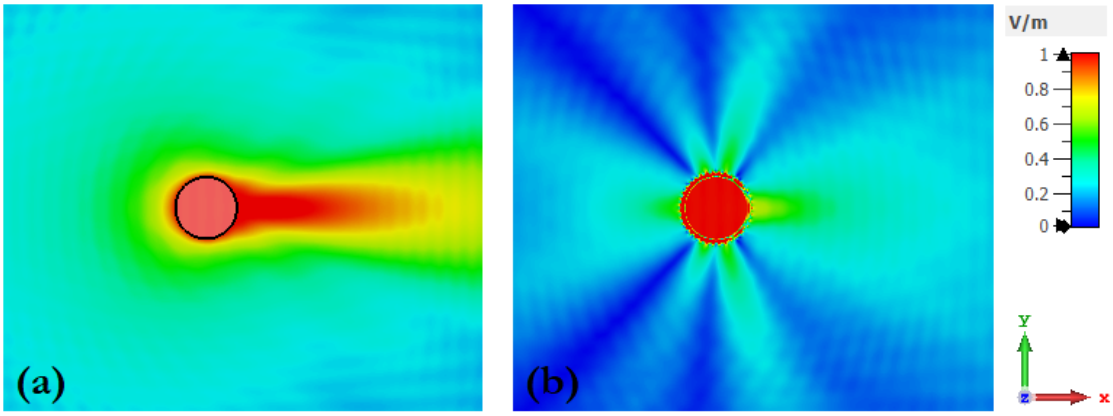

Figure 5.13: Absolute value of the electric field scattered by the bare (a) and the cloaked cylinder with the inhomogeneous stripline based metasurface, at the cloaking frequencies f_1 = 13.9 GHz.

Moreover, the analysis of the scattering coefficients is performed by using the projection method presented previously, and it is reported in Fig. 5.14. For the bare case the predominant coefficients are c_4, c_1 and c_5. It can be seen that with the presence of the inhomogeneous metasurface coat, the coefficients are strongly reduced, and the two dominant coefficients are now c_3 and c_1, however, their value does not exceed 0.6.

Therefore, the use of an inhomogeneous metasurface can be useful to improve the cloaking of cylinders also beyond the quasi-static limit, in all those cases in which the incident field direction is known. Without the addition of a second cloaking layer of the use of active elements, it can be used to both have a dual band application or to further reduce the scattering and to improve the cloaking bandwidth.

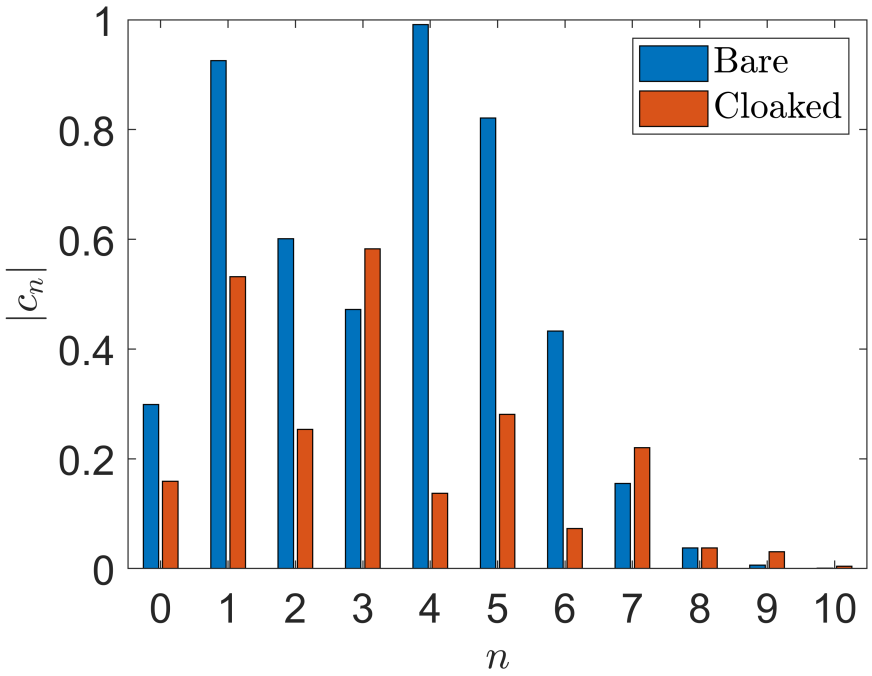

Figure 5.14: Scattering coefficients associated to the bare and the cloaked cylinder considering the inhomogeneous stripline based metasurface, at the cloaking frequencies $f_1 = 13.9$ GHz.

Chapter 6

Conclusions

In this dissertation an analysis of the electromagnetic cloaking of metallic cylinder has been proposed by exploiting thin passive metasurface cloaking.

A particular attention was given to the harmonic composition of the field scattered by a metasurface cloaked cylinder, showing how the metasurface affects the scattering coefficients and the harmonic composition of the scattered field. The metasurface was first considered homogeneous and it was modeled as a surface impedance boundary condition imposed on the cylinder boundary, moreover a dielectric layer needs to be presents between the cylinder and the metasurface in the case of metallic structures.

A closed form formulation of the scattering coefficients associated to the metasurface coated cylinder was derived. Moreover, an analytical expression of the surface impedance condition which annuls a scattering harmonics is computed in a closed and compact form.

An analysis of the surface impedance which minimises the scattered field is performed for different design parameters of the dielectric layer and the cylinder radius. It was shown that for electrically small cylinder, for which the radius is much smaller than the wavelength of the incident field, a minimum of the scattering is obtained when a negative value of surface reactance is considered, however, it is proven that beyond the low frequency regime is still possible to partially reduce the scattered field even with passive single layer metasurfaces by employing an inductive value of surface impedance.

In the second part of the dissertation, the analysis performed in the first part was applied to the realisation of a practically metasurface cloaking. An example of a simple metasurface design based on a square patch unit cell was proposed to cloaking an electrically small cylinder, giving indication to compute the design

parameters value such to obtain the proper surface impedance and showing the strong scattering reduction caused by the metasurface.

The same concepts were then adjusted for the cloaking of a cylinder with radius comparable with the wavelength of the incident field. In this case a metallic strip based metasurface was considered to obtain the inductive surface reactance required to minimize the scattering.

Then, in order to enlarge the cloaking bandwidth and to further reduce the scattered field, an inhomogeneous metasurface is proposed. Starting from the homogeneous design of the square patch metasurface, it was demonstrated that by using two patches with different length and by opportunely arranging them, it is possible to improve the cloaking performances, and a reduction of 8.2 dB of the scattering width (which is a measure of the scattered field power) and a bandwidth of 16.4% was obtained for a cylinder with normalised radius with respect to the incident field wavelength λ equal to 0.43λ.

Moreover, an inhomogeneous metasurface based on the arrangement of metallic strips unit cells with different widths was also proposed to improve the cloaking of a cylinder with radius comparable with the incident field wavelength. It was shown that with the proposed metasurface, a reduction of 9.4 dB of the scattering width with respect to the bare cylinder case is obtained for a value of $a/\lambda = 0.93$.

Bibliography

[1] M. Kerker, "Invisible bodies", *J. Opt. Soc. Am.*, vol. 65, no. 4, pp. 376–379, 1975.

[2] H. Chew and M. Kerker, "Abnormally low electromagnetic scattering cross sections", *J. Opt. Soc. Am.*, vol. 66, no. 5, pp. 445–449, 1976.

[3] R. M. Walser, "Electromagnetic metamaterials", in *Complex Mediums II: Beyond Linear Isotropic Dielectrics*, A. Lakhtakia, W. S. Weiglhofer, and I. J. Hodgkinson, Eds., International Society for Optics and Photonics, vol. 4467, SPIE, 2001, pp. 1–15.

[4] V. G. Veselago, "The electrodinamics of substances with simultaneously negative values of ε and μ", *Soviet Physics Uspekhi*, vol. 10, no. 4, pp. 509–514, 1968.

[5] J. B. Pendry, A. J. Holden, D. J. Robbins, and W. J. Stewart, "Magnetism from conductors and enhanced nonlinear phenomena", *IEEE Trans. Microwave Theory Tech.*, vol. 47, no. 11, pp. 2075–2084, 1999.

[6] D. R. Smith, W. J. Padilla, D. C. Vier, S. C. Nemat-Nasser, and S. Schultz, "Composite medium with simultaneously negative permeability and permittivity", *Phys. Rev. Lett.*, vol. 84, pp. 4184–4187, 18 2000.

[7] J. B. Pendry, "Negative refraction makes a perfect lens", *Phys. Rev. Lett.*, vol. 85, pp. 3966–3969, 18 2000.

[8] R. A. Shelby, D. R. Smith, and S. Schultz, "Experimental verification of a negative index of refraction", *Science*, vol. 292, no. 5514, pp. 77–79, 2001.

[9] D. R. Smith, J. B. Pendry, and M. C. K. Wiltshire, "Metamaterials and negative refractive index", *Science*, vol. 305, no. 5685, pp. 788–792, 2004.

[10] W. J. Padilla, D. N. Basov, and D. R. Smith, "Negative refractive index metamaterials", *Materials Today*, vol. 9, no. 7, pp. 28–35, 2006.

[11] E. Abdo-Sánchez, M. Chen, A. Epstein, and G. V. Eleftheriades, "A leaky-wave antenna with controlled radiation Using a bianisotropic Huygens' metasurface", *IEEE Trans. Antennas Propag.*, vol. 67, no. 1, pp. 108–120, 2019.

[12] S. Ramalingam, C. A. Balanis, C. R. Birtcher, S. Pandi, and H. N. Shaman, "Axially modulated cylindrical metasurface leaky-wave antennas", *IEEE Antennas Wireless Propag. Letters*, vol. 17, no. 1, pp. 130–133, 2018.

[13] J. Chen, W. Yuan, C. Zhang, W. X. Tang, L. Wang, Q. Cheng, and T. J. Cui, "Wideband leaky-wave antennas loaded with gradient metasurface for fixed-beam radiations with customized tilting angles", *IEEE Trans. Antennas Propag.*, vol. 68, no. 1, pp. 161–170, 2020.

[14] X. Liu, K. Fan, I. V. Shadrivov, and W. J. Padilla, "Experimental realization of a terahertz all-dielectric metasurface absorber", *Opt. Express*, vol. 25, no. 1, pp. 191–201, 2017.

[15] Y. Yao, R. Shankar, M. A. Kats, Y. Song, J. Kong, M. Loncar, and F. Capasso, "Electrically tunable metasurface perfect absorbers for ultrathin mid-infrared optical modulators", *Nano Letters*, vol. 14, no. 11, pp. 6526–6532, 2014.

[16] Y. Cheng, H. Luo, and F. Chen, "Broadband metamaterial microwave absorber based on asymmetric sectional resonator structures", *J. Appl. Phys.*, vol. 127, no. 21, p. 214 902, 2020.

[17] H. Li, G. Wang, J. Liang, X. Gao, H. Hou, and X. Jia, "Single-layer focusing gradient metasurface for ultrathin planar lens antenna application", *IEEE Trans. Antennas Propag.*, vol. 65, no. 3, pp. 1452–1457, 2017.

[18] A. She, S. Zhang, S. Shian, D. R. Clarke, and F. Capasso, "Large area metalenses: design, characterization, and mass manufacturing", *Opt. Express*, vol. 26, no. 2, pp. 1573–1585, 2018.

[19] S. Shi, K. Qian, W. Gao, J. Dai, M. Li, and J. Dong, "Dual-band reflection polarization converter for circularly polarized waves based on a zigzag asymmetric split ring resonator", *J. Appl. Phys.*, vol. 129, no. 1, p. 014 901, 2021.

[20] X. Gao, W. Yang, H. Ma, Q. Cheng, X. Yu, and T. Cui, "A reconfigurable broadband polarization converter based on an active metasurface", *IEEE Trans. Antennas Propag.*, vol. 66, no. 11, pp. 6086–6095, 2018.

[21] J. Xu, R. Li, S. Wang, and T. Han, "Ultra-broadband linear polarization converter based on anisotropic metasurface", *Opt. Express*, vol. 26, no. 20, pp. 26 235–26 241, 2018.

[22] L. Wu, Z. Yang, Y. Cheng, R. Gong, M. Zhao, Y. Zheng, J. Duan, and X. Yuan, "Circular polarization converters based on bi-layered asymmetrical split ring metamaterials", *Applied Physics A: Materials Science and Processing*, vol. 116, no. 2, pp. 643–648, 2014.

[23] L. Dolin, "On the possibility of comparison of three-dimensional electromagnetic systems with nonuniform anisotropic filling", *Izv. Vyssh. Uchebn. Zaved. Radiofiz.*, vol. 4, pp. 964–967, 1961.

[24] J. B. Pendry, D. Schurig, and D. R. Smith, "Controlling electromagnetic fields", *Science*, vol. 312, no. 5781, pp. 1780–1782, 2006.

[25] U. Leonhardt, "Optical conformal mapping", *Science*, vol. 312, no. 5781, pp. 1777–1780, 2006.

[26] D. Schurig, J. J. Mock, B. J. Justice, S. A. Cummer, J. B. Pendry, A. F. Starr, and D. R. Smith, "Metamaterial electromagnetic cloak at microwave frequencies", *Science*, vol. 314, no. 5801, pp. 977–980, 2006.

[27] J. Li and J. B. Pendry, "Hiding under the carpet: a new strategy for cloaking", *Phys. Rev. Lett.*, vol. 101, p. 203 901, 20 2008.

[28] R. Liu, C. Ji, J. J. Mock, J. Y. Chin, T. J. Cui, and D. R. Smith, "Broadband ground-plane cloak", *Science*, vol. 323, no. 5912, pp. 366–369, 2009.

[29] J. Valentine, J. Li, T. Zentgraf, G. Bartal, and X. Zhang, "An optical cloak made of dielectrics", *Nature materials*, vol. 8, pp. 568–71, 2009.

[30] M. Gharghi, C. Gladden, T. Zentgraf, Y. Liu, X. Yin, J. Valentine, and X. Zhang, "A carpet cloak for visible light", *Nano Letters*, vol. 11, no. 7, pp. 2825–2828, 2011.

[31] F. Frezza, F. Mangini, and N. Tedeschi, "Introduction to electromagnetic scattering: tutorial", *J. Opt. Soc. Am. A*, vol. 35, no. 1, pp. 163–173, 2018.

[32] A. Alù and N. Engheta, "Achieving transparency with plasmonic and metamaterial coatings", *Phys. Rev. E*, vol. 72, p. 016 623, 1 2005.

[33] B. Edwards, A. Alù, M. G. Silveirinha, and N. Engheta, "Experimental verification of plasmonic cloaking at microwave frequencies with metamaterials", *Phys. Rev. Lett.*, vol. 103, p. 153 901, 15 2009.

[34] M. G. Silveirinha, A. Alù, and N. Engheta, "Parallel-plate metamaterials for cloaking structures", *Phys. Rev. E*, vol. 75, p. 036 603, 3 2007.

[35] D. Rainwater, A. Kerkhoff, K. Melin, J. C. Soric, G. Moreno, and A. Alù, "Experimental verification of three-dimensional plasmonic cloaking in free-space", *New J. Phys.*, vol. 14, no. 1, p. 013 054, 2012.

[36] A. Alù and N. Engheta, "Plasmonic and metamaterial cloaking: physical mechanisms and potentials", *J. Opt. A: Pure Appl. Opt.*, vol. 10, no. 9, p. 093 002, 2008.

[37] A. Alù and N. Engheta, "Cloaking and transparency for collections of particles with metamaterial and plasmonic covers", *Opt. Express*, vol. 15, no. 12, pp. 7578–7590, 2007.

[38] A. Alù and N. Engheta, "Plasmonic materials in transparency and cloaking problems: mechanism, robustness, and physical insights", *Opt. Express*, vol. 15, no. 6, pp. 3318–3332, 2007.

[39] A. Alù, D. Rainwater, and A. Kerkhoff, "Plasmonic cloaking of cylinders: finite length, oblique illumination and cross-polarization coupling", *New J. Phys.*, vol. 12, no. 10, p. 103 028, 2010.

[40] A. Alù and N. Engheta, "Multifrequency optical invisibility cloak with layered plasmonic shells", *Phys. Rev. Lett.*, vol. 100, no. 11, 2008.

[41] A. Alù and N. Engheta, "Theory and potentials of multi-layered plasmonic covers for multi-frequency cloaking", *New J. Phys.*, vol. 10, no. 11, p. 115 036, 2008.

[42] O. Luukkonen, C. Simovski, G. Granet, G. Goussetis, D. Lioubtchenko, A. V. Raisanen, and S. A. Tretyakov, "Simple and accurate analytical model of planar grids and high-impedance surfaces comprising metal strips or patches", *IEEE Trans. Antennas Propag.*, vol. 56, no. 6, pp. 1624–1632, 2008.

[43] A. Alù, "Mantle cloak: Invisibility induced by a surface", *Phys. Rev. B*, vol. 80, p. 245 115, 24 2009.

[44] P.-Y. Chen and A. Alù, "Mantle cloaking using thin patterned metasurfaces", *Phys. Rev. B*, vol. 84, p. 205 110, 20 2011.

[45] Y. R. Padooru, A. B. Yakovlev, P.-Y. Chen, and A. Alù, "Analytical modeling of conformal mantle cloaks for cylindrical objects using sub-wavelength printed and slotted arrays", *J. Appl. Phys.*, vol. 112, no. 3, p. 034 907, 2012.

[46] R. S. Schofield, J. C. Soric, D. Rainwater, A. Kerkhoff, and A. Alù, "Scattering suppression and wideband tunability of a flexible mantle cloak for finite-length conducting rods", *New J. Phys.*, vol. 16, no. 6, p. 063 063, 2014.

[47] J. Soric, P.-Y. Chen, A. Kerkhoff, D. Rainwater, K. Melin, and A. Alú, "Demonstration of an ultralow profile cloak for scattering suppression of a finite-length rod in free space", *New J. Phys.*, vol. 15, no. 3, p. 033 037, 2013.

[48] J. C. Soric, A. Monti, A. Toscano, F. Bilotti, and A. Alù, "Multiband and wideband bilayer mantle cloaks", *IEEE Trans. Antennas Propag.*, vol. 63, no. 7, pp. 3235–3240, 2015.

[49] A. Monti, J. Soric, M. Barbuto, D. Ramaccia, S. Vellucci, F. Trotta, A. Alù, A. Toscano, and F. Bilotti, "Mantle cloaking for co-site radio-frequency antennas", *App. Phys. Lett.*, vol. 108, no. 11, p. 113 502, 2016.

[50] H. Bernety and A. Yakovlev, "Reduction of mutual coupling between neighboring strip dipole antennas using confocal elliptical metasurface cloaks", *IEEE Trans. Antennas Propag.*, vol. 63, no. 4, pp. 1554–1563, 2015.

[51] A. Monti, J. Soric, A. Alu, F. Bilotti, A. Toscano, and L. Vegni, "Overcoming mutual blockage between neighboring dipole antennas using a low-profile patterned metasurface", *IEEE Antennas Wireless Propag. Letters*, vol. 11, pp. 1414–1417, 2012.

[52] P. H. Rao, I. Balakrishna, and B. J. Sherlin, "Radiation blockage reduction in antennas using radio-frequency cloaks", *IEEE Antennas Propag. Magazine*, vol. 60, no. 3, pp. 91–100, 2018.

[53] J. Ghosh and D. Mitra, "Restoration of antenna performance in the vicinity of metallic cylinder in implantable scenario", *IET Microwaves, Antennas Propag.*, vol. 14, no. 12, pp. 1440–1445, 2020.

[54] S. Vellucci, A. Monti, M. Barbuto, A. Toscano, and F. Bilotti, "Use of mantle cloaks to increase reliability of satellite-to-ground communication link", *IEEE Journal on Multiscale and Multiphysics Computational Techniques*, vol. 2, pp. 168–173, 2017.

[55] S. Vellucci, A. Monti, M. Barbuto, A. Toscano, and F. Bilotti, "Waveform-selective mantle cloaks for intelligent antennas", *IEEE Trans. Antennas Propag.*, vol. 68, no. 3, pp. 1717–1725, 2020.

[56] E. Shokati, N. Granpayeh, and M. Danaeifar, "Wideband and multi-frequency infrared cloaking of spherical objects by using the graphene-based metasurface", *Appl. Opt.*, vol. 56, no. 11, pp. 3053–3058, 2017.

[57] M. Naserpour, C. Zapata-Rodríguez, S. Vuković, H. Pashaeiadl, and M. Belić, "Tunable invisibility cloaking by using isolated graphene-coated nanowires and dimers", *Sci. Rep.*, vol. 7, no. 1, 2017.

[58] Z. Hamzavi-Zarghani, A. Yahaghi, L. Matekovits, and A. Farmani, "Tunable mantle cloaking utilizing graphene metasurface for terahertz sensing applications", *Opt. Express*, vol. 27, no. 24, pp. 34 824–34 837, 2019.

[59] P.-Y. Chen, J. Soric, Y. R. Padooru, H. M. Bernety, A. B. Yakovlev, and A. Alù, "Nanostructured graphene metasurface for tunable terahertz cloaking", *New J. Phys.*, vol. 15, no. 12, p. 123 029, 2013.

[60] P.-Y. Chen and A. Alù, "Atomically thin surface cloak using graphene monolayers", *ACS Nano*, vol. 5, no. 7, pp. 5855–5863, 2011.

[61] H. Bernety and A. Yakovlev, "Cloaking of single and multiple elliptical cylinders and strips with confocal elliptical nanostructured graphene metasurface", *J. .Phys. Cond. Matter*, vol. 27, no. 18, p. 185 304, 2015.

[62] A. Norris, "Acoustic cloaking theory", *Proceedings of the Royal Society A: Mathematical, Physical and Engineering Sciences*, vol. 464, no. 2097, pp. 2411–2434, 2008.

[63] M. Guild, A. Al, and M. Haberman, "Cancellation of acoustic scattering from an elastic sphere", *J. Acoustical Soc. Am.*, vol. 129, no. 3, pp. 1355–1365, 2011.

[64] X. Zhu, B. Liang, W. Kan, X. Zou, and J. Cheng, "Acoustic cloaking by a superlens with single-negative materials", *Phys. Rev. Lett.*, vol. 106, no. 1, p. 014 301, 2011.

[65] R. Schittny, M. Kadic, S. Guenneau, and M. Wegener, "Experiments on transformation thermodynamics: molding the flow of heat", *Phys. Rev. Lett.*, vol. 110, p. 195 901, 19 2013.

[66] I. Peralta, V. D. Fachinotti, and J. C. Álvarez Hostos, "A brief review on thermal metamaterials for cloaking and heat flux manipulation", *Advanc. Eng. Materials*, vol. 22, no. 2, p. 1 901 034, 2020.

[67] M. Imran, L. Zhang, and A. Gain, "Advanced thermal metamaterial design for temperature control at the cloaked region", *Sci. Rep.*, vol. 10, no. 1, 2020.

[68] M. Farhat, P.-Y. Chen, H. Bagci, C. Amra, S. Guenneau, and A. Alù, "Thermal invisibility based on scattering cancellation and mantle cloaking", *Sci. Rep.*, vol. 5, 2015.

[69] M. Bisht, V. Vinubhai, and K. Srivastava, "Analysis and realization of a wideband mantle cloak with improved cloaking performance", *J. Electromag. Waves Appl.*, vol. 34, no. 10, pp. 1386–1399, 2020.

[70] G. Moreno, A. B. Yakovlev, H. M. Bernety, D. H. Werner, H. Xin, A. Monti, F. Bilotti, and A. Alù, "Wideband elliptical metasurface cloaks in printed antenna technology", *IEEE Trans. Antennas Propag.*, vol. 66, no. 7, pp. 3512–3525, 2018.

[71] M. Danaeifar and N. Granpayeh, "Wideband invisibility by using inhomogeneous metasurfaces of graphene nanodisks in the infrared regime", *J. Opt. Soc. Am. B*, vol. 33, no. 8, pp. 1764–1768, 2016.

[72] E. Shokati and N. Granpayeh, "Wideband cloaking by using inhomogeneous nanostructured graphene metasurface for tunable cloaking in the terahertz regime", in *2016 Fourth International Conference on Millimeter-Wave and Terahertz Technologies (MMWaTT)*, 2016, pp. 9–13.

[73] E. Shokati, N. Granpayeh, and M. Danaeifar, "Wideband and multi-frequency infrared cloaking of spherical objects by using the graphene-based metasurface", *Appl. Opt.*, vol. 56, no. 11, pp. 3053–3058, 2017.

[74] D. L. Sounas, R. Fleury, and A. Alù, "Unidirectional cloaking based on metasurfaces with balanced loss and gain", *Phys. Rev. Applied*, vol. 4, p. 014 005, 1 2015.

[75] P.-Y. Chen, C. Argyropoulos, and A. Alú, "Broadening the cloaking bandwidth with non-Foster metasurfaces.", *Phys. Rev. Lett.*, vol. 111 23, p. 233 001, 23 2013.

[76] S. Liu, H.-X. Xu, H. C. Zhang, and T. J. Cui, "Tunable ultrathin mantle cloak via varactor-diode-loaded metasurface", *Opt. Express*, vol. 22, no. 11, pp. 13 403–13 417, 2014.

[77] M. Selvanayagam and G. Eleftheriades, "Experimental demonstration of active electromagnetic cloaking", *Phys. Rev. X*, vol. 3, no. 4, p. 041 011, 2014.

[78] E. G. Mizuji, A. Abdolali, and F. Aghamohamadi, "Analytical approach for making multilayer and inhomogeneous structures invisible based on mantle cloak", *J. Microw. Optoelectron. Electromagn. Appl.*, vol. 17, pp. 121–133, 2018.

[79] A. Serna, L. Molina, J. Rivero, L. Landesa, and J. Taboada, "Multilayer homogeneous dielectric filler for electromagnetic invisibility", *Sci. Rep.*, vol. 8, no. 1, 2018.

[80] A. Abouelsaood, I. Afifi, and I. Eshrah, "Nonresonant and resonant cloaking of an electrically large dielectric spherical object by a multilayer isotropic metamaterial cover", *Appl. Opt.*, vol. 54, no. 21, pp. 6598–6607, 2015.

[81] Z. H. Jiang and D. H. Werner, "Exploiting metasurface anisotropy for achieving near-perfect low-profile cloaks beyond the quasi-static limit", *J. Phys. D: Appl. Phys.*, vol. 46, no. 50, p. 505 306, 2013.

[82] D.-H. Kwon, "Lossless tensor surface electromagnetic cloaking for large objects in free space", *Phys. Rev. B*, vol. 98, p. 125 137, 12 2018.

[83] S. Nanz, *Toroidal Multipole Moments in Classical Electrodynamics*. Springer, 2016.

[84] T. Kaelberer, V. A. Fedotov, N. Papasimakis, D. P. Tsai, and N. I. Zheludev, "Toroidal dipolar response in a metamaterial", *Science*, vol. 330, no. 6010, pp. 1510–1512, 2010.

[85] G. N. Afanasiev and V. M. Dubovik, "Some remarkable charge-current configurations", *Physics of Particles and Nuclei*, vol. 29, no. 4, pp. 366–391, 1998.

[86] B. Cappello, A. Ospanova, L. Matekovits, and A. Basharin, "Mantle cloaking due to ideal magnetic dipole scattering", *Sci. Rep.*, vol. 10, no. 1, 2020.

[87] B. Cappello and L. Matekovits, "Harmonic analysis and reduction of the scattered field from electrically large cloaked metallic cylinders", *Appl. Opt.*, vol. 59, no. 12, pp. 3742–3750, 2020.

[88] B. Cappello, G. Labate, and L. Matekovits, "A surface impedance model for a microstrip-line based metasurface", in *2017 International Conference on Electromagnetics in Advanced Applications (ICEAA)*, 2017, pp. 429–432.

[89] B. Cappello and L. Matekovits, "Spectral Composition of the Scattered Field from a Large Metallic Cloaked Cylinder", in *2018 International Conference on Electromagnetics in Advanced Applications (ICEAA)*, 2018, pp. 240–243.

[90] C. A. Balanis, *Advanced Engineering Electromagnetics*. John Wiley & Sons, Inc, 1989.

[91] I. A. S. M. Abramowitz, *Handbook of mathematical functions, with Formulas, graphs, and mathematical tables*. Dover Publications, New York, 1965.

[92] N. Xiang, Q. Cheng, H. B. Chen, J. Zhao, W. X. Jiang, H. F. Ma, and T. J. Cui, "Bifunctional metasurface for electromagnetic cloaking and illusion", *Applied Physics Express*, vol. 8, no. 9, p. 092 601, 2015.

[93] K. Barkeshli, *Advanced electromagnetics and scattering theory*. Springer, 2015.

[94] S. Liu, H. C. Zhang, H.-X. Xu, and T. J. Cui, "Nonideal ultrathin mantle cloak for electrically large conducting cylinders", *J. Opt. Soc. Am. A*, vol. 31, no. 9, pp. 2075–2082, 2014.

[95] H. Younesiraad, M. Bemani, and S. Nikmehr, "Scattering suppression and cloak for electrically large objects using cylindrical metasurface based on monolayer and multilayer mantle cloak approach", *IET Microwaves, Antennas Propagation*, vol. 13, no. 3, pp. 278–285, 2019.

[96] B. Cappello, Y. Shestopalov, and L. Matekovits, "Analysis of the surface impedance of a sinusoidally modulated metasurface", in *2019 International Conference on Electromagnetics in Advanced Applications (ICEAA)*, 2019, pp. 0075–0077.

[97] B. Cappello and L. Matekovits, "Inhomogeneous metasurface to enlarge cloaking bandwidth", in *2020 IEEE International Symposium on Antennas and Propagation and North American Radio Science Meeting*, 2020, pp. 813–814.

This Ph.D. thesis has been typeset by means of the TEX-system facilities. The typesetting engine was pdfLATEX. The document class was `toptesi`, by Claudio Beccari, with option `tipotesi=scudo`. This class is available in every up-to-date and complete TEX-system installation.